DETERMINATION OF THREE-DIMENSIONAL AQUIFER ANISOTROPY OF AN UNCONFINED AQUIFER UNDER PARTIALLY PENETRATING PUMPING CONDITIONS

By

Chia-Shyun Chen
Principal Investigator

And

Christopher Holmes, Weidong Li, David Chace,
Mike Fort, Jingfang He, Jim Liu

Graduate Research Assistants

Department of Geoscience
New Mexico Institute of Mining and Technology

TECHNICAL COMPLETION REPORT

Account Numbers 1423640 and 01423952

November 1993

New Mexico Water Resources Research Institute

in cooperation with

Department of Geoscience
New Mexico Institute of Mining and Technology

The research on which this report is based was financed in part by the U.S. Department of the Interior, Geological Survey, through the New Mexico Water Resources Research Institute.

DISCLAIMER

The purpose of Water Resources Research Institute technical reports is to provide a timely outlet for research results obtained on projects supported in whole or in part by the institute. Through these reports, we are promoting the free exchange of information and ideas, and hope to stimulate thoughtful discussion and actions that may lead to resolution of water problems. The WRRI, through peer review of draft reports, attempts to substantiate the accuracy of information contained in its reports, but the views expressed are those of the author(s) and do not necessarily reflect those of the WRRI or its reviewers. Contents of this publication do not necessarily reflect the views and policies of the U.S. Department of the Interior, nor does mention of trade names or commercial products constitute their endorsement by the United States government.

ACKNOWLEDGEMENTS

This project was supported by the New Mexico Water Resources Research Institute through grant numbers 1423640 and 01423952. The pumping tests for this project were carried out using the research facilities supported by the U.S. Geological Survey (grant number 14-08-0001-G1744) for research on a three-dimensional solute transport. New Mexico Tech provided matching funds for both projects by waiving the overhead and supporting computer costs. We are indebted to the three sponsors. We also wish to thank Darlene Reeves and Catherine Ortega Klett of the New Mexico Water Resources Research Institute, Anna Mclain of New Mexico Tech, Nedra Stalline, Melvin Lew, and Mary-Eileen Mathey of the U.S. Geological Survey for their dedicated help in administering this research. We express our appreciation to Irl Downes, Walter Gage, and Cathy Aimone of New Mexico Tech for their valuable assistance in the drilling work, and to William Stone of New Mexico Tech's Mathematics Department for his helpful suggestions. Thanks are due to Ted Stans of U.S. Fish and Wildlife Service for his permission and assistance in using the Sevilleta Wildlife Refuge research site. Particularly, we thank Edith Montoya for her tremendous patience and excellent skill in typing this report; equations involved are a nightmare to us even when writing in longhand.

ABSTRACT

Field and theoretical investigations were made to study the three-dimensional hydraulic conductivity anisotropy of an unconfined aquifer. A well field, consisting of three multilevel samplers/piezometers (MLSP), ten fully screened observation wells, and two pumping wells, was developed in the Sevilleta Wildlife Refuge, north of New Mexico Tech. The MLSP can give depth-specific drawdown and groundwater samples for the three-dimensional analysis. The fully screened observation well can yield vertically-averaged drawdown and groundwater samples for the two-dimensional analysis. The three-dimensional aquifer anisotropy is characterized using the depth-specific drawdown data and a method based on the Laplace-Hankel domain solution of a pertinent three-dimensional unconfined well hydraulics theory. The Laplace-Hankel domain solution involves three mathematically simple terms representing the Theis solution, the water-table effect, and the partially penetrating effect, respectively. The fast Hankel transform (FHT) technique and the Stehfest Laplace inverse method are employed to calculate the drawdown of interest from the Laplace-Hankel domain counterpart. This Laplace-Hankel domain analysis provides an effective way to evaluate and understand complicated well hydraulics theories.

Also, a mapping function technique was developed to diagnose the drawdown data. The mapping function essentially represents any difference between the actual hydrogeological conditions embedded in the field data and the idealistic assumptions invoked in the Theis solution. A new analytical solution for well hydraulics involving the temporal mapping function was obtained. Based on this solution, a robust method was developed to find the mapping function from available field drawdown data.

A few case studies demonstrated that the mapping function indeed can yield diagnostic curve characteristics pertinent to important hydrogeological conditions. During the course of reviewing currently available well hydraulics, it was found that the method normally used in finding the asymptotic solutions from the Laplace domain can lead to incorrect results. To avoid this pitfall, it is suggested that the Tauberian Theorem be used to check the validity of the asymptotic solutions obtained using the normally accepted method.

Keywords: three-dimensional anisotropy, well hydraulics, pumping tests, Laplace-Hankel solutions, mapping functions, drawdown data analysis.

TABLE OF CONTENTS

LIST OF FIGURES

LIST OF TABLES

1. INTRODUCTION AND SUMMARY

1.1 BACKGROUND AND PROBLEM OF INTEREST

Under field conditions, groundwater movement is three-dimensional in nature. A detailed study of three-dimensional groundwater problems requires appropriate three-dimensional theories and depth-specific field data (i.e., drawdown or groundwater quality) at different locations in the aquifer. For this project dealing with three-dimensional solute transport under anisotropic conditions, a well field was developed to generate depth-specific and vertically averaged field data. The depth-specific drawdown data collected form a three-dimensional data base, which is suitable for characterizing the three-dimensional aquifer anisotropy. The aquifer anisotropy has been normally studied in a two-dimensional, planar sense. Little work has been done to estimate three-dimensional aquifer anisotropy for granular aquifers. Due to the availability of three-dimensional drawdown data and the practical importance of three-dimensional aquifer anisotropy, this project sought a method that can be used to determine the three-dimensional aquifer anisotropy.

It should be noted that this project was a continuation of an earlier study of three-dimensional solute transport and does not require a storage coefficient and the specific yield. Thus, for the current project, these two parameters are not of primary concern and we did not develop a method to estimate them. The problem of interest was to determine the three-dimensional aquifer anisotropy using appropriate depth-specific drawdown data. Literature related to this subject is reviewed below in appropriate chapters of the report.

1.2 PURPOSES AND SCOPE

The purposes of the project are to conduct three-dimensional pumping tests to produce drawdown data appropriate for three-dimensional determination of the aquifer anisotropy tensor, and to develop a method to estimate the three-dimensional aquifer anisotropy tensor.

Due to the concurrence of the current and previous projects, some pumping tests involved tracer injection (as discussed in Chapters 2 and 3). Since this project was limited to the study of aquifer anisotropy, the briefly mentioned tracer tests and related information are not elaborated on here.

1.3 SUMMARY OF ACHIEVEMENT

During the course of this project, the following was achieved:

(1) A well field (see Figure 1) including two pumping wells, 15.24 cm (6 inches) in diameter, ten observation wells, 5.08 cm (2 inches) in diameter, and three multilevel samplers/piezometers (MLSP), was developed. This well field can produce both depth-specific and vertically averaged data of drawdown and tracer concentration distributions.

(2) A new method for aquifer characterization was developed. It calls for the use of a temporal mapping function, which represents the possible hydrogeological conditions imbedded in the field data. The mapping function can be used to diagnose the hydrogeological conditions involved in drawdown data, to quantify a few hydrogeological parameters, and to justify the pressure-derivative method developed by petroleum reservoir engineers.

(3) A new method for calculating complicated well hydraulics solutions of various unconfined conditions was developed. This method is based on the Laplace-Hankel domain analysis. Complicated numerical integration was avoided

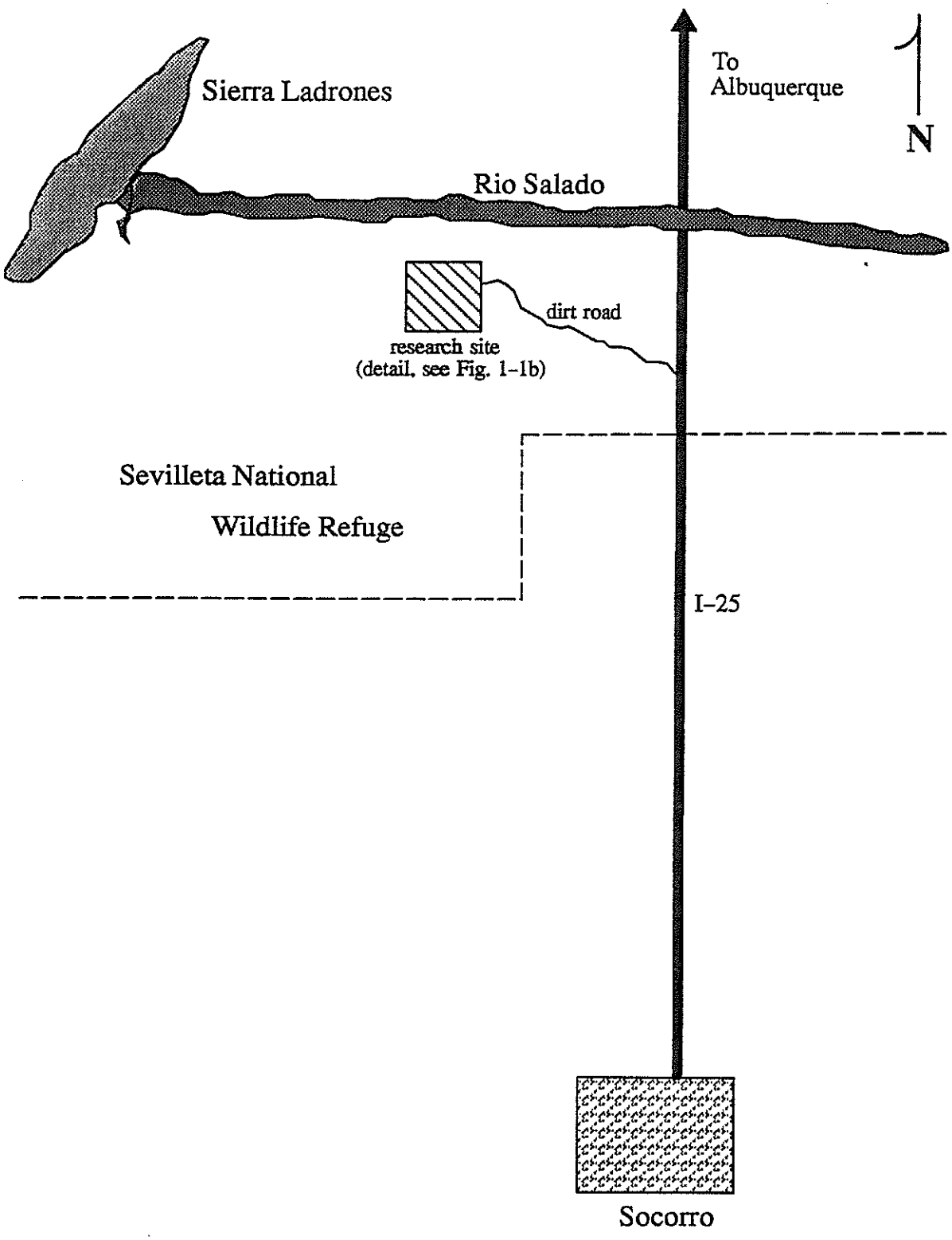

Figure 1-1a. Research Site Inside the Sevilleta National Wildlife Refuge North of Socorro, New Mexico.

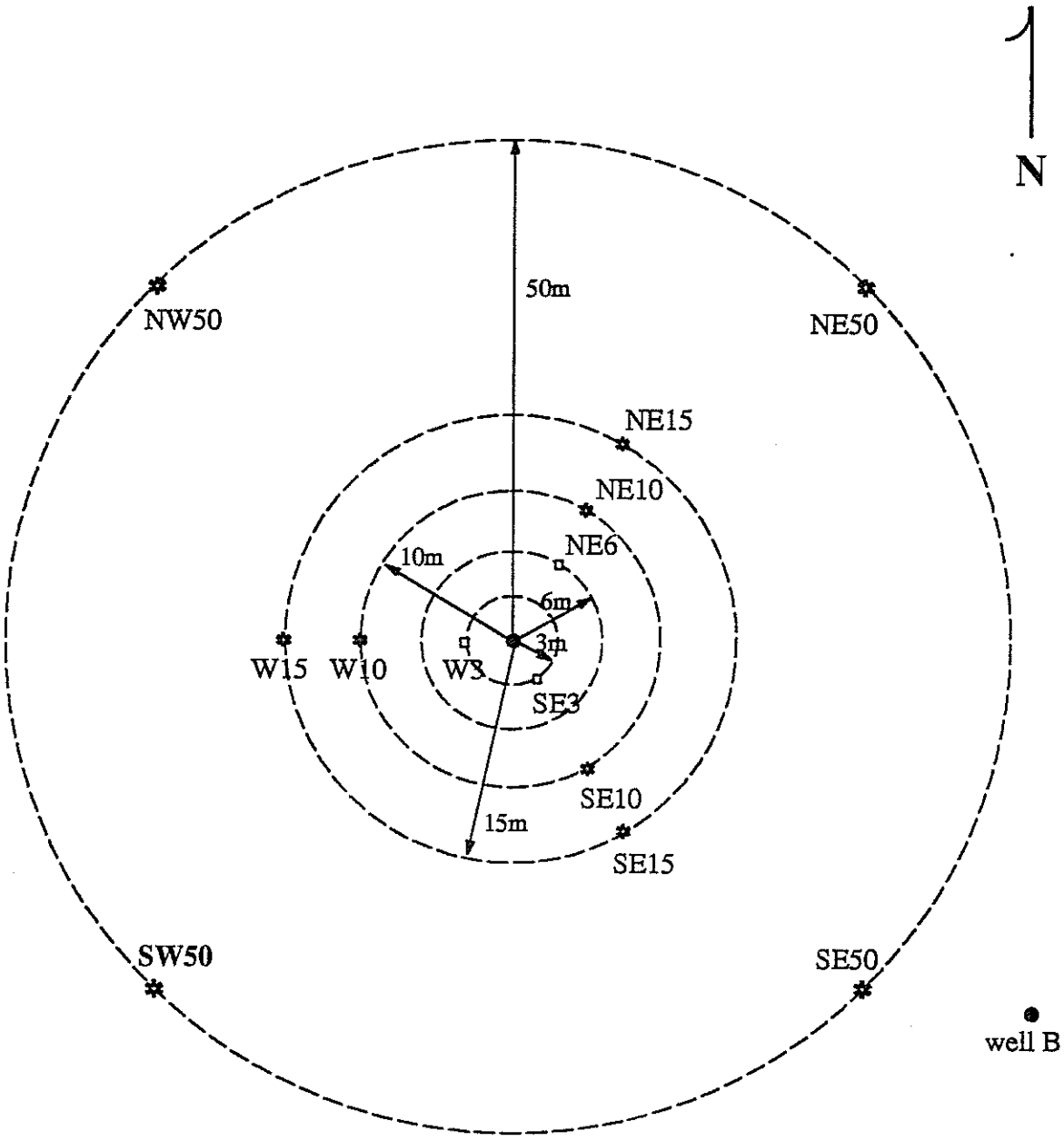

● – 6–inch well A, approximately 60 meters from 6–inch well B

✱ – 2–inch observation well

▫ – functional multilevel samplers/piezometers (MLSP)

Figure 1–1b. Locations of Observation Wells and MLSP's at the Sevilleta Research Site.

by using the Fast Hankel Transform (FHT) and easily implemented numerical Laplace inverse techniques. The Laplace-Hankel domain solutions explicitly show the influence of the water table and partially penetrating pumping on the drawdown distributions.

(4) A method of estimating the three-dimensional anisotropy tensor for an unconfined aquifers was developed. This method uses the large-time depth-specific drawdown data and the mathematical properties demonstrated in the appropriate Laplace-Hankel domain solutions.

(5) A possible pitfall in calculating asymptotic well hydraulics solutions was found. An alternative way to handle the asymptotic calculation, which avoids the pitfall, was suggested.

2. SITE DEVELOPMENT AND MEASURING DEVICES INSTALLATION

The research site for the field experiments is located on the flood plain of the Rio Salado in the Sevilleta National Wildlife Refuge (Figure 1-1a) approximately 32 km north of Socorro, New Mexico. Two 15.24-cm (6 inch) wells, three multilevel samplers/piezometers (MLSP) and ten 5.08-cm (2 inch) observation wells have been installed at the site (Figure 1-1b). Well B, 60 m southeast of Well A, was used primarily for water supply. Both Well A and B are 15.2 cm in diameter. Well A is at the center of the well field for field experiments. The MLSPs and observation wells were installed on three rays west (W), northeast (NE) and southeast (SE), on five concentric circles surrounding Well A. The concentric circles have a radius of 3 m, 6 m, 10 m, 15 m and 50 m. Each MLSP or observation well was designated by its direction and distance measured with respect to Well A. For example, SE 3 represents the MLSP located in the SE direction and 3 m away from Well A. All MLSP's were installed at the 3-m and 6-m circles, and the observation wells at 10-m, 15-m, and 50-m circles. The four observation wells, NW50, NE50, SW50, and SE50, primarily were used to monitor the regional groundwater flow field. The regional groundwater movement monitored by these four observation wells, in general, was relatively uniform from NW to SE with a small hydraulic gradient of about 10^{-3} m/m and provided no significant rainfall effects. Due to the small pumping rates (no more than 6.3×10^{-3} m^3/s, or 100 gpm) used in the pumping/tracer tests, drawdown or tracer never reached these four observation wells.

The Rio Salado, located north of the research site, is an ephemeral stream with the channel dry on the average of 320 days per year. The Sevilleta aquifer is unconfined with a

shallow water table approximately 3-m below the ground surface. This aquifer consists of Holocene Rio Salado alluvium overlying Pleistocene axial stream deposits of the Sierra Ladrones Formation. The Rio Salado alluvium consists of interbedded sand, gravel, and silt. The axial stream deposits also consist of interbedded sand and silt with occasional gravel and clay layers. Split-spoon samples taken from three boreholes show the contact between the Rio Salado and axial stream deposits is located between 13.72 m and 19.81 m below the ground surface. This supports the seismological studies made by Stephens et al. (1988), which proclaimed that Rio Salado alluvium was in contact with the Sierra Ladrones.

The contact depth between these two formations increases from north to south, indicating the original channel of the Rio Salado was located farther south than the present channel. Although the exact thickness of the aquifer is unknown, our drilling indicated that the thickness is more than 24.38 m. Seismological studies indicate that the aquifer thickness should be more than 100 m (Knapp, personal communication, 1991).

The Loma Blanca fault cuts across the aquifer in an almost due north-south direction. Zody (1989) noted that there was a marked steepening of the hydraulic gradient extending about 300 m west of the fault. Effects of the Loma Blanca fault and the steepening of the hydraulic gradients on the test area are unknown. Little or no tilting of the Sierra Ladrones formation outcropping beds was noticed in the test vicinity.

2.1 DESIGN OF MULTILEVEL SAMPLERS/PIEZOMETERS (MLSP)

The original plan for the well field called for the use of several multilevel samplers for collecting depth-specific groundwater samples and several piezometers for measuring depth-specific drawdown. Since drilling with the equipment available to New Mexico Tech

was rather difficult in the Sevilleta's unconsolidated sandy materials, we decided to reduce drilling by developing the MLSP technique.

As shown in Figure 2-1, one MLSP includes a cluster of eleven 0.64-cm (1/4 inch) polyethylene tubes for groundwater sampling and seven 1.27-cm (1/2 inch) PVC standing pipes connected to 0.95-cm (3/8 inch) flexible tubing for drawdown measurement. Each standing pipe is 6.1 m in length and connected to a 0.95-cm flexible tube of which the length depends on the water intake depth. The water intake was made of a 1.27-cm PVC pipe 7.62-cm (3 inches) long. Holes were drilled and a nylon mesh placed on this section. As a result, one MLSP allowed the collection of groundwater samples from eleven different depths and drawdown data at seven different depths. Little vertical averaging can occur inside the small water intakes, and thus data yielded by the MLSP were depth-specific. The total cross-sectional area of the eleven 0.64-cm polyethylene tubes and the seven 1.27-cm PVC standing pipes is the maximum possible area that can fit in a 9.53-cm (3-3/4 inches) hollow stem auger, which was used for drilling and installation of the MLSP.

The depth-specific drawdown was measured with 0.64-cm pressure transducers. Before the pump started, the pressure transducers were dropped into the 1.27 cm standing pipes to a depth approximately 1 m below the groundwater table considering that the maximum drawdown occurring in the pumping well for a pumping rate of 378.5 l/min was only 1.5 m. This pumping rate was the maximum one used in the field experiments for the project. A datalogger with ten channels was used to measure and record the depth-specific drawdown histories at ten different locations in the aquifer. As shown in

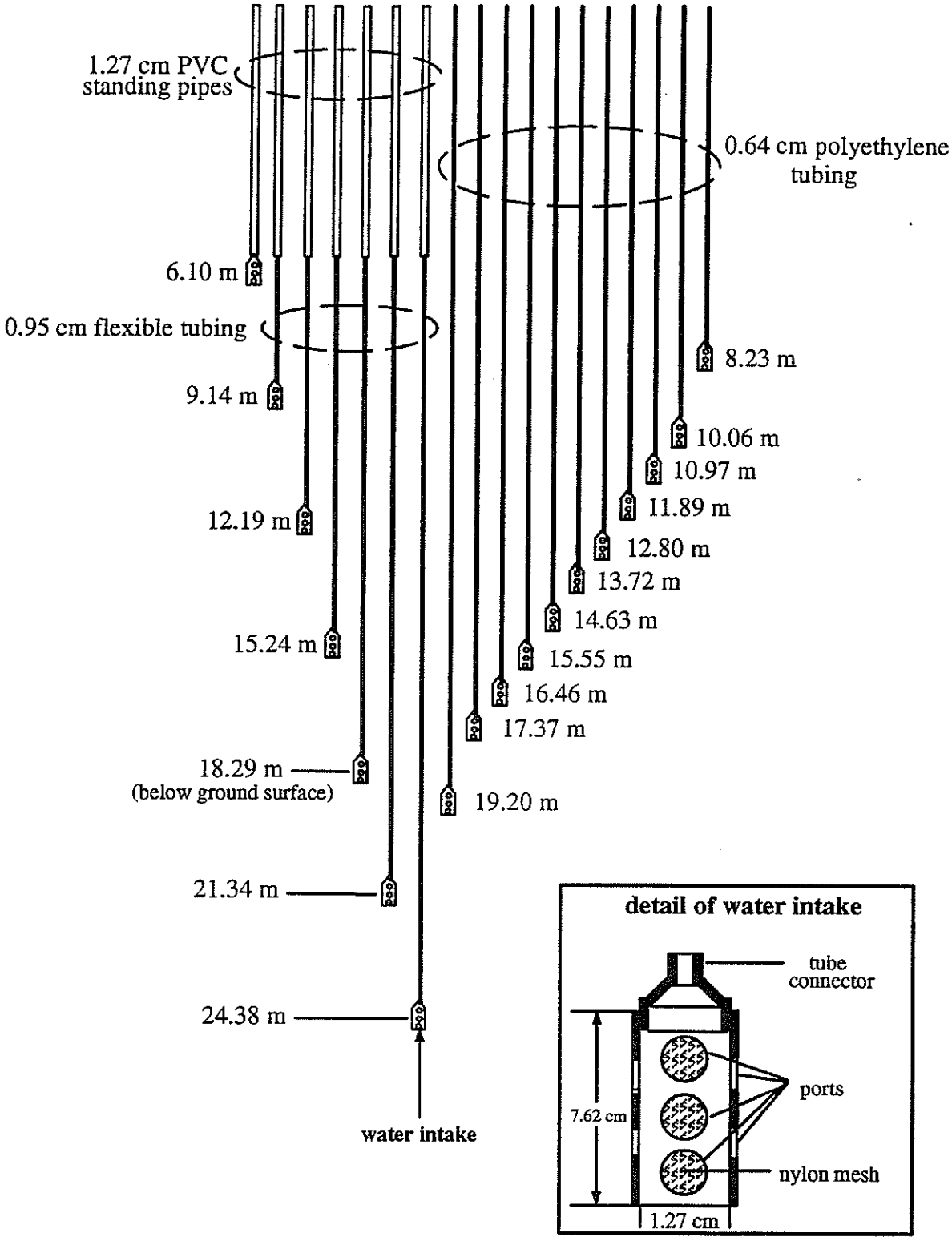

Figure 2–1 Design of the Multilevel Sampler/Piezometer (MLSP).

Figure 2-2, a groundwater sampling manifold (GSM) was developed to simultaneously collect ten groundwater samples from ten different 0.64 cm polyethylene tubes using one vacuum pump. This device is a modification of the design given by Hitchman [1988]. The GSM uses ten polyethylene syringe barrels as storage chambers for groundwater. Each of the ten polyethylene syringe barrels has a volume of 60 cubic centimeters and is connected to the vacuum pump through the 0.64 cm copper tubing. A three-way teflon stopcock (the stopcock No. 1) is used to control the bypass of the suction from the pump to the chambers.

When stopcock No. 1 is in the closed position, the chamber is not subject to the suction. Another three-way teflon stopcock (the stopcock No. 2) controls the drainage of groundwater stored in the chamber. When the chamber is filled with groundwater and the stopcock No. 1 is closed, the chamber is drained by turning on the stopcock No. 2. The drained groundwater is stored in collection bottles, which are shipped to the laboratory for tracer concentration analysis. The chamber can be connected to the MLSP sampling tubes through the 0.64 cm copper tubing that does not have a teflon stopcock.

The field operation procedure of the GSM is:

(1) connect the GSM to the vacuum pump and to ten sampling tubes of the MLSP's;

(2) set the stopcock No. 1 of each chamber to the open position, and the stopcock No. 2 to the closed position;

(3) turn on the vacuum pump and start the collection of groundwater;

(4) turn off the stopcock No. 1 before the water level inside the chamber reaches the 1/4" copper tubing opening;

(5) turn on the stopcock No. 2 and collect the groundwater drained from the chamber;

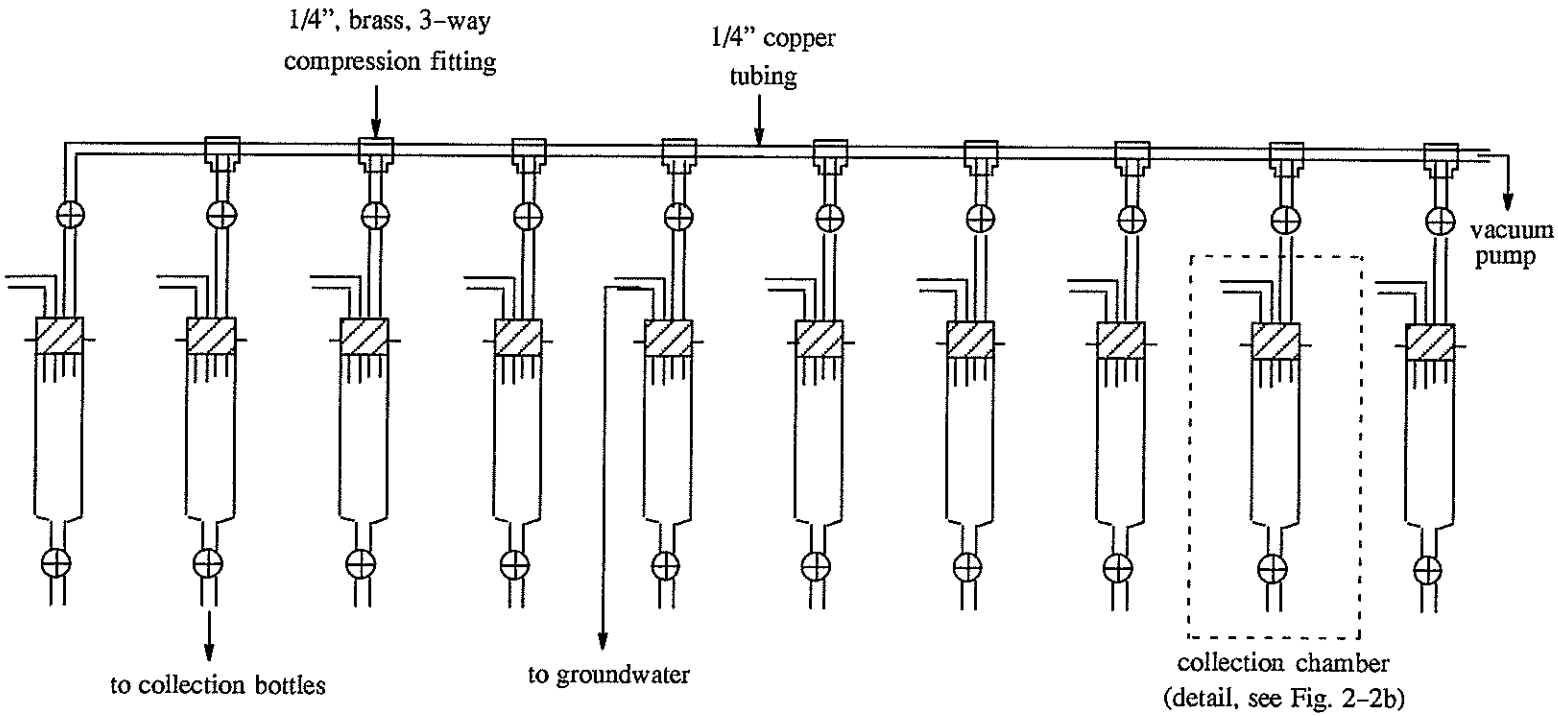

Figure 2-2a. Design of groundwater sampling manifold system.

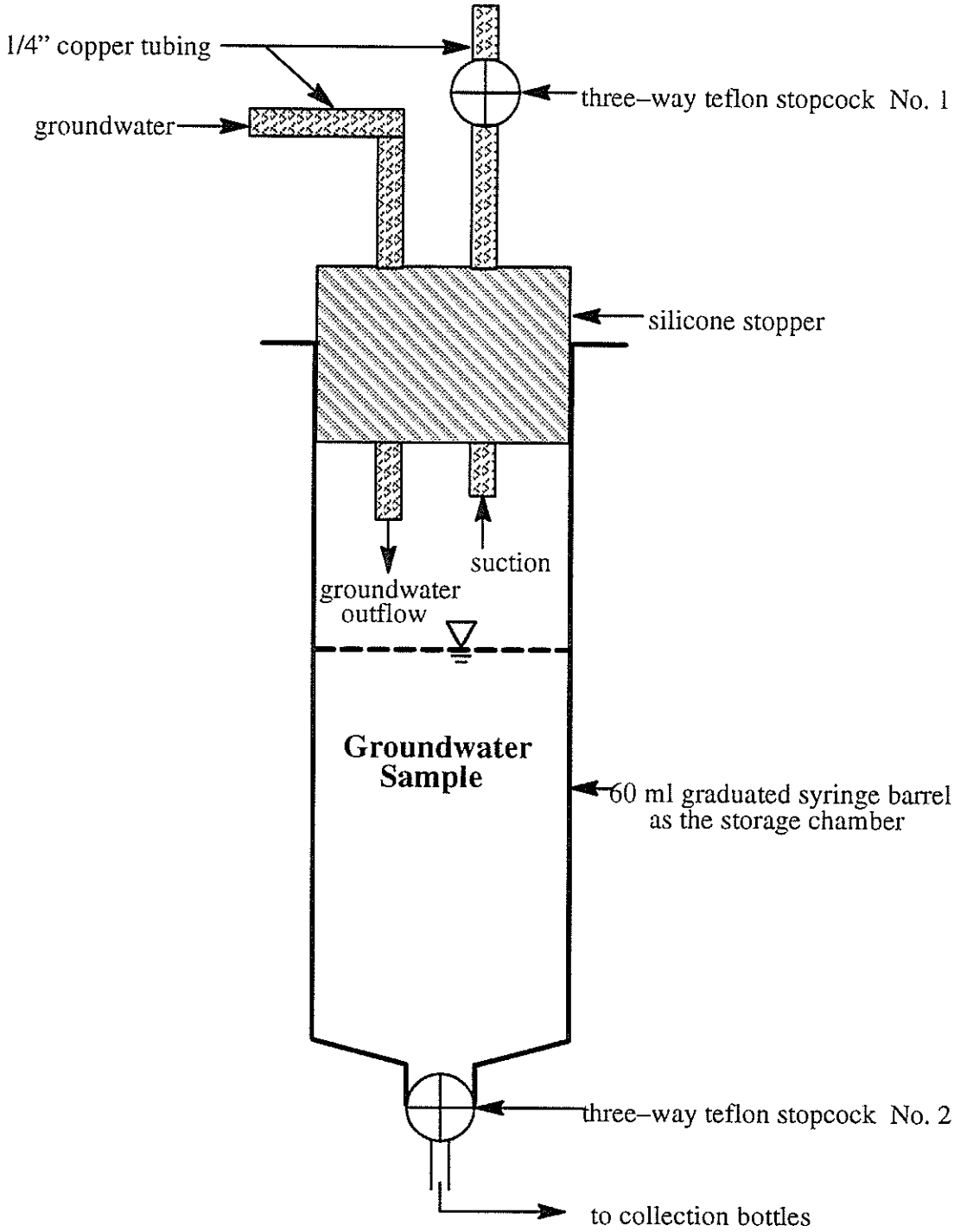

Figure 2–2b. Detail of the collection chamber.

(6) turn off the stopcock No. 2 after the chamber is drained and turn on the stopcock No. 1 to activate the suction and continue the groundwater collection.

The GSM has been successfully used in the field to collect groundwater samples.

2.2 DRILLING HISTORY AND MEASURING DEVICE INSTALLATION

Drilling for the project began on March 21, 1990, using a 18.73 cm (7-3/8 inches) tricone rotary bit. In order to avoid the formation of wall cake, a foaming agent instead of drilling mud was used with air lift to remove the cuttings. The first borehole was completed to a depth of 25.91 m and the 15.24 cm well screen was inserted to a depth of 13.92 m where it was stopped by an obstruction possibly caused by caving in the lower portion of the borehole. The 15.24 cm well screen is made of a 15.24 cm PVC pipe with machine cut slots. After an unsuccessful attempt to free the screen by drilling below it with a 10.08 cm (4 inches) bit, it was decided to use this well (Well B) for water supply well. A second borehole, 46 m west of Well B, was drilled and completed to a depth of 25.91 m. The high water velocities needed for air lift had, however, caused severe caving near the ground surface, and this borehole had to be completely abandoned.

The third borehole was drilled using a synthetic polymer viscosifier added to the drilling fluid to keep the borehole open. After mixing with water, this polymer is decomposed into aqueous components and thus will not create any wall cake. The third borehole was drilled and kept open to 25.91 m below the ground surface. It was successfully cased from the ground surface to 6.1 m with a solid 15.24 cm PVC pipe, and screened from 6.1 m to 25.91 m with a 15.24 cm well screen. This well, Well A, was pumped using air lift to remove the drilling fluid and the annulus was backfilled with drilling cuts. Well A

was then left for three days to allow the breakdown of any remaining polymer and was developed again using air surging and air lift pumping. Well A is about 60 m west of Well B. A 5.08-cm PVC pipeline exists between these two wells, used to convey groundwater pumped from Well B to Well A when needed.

A total of six MLSPs (only three are functional) and ten 5.08-cm observation wells were installed at different locations surrounding Well A as shown in Figure 1-1b. From the experience of drilling Well A and B, it was decided that a 9.53-cm hollow stem auger would be used to drill the boreholes for the MLSPs and observations wells. To do so, the hollow stem auger keeps the borehole open without needing polymer nor is there any worry of caving problems. In addition, split-spoon soil samples became possible. However, the split spoon was easily sand locked inside the hollow stem auger and split-spoon sampling was not successful for many boreholes. Only during the last three drillings of NW50, SE15 and SE50 was the difficulty overcome by a water-circulation technique. It consisted of circulating water through the borehole while drilling was in progress. In the meantime, the hollow stem was filled with water while soil samples were taken. Circulation of water kept aquifer materials from lodging in between the drill stem and the inside wall of the hollow auger. Water in the hollow stem creating a head that inhibited any aquifer materials from rushing into the hollow stem while the drill bit was taken out of the borehole and replaced with the split spoon. Split-spoon soil samples were successfully collected with this water-circulation method at various depths for NW50, SE15 and SE50. A total of 44 soil samples was obtained. Each sample underwent laboratory analysis for soil classification and other purposes as discussed below.

While the hollow stem was in the borehole drilled, the 0.64 cm polyethylene tubes and the 0.95 cm flexible tubings were tightly bundled with a weight attached to the end. The bundle then was carefully lowered into the hollow stem. After the entire section, including the standing pipes, was lowered into the augers, the augers were simply pulled out, leaving the bundle in place. To keep the bundle straight, a nylon rope running the entire section of the bundle was kept taut during the pullout. After the augers were pulled out, sand caved in very rapidly that little time was available to isolate water intakes by backfilling the spaces among them with bentonite or grout. Had there been sufficient time, the backfilling might have easily jeopardized the water intake function by blocking the water intakes due to their smallness and very tight space inside the boreholes for actual filling operation. However, this naturally occurring event was neither problematic nor short circuit the vertical flow paths between water intakes, as evidenced by the fact that depth-specific drawdown taken at different depths from the MLSP's indeed demonstrate distinctive and expected trends. The ten observation wells were installed in a similar manner; the 5.08 cm PVC pipes were lowered into the hollow stem augers and then the augers were pulled out. The top 6.1 m of these observations wells are of solid PVC pipes. From 6.1 m to various depths are of slotted screens. Figure 2-3 gives the screen locations for these 5.08 cm observation wells and Well A; all these were measured with respect to the top point of the casing of Well A.

After installation, the MLSP's, 5.08 cm observation wells and 15.24 cm wells were developed using both air surge and water surge methods. It was found that three of the six MLSP's were dysfunctional; they failed to yield drawdown or groundwater samples after extensive development. These three MLSP's were abandoned and not indicated in Figure 1b.

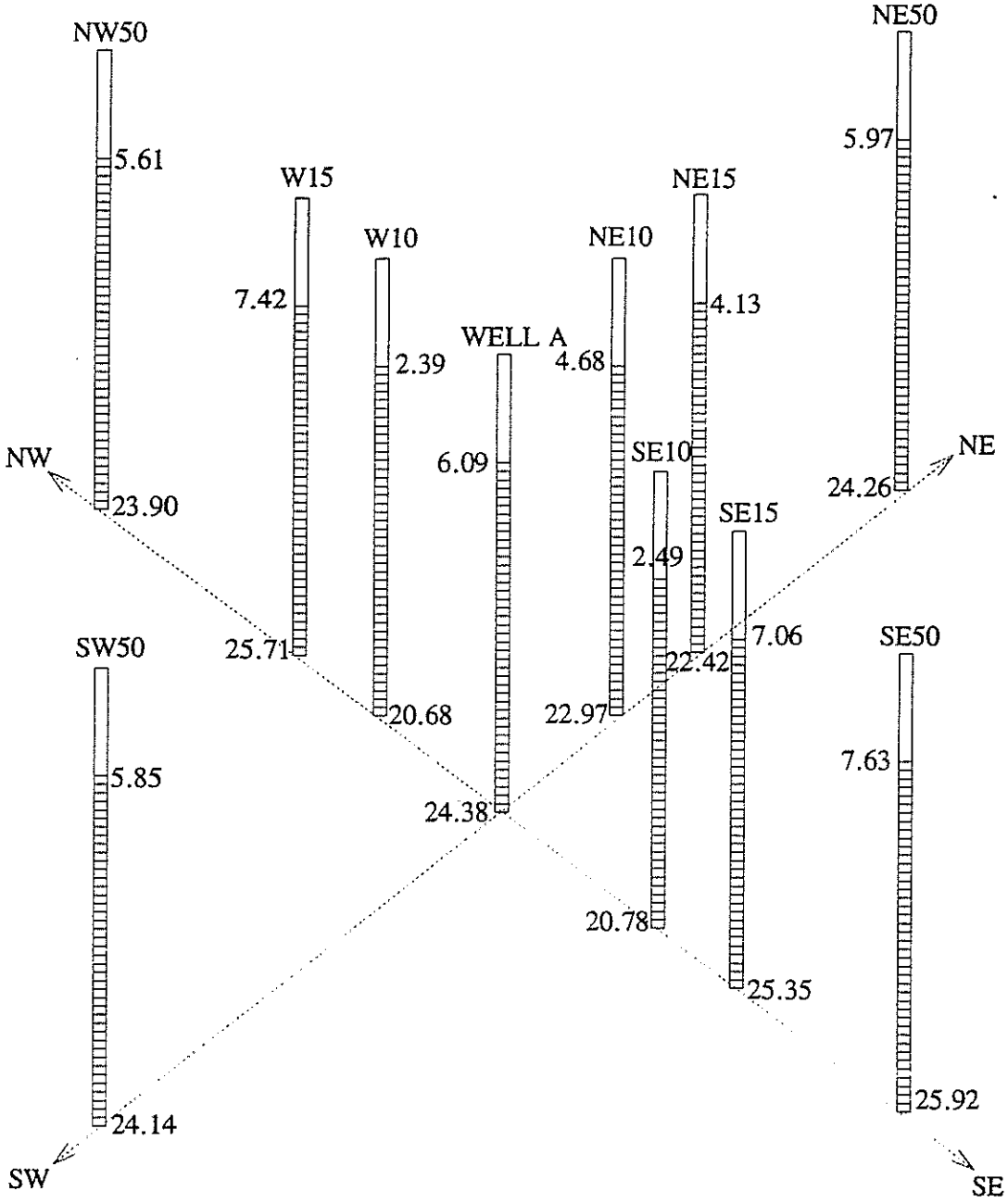

Figure 2-3. Depths of well screens measured with respect to top of Well A.

Drilling, installation and development of the well field were completed in March, 1992. Nevertheless, the observation wells, the pumping well and the MLSP's were water surged before most pumping tests.

2.3 SOIL SAMPLE ANALYSIS

The 44 soil samples collected from NW50, SE15 and SE50 were analyzed for soil classification, porosity determination, and hydraulic conductivity estimation. The soil classification was based on the Udden-Wentworth system as described by Boggs [1987]. This method allows soil samples to be classified according to their mean grain sizes, to sorting and to skewness by the cumulative distribution curves. The hydraulic conductivities of the soil samples were estimated using the empirical equations given by Vukovic and Soro [1992], and the constant-head laboratory method. Information gained from soil sample analysis is useful, as a first approximation, in understanding the hydrogeological conditions of the Sevilleta site.

2.3.1 Soil Classification

Classification of soil types and estimation of hydraulic conductivities by the empirical equations require the grain-size distributions of the soil samples. The grain-size distribution of a soil sample can be determined by using the sieve analysis. The sieve analysis consists of placing a soil sample in the uppermost sieve in a nest of sieves (largest openings are found in the uppermost sieve with progressively smaller openings on lower sieves), and the nest of sieves is vibrated to allow the individual particles to fall through the sieve openings. Then the weight of soil retained on each of the sieves is determined by weighing, and the cumulative percent of the sample retained is plotted against the various grain sizes. From

these cumulative grain-size distribution curves, the mean grain size, effective grain size, and other information, can be determined for use in classifying the soil samples. The standard procedure of ASTM D422-63, given by the American Society of Testing Materials [1963], was used for the sieve analysis. It should be noted that this procedure is for the Type C soil, where clay, cementing agents or soluble salts are absent.

The Udden-Wentworth soil classification is based on the cumulative distribution curve, where the cumulative percent retained by weight is plotted against the "ϕ" size. The ϕ-size is defined as [Boggs, 1987]

$$\phi = -\log_2 d = -3.32\log_{10} d \qquad \textbf{(2-1)}$$

where d is the soil grain size in millimeter (mm). It can be seen that ϕ is zero for the soil grain size equal to 1 mm. For d is less than 1 mm ϕ is positive, and for d is greater than 1 mm ϕ is negative. This indicates that the fine fraction of a soil sample is represented by positive ϕ's and the coarse fraction by negative ϕ's. The cumulative distribution curves for all of the soil samples are presented in Figures 2-4, 2-5 and 2-6.

Any soil samples can be classified by the Udden-Wentworth system in three different ways; namely, classification according to the mean size, M_z, classification according to the standard deviation, σ, and classification according to the skewness, SK. These three quantities are determined from the cumulative distribution curves, or

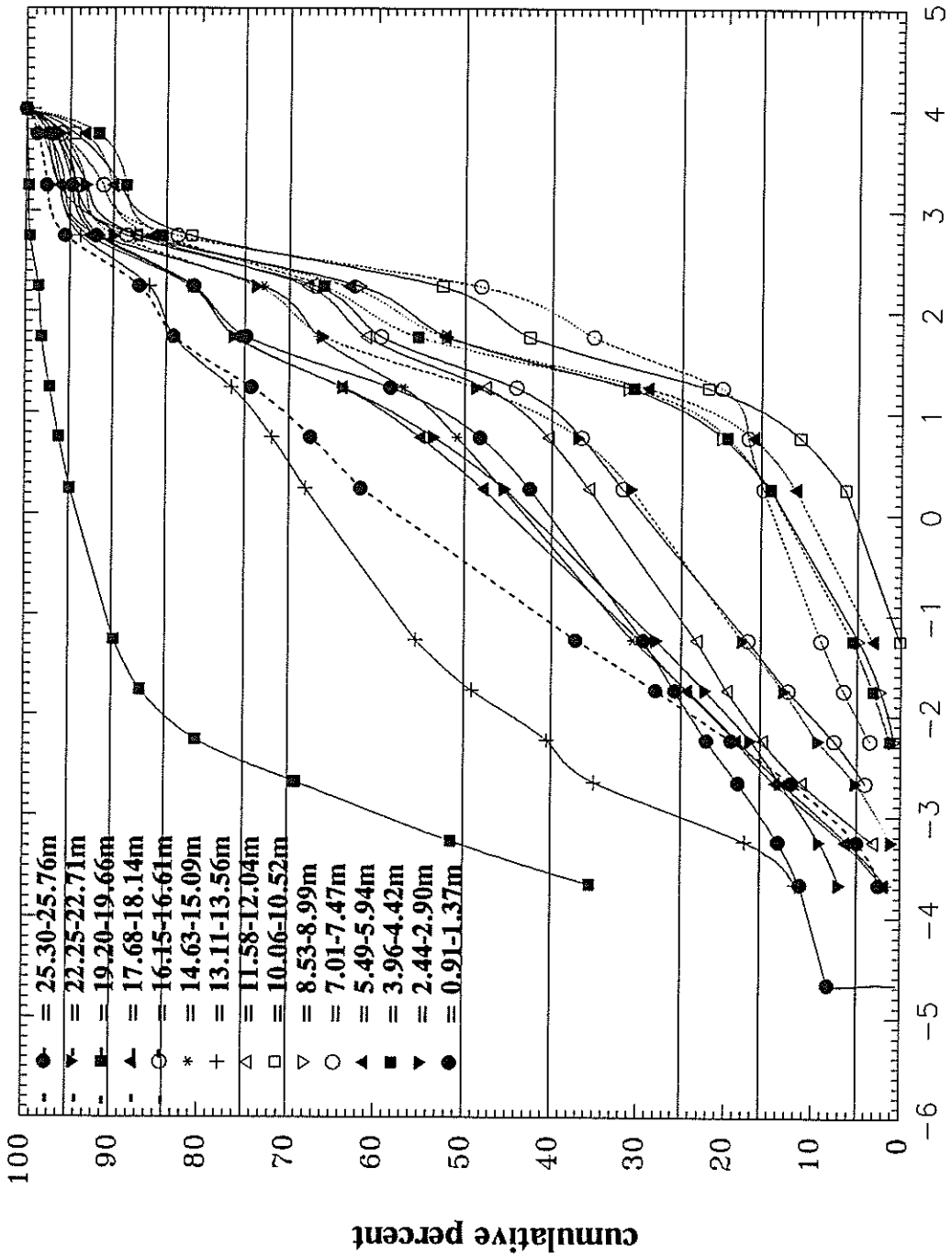

Figure 2-4. Cumulative distribution curves for soil samples from NW50

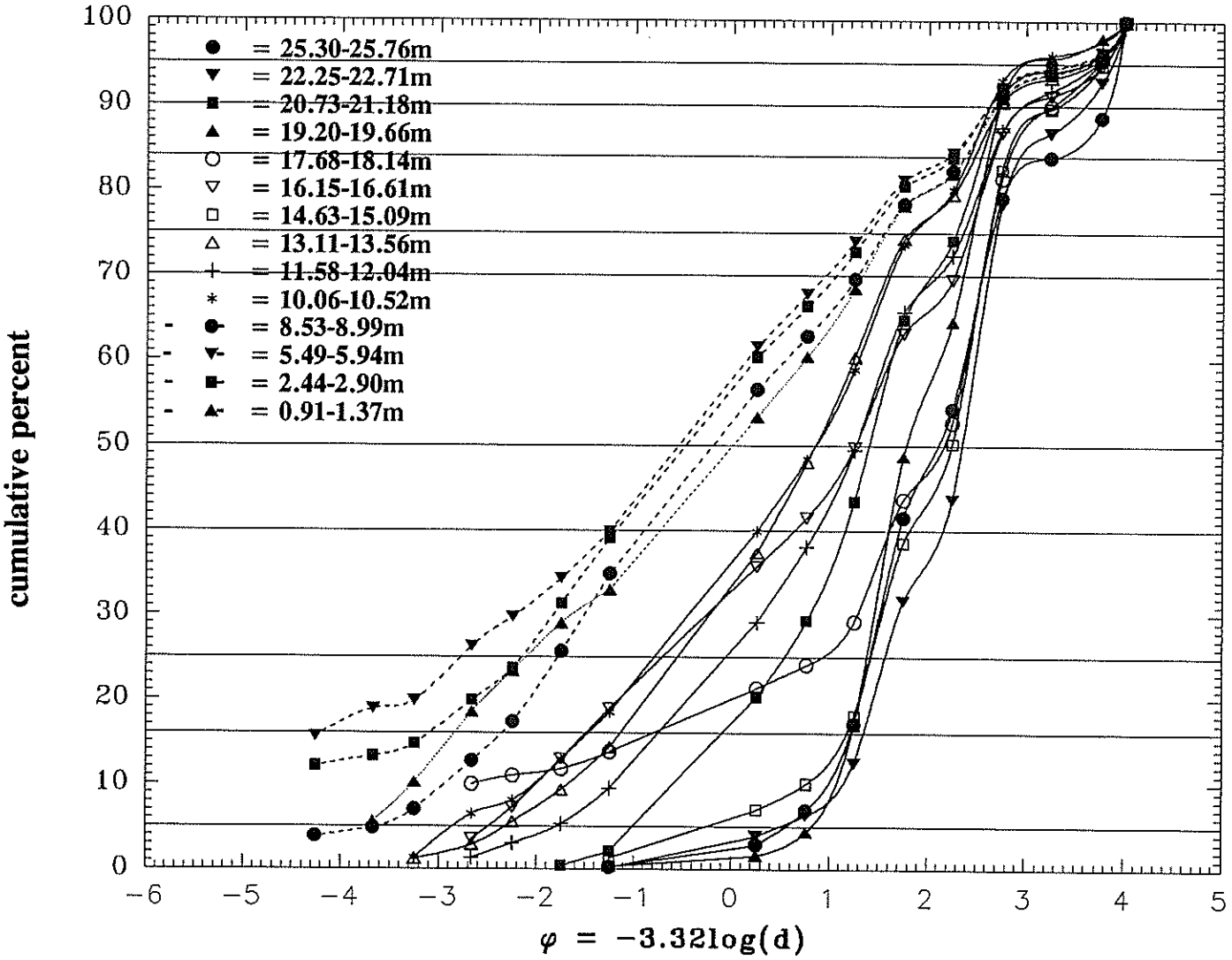

Figure 2-5. Cumulative distribution curves for soil samples from SE15

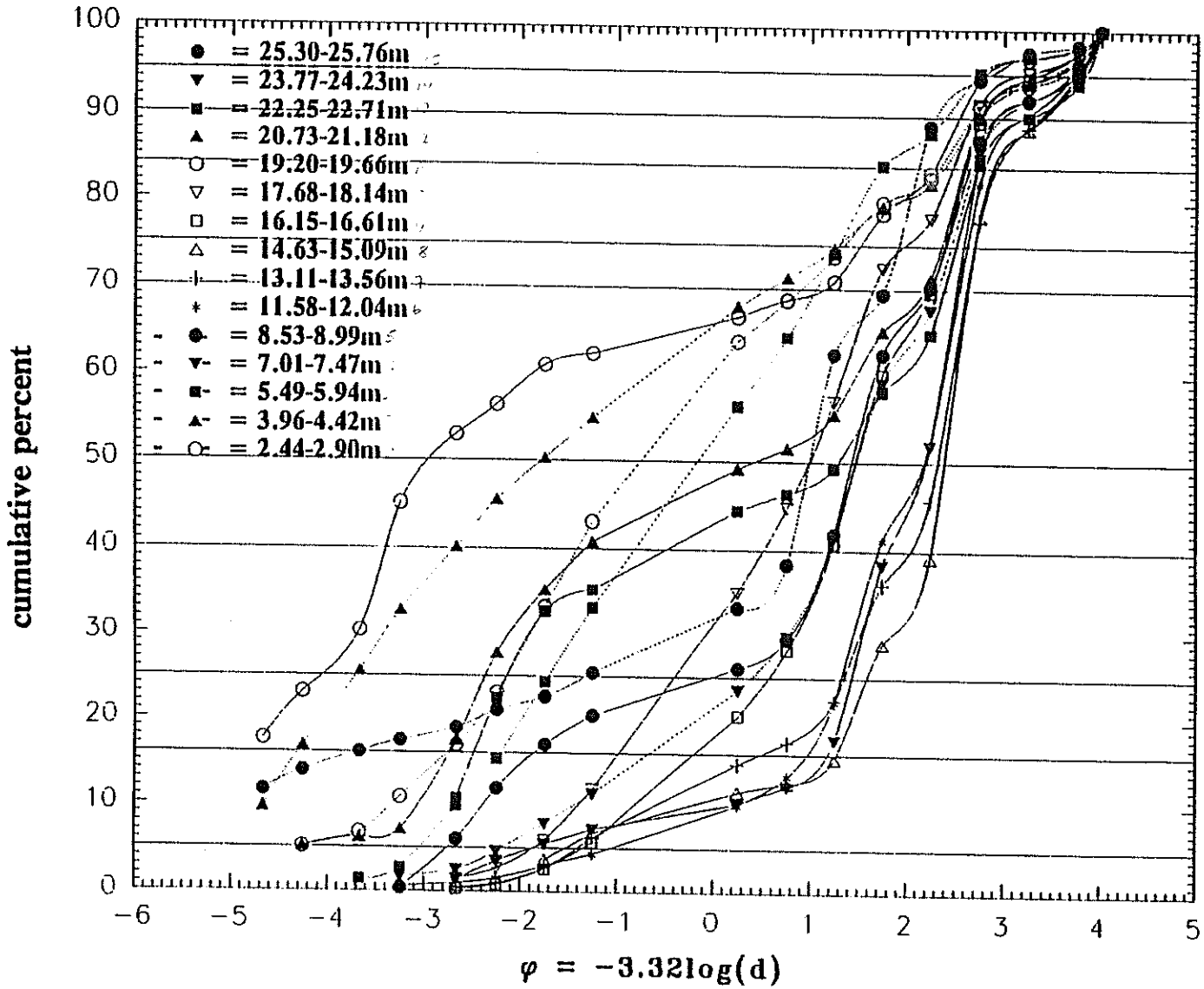

Figure 2-6. Cumulative distribution curves for soil samples from SE50

$$M_z = \frac{\phi_{16} + \phi_{50} + \phi_{84}}{3} \quad \textbf{(2-2)}$$

$$\sigma = \frac{\phi_{84}-\phi_{16}}{4} + \frac{\phi_{95}-\phi_5}{6.6} \quad \textbf{(2-3)}$$

$$SK = \frac{(\phi_{84} + \phi_{16}-2\phi_{50})}{2(\phi_{84}-\phi_{16})} + \frac{(\phi_{95} + \phi_5-2\phi_{50})}{2(\phi_{95}-\phi_5)} \quad \textbf{(2-4)}$$

where ϕ_n corresponds to d_n. The parameter d_n is the grain size of which n percent of the soil is finer. For example, d_{10} refers to the grain size that 10% of soil is finer and 90% is coarser. In other words, d_{10} corresponds to the 90th percentile of the cumulative percent in the cumulative distribution curves. Classification according to M_z gives the soil types based on the average grain size, as shown in Table 2-1a. Classification according to σ gives the sorting conditions as shown in Table 2-1b. Classification according to SK gives the description of skewness of the grain size distribution (see Table 2-1C), that is, the most frequently occurring grain sizes in the soil sample.

Taking the soil sample from 17.68 to 18.14 m of SE15 as an example, ϕ_{16}, ϕ_{50} and ϕ_{84} were determined as -0.84, 2.16 and 2.81, respectively. As a result, M_z was 1.37, which correlates to a medium sand in Table 2-1a. The value for ϕ_{95} is 3.71 and the value for ϕ_5 is -5.23, which yields a value of 2.26 for σ. From Table 2-1b, classification according to σ

Table 2–1. Soil Classification by the Udden–Wentworth System

[from Table 5.1 in Boggs 1987]

a. Soil Classification According to Size

d (millimeters)	M_z	Classification
> 4.0	< –2.0	Pebble
2.0 < d < 4.0	–2.0 < M_z < –1.0	Granule
1.0 < d < 2.0	–1.0 < M_z < 0.0	Very Coarse Sand
0.5 < d < 1.0	0.0 < M_z < 1.0	Coarse Sand
0.25 < d < 0.5	1.0 < M_z < 2.0	Medium Sand
0.125 < d < 0.25	2.0 < M_z < 3.0	Fine Sand

b. Soil Classification According to Sorting

ϕ Standard Deviation	Classification
<0.35	very well sorted
0.35 to 0.50	well sorted
0.50 to 0.71	moderately well sorted
0.71 to 1.00	moderately sorted
1.00 to 2.00	poorly sorted
2.00 to 4.00	very poorly sorted
>4.00	extremely poorly sorted

c. Soil Classification According to Skewness

Skewness	Classification
> +0.30	strongly fine skewed
+0.30 to +0.10	fine skewed
+0.10 to –0.10	near symmetrical
–0.10 to –0.30	coarse skewed
< –0.30	strongly coarse skewed

indicates this soil sample is very poorly sorted. The skewness was determined to be -0.65, which indicates that the soil sample is strongly coarse skewed. Therefore, this particular soil sample can be described as very poorly sorted medium sands where coarse grain sizes dominate the grain-size distribution. Using this method, the soil profiles for NE50, SE10 and SE50 are demonstrated in Figures 2-7, 2-8 and 2-9. These profiles are marked by poorly sorted coarse sand and gravel with fines randomly mixed throughout the sampling sequence. In general, this aquifer is unconfined consisting of nonindurated poorly sorted sand and gravel.

2.3.2 Estimation of Porosity

The porosity of a porous medium is defined as the ratio of the volume of the void space to the total volume of that porous medium. The porosity of each of the 44 soil samples from the Sevilleta research site was determined by a water displacement technique described by Freeze and Cherry (1979). This technique consisted of weighing an empty graduated cylinder, pouring a quantity of the soil sample into the graduated cylinder and reweighing it to obtain the sample's mass. With the mass and volume of the soil sample known, a known volume of water is added to the graduated cylinder. From this, the volume of the void space in the soil sample can be determined. Using this information, the soil sample's porosity can be calculated from the following relationship:

$$n = 1 - \frac{\rho_b}{\rho_s} \qquad \textbf{(2-5)}$$

where ρ_b is the bulk mass density (the mass weight of the soil sample divided by the volume

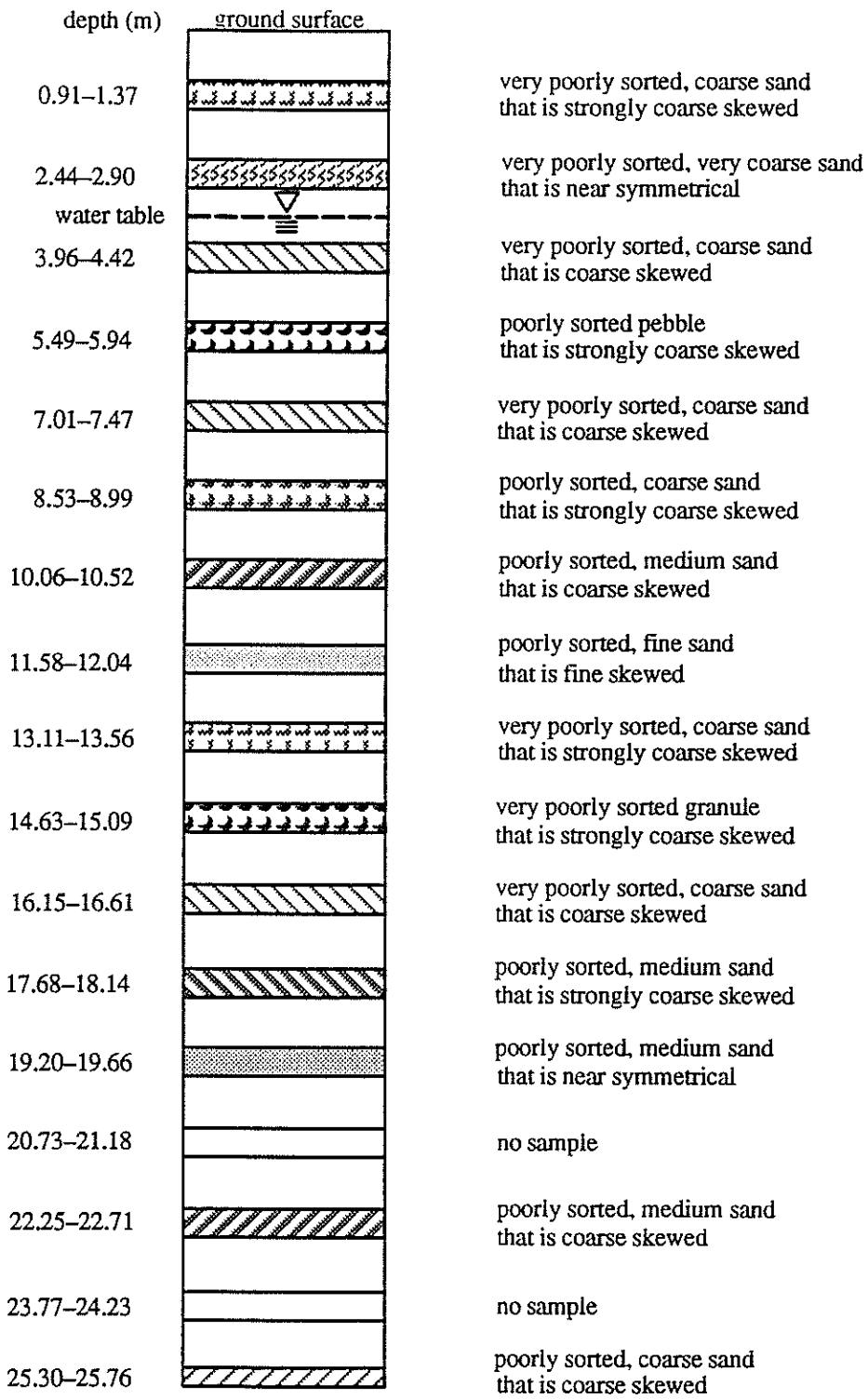

Figure 2–7. Soil classification by the Udden–Wentworth method for soil samples from NW50.

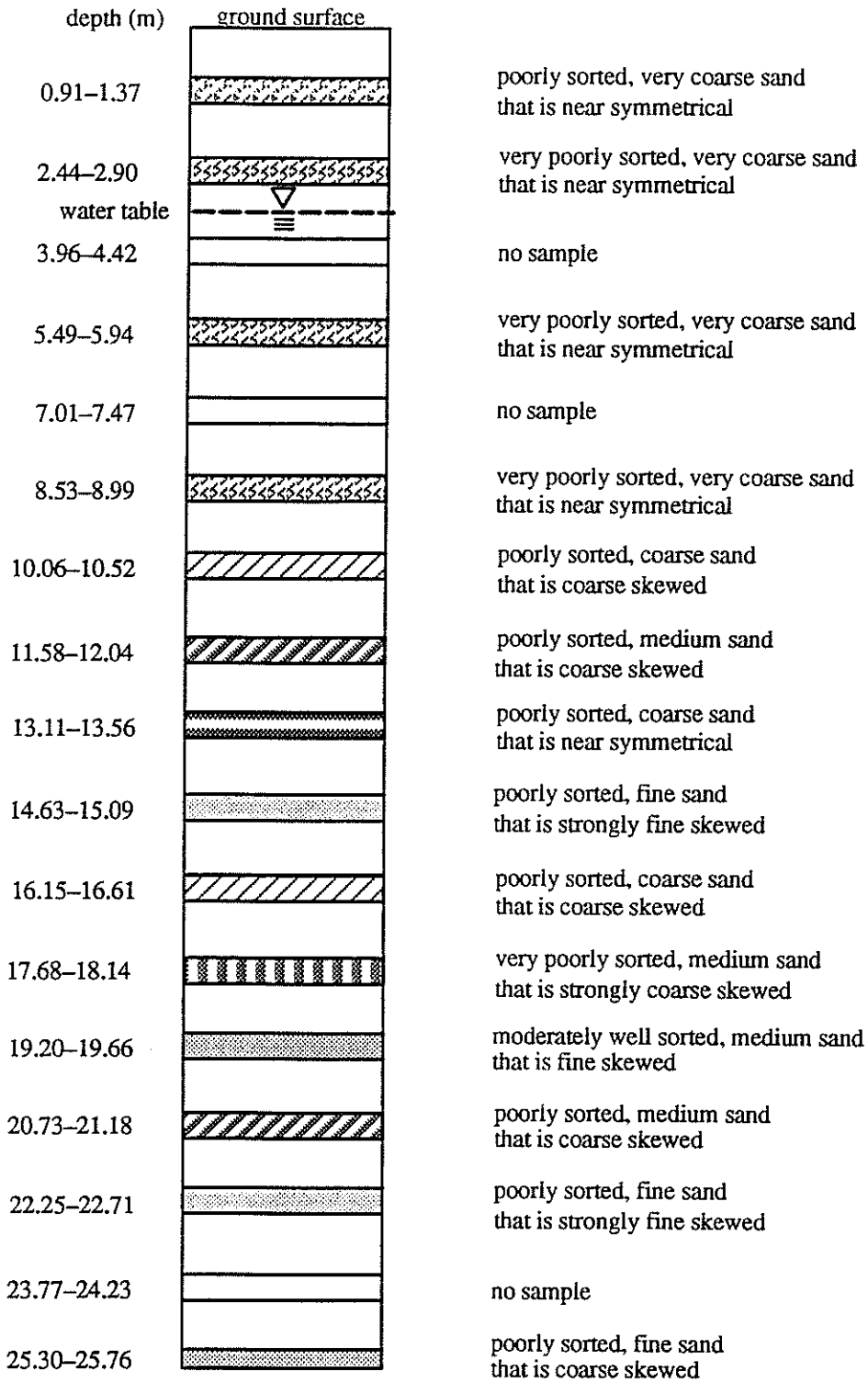

Figure 2–8. Soil classification by the Udden–Wentworth method for soil samples from SE15.

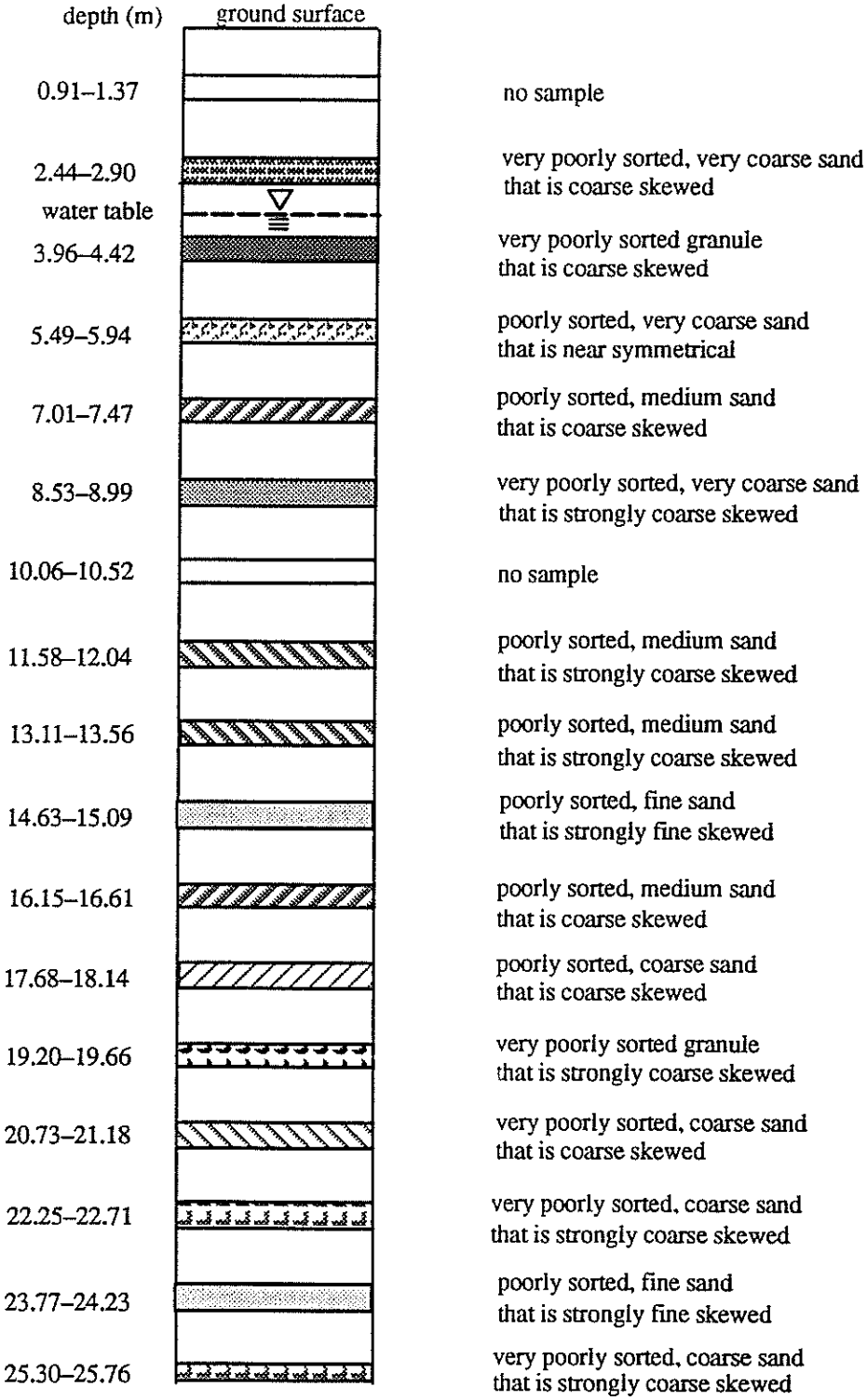

Figure 2–9. Soil classification by the Udden–Wentworth method for soil samples from SE50.

of the soil sample) and ρ_s is the particle grain density (the mass of the soil sample divided by the volume of the solid particles, i.e., the volume calculated from the displacement technique).

The porosities of the 44 soil samples from the Sevilleta research site ranged from 0.2 to 0.35. Since the soil samples were disturbed and subject to no overburden stress, porosities determined in the laboratory are typically higher than actual insitu values. A value of 0.25 is used as the standard porosity for any calculations that require this parameter.

2.3.3 Estimation of Hydraulic Conductivity

The hydraulic conductivities of the 44 soil samples were estimated with the ten empirical equations listed in Table 2-2 and by the constant-head test. As discussed by Vukovic and Soro [1992], these ten empirical equations are of a fundamental form

$$K = \frac{g}{\nu} C\varphi(n) d_e^2 \qquad \textbf{(2-6)}$$

where g is the gravitational acceleration, ν is the kinematic viscosity, C is an empirical coefficient, φ(n) is the empirical function of porosity, and d_e is the effective grain size. The ten empirical equations differ in the definitions of C, φ(n) and d_e. The range of applicability for each of them is also given in Table 2.2. A computer program was written for these equations, and it screens out the inappropriate methods according to the ranges of applicability. It was noted that methods of Slichter, Beyer and Sauerbrei were the most appropriate three for the 44 soil samples. The averaged value from these three methods for each soil sample is given in Figure 2-10, which shows the vertical hydraulic conductivity

Table 2–2. Empirical equations for estimating hydraulic conductivity

(from Table 7 of Vukovic and Soro 1992)

	Author	Value of Coefficient C	Function of Porosity $\phi(n)$	Effective Grain Diameter (d_e)	Domain of Applicability
1	Hazen	6×10^{-4}	$[1+10(n-0.26)]$	$d_e = d10$	$0.1mm < de < 3mm$ $C_u < 5$
2	Slichter	1×10^{-2}	$n^{3.287}$	$d_e = d10$	$0.01mm < de < 5mm$
3	Terzaghi	$10.7 \times 10^{-3} > Ct$ $Ct > 6.1 \times 10^{-3}$	$[(n-0.13)/(1-n)^{1/3}]^2$	$d_e = d10$	large–grain sands
4	Beyer	$6 \times 10^{-4} \log(500/\_)$	1	$d_e = d10$	$0.06mm < de < 0.6mm$ $1 < C_u < 20$
5	Sauerbrei	3.75×10^{-3}	$[n^3/(1-n)^2]$	$d_e = d17$	sand and sandy clay $d < 0.5mm$
6	Kruger	4.35×10^{-5}	$[n/(1-n)^2]$	$1/d_e = \Sigma \Delta g_i (2)/(d_i^g + d_i^d)$	medium–grain sands $C_u > 5$
7	Kozeny	8.3×10^{-3}	$[n^3/(1-n)^2]$	$1/d_e = 3/2 \Delta g_i / d_i + \Sigma \Delta g_i (d_i^g d_i^d)/(2 d_i^g)$	large–grain sands
8	Zunker	$0.7 \times 10^{-4} > Cz$ $Cz > 2.4 \times 10^{-3}$	$[n/(1-n)]$	$1/d_e = 3/2 \Delta g_i / d_i + \Sigma \Delta g_i (d_i^g d_i^d / d_i^g \{\ln d_i^g - \ln d_i^d\})$	fine and medium grain sands
9	Zamarin	8.3x10	$[n^3/(1-n)^2] \cdot (1.275-1.5n)^2$	$1/d_e = 3/2 \Delta g_i + \Sigma \Delta g_i (\ln d_i^g - \ln d_i^d)/(d_i^g - d_i^d)$	large–grain sands
10	USBR	$4.8 \times 10^{-4} d20^{0.3}$	1	$d_e = d20$	medium–grain sands $C_u < 5$

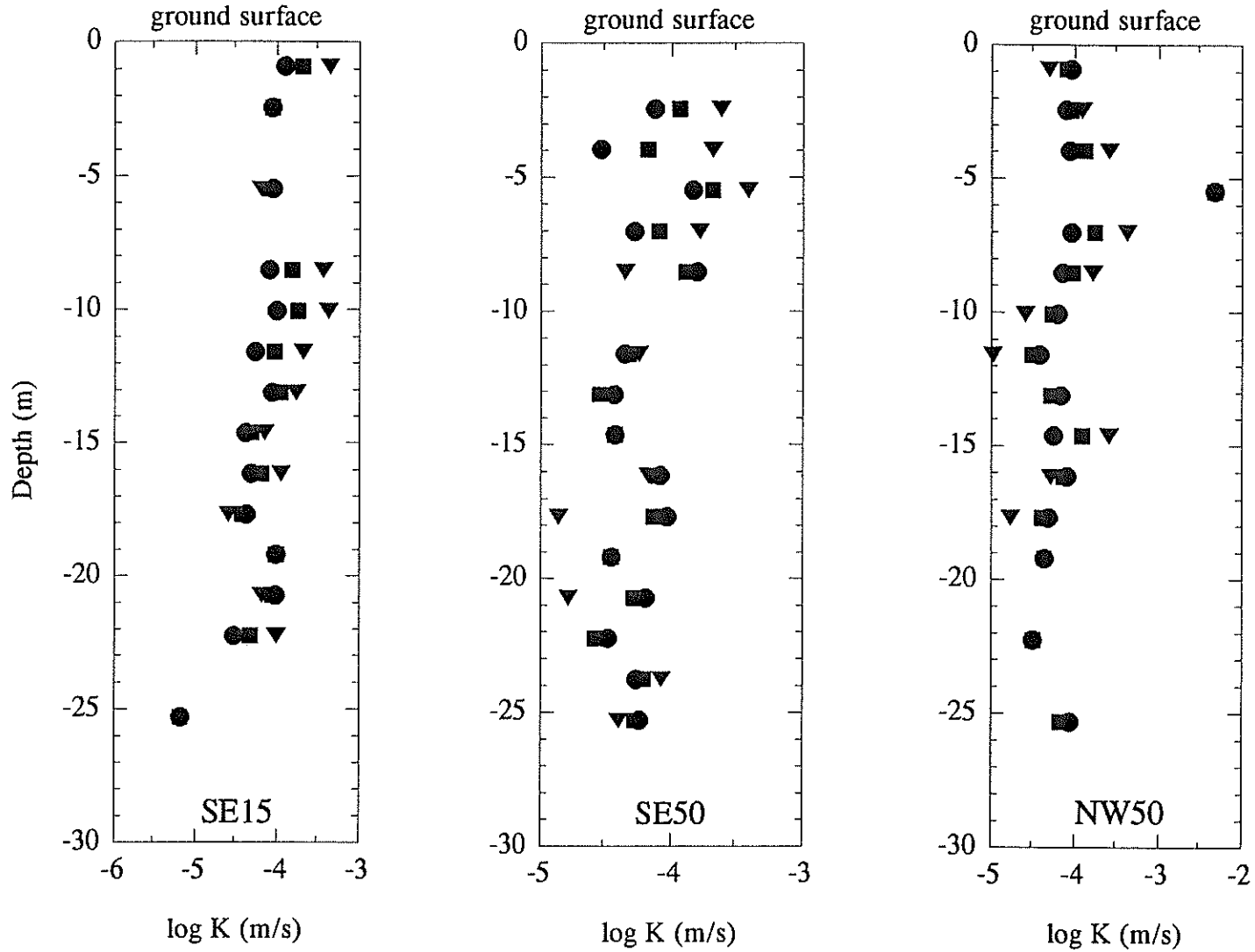

Figure 2-10. Hydraulic conductivity distribution determined by constant-head test and empirical equations for the soil samples (dots for empirical equations, inverse triangles for constant-head test, and squares for the average of the two methods).

distributions at the three locations of NW50, SE15 and SE50. Again, the distributions shown in Figure 2-10 are not representative of insitu conditions, and are used for reference purposes only.

The hydraulic conductivity of the soil samples was also determined in the laboratory by performing a constant-head test. In a constant-head test, a soil sample of length L and cross-sectional area A is enclosed between two porous plates in a cylindrical tube, and a constant-head differential H is set up across the sample. An application of Darcy's law leads to the expression

$$K = \frac{QL}{AH} \tag{2-7}$$

where Q is the steady volumetric discharge through the system. This test was done for all of the soil samples and the values of hydraulic conductivity are shown in Figure 2-10.

3. PUMPING TEST

Numerous pumping tests with durations ranging from a few hours to a few days have been conducted on the Sevilleta site. Most were performed to evaluate the applicability and appropriateness of the MLSPs, the observation wells, the automated datalogger, the groundwater sampling manifold, the operational procedure and field setup of the pumping/tracer tests, and to understand the local hydrogeology. A large amount of drawdown and tracer concentration data was collected and the most pertinent data are shown below.

3.1 GENERAL INFORMATION

Many short-term (less than two hours in duration) pumping tests were conducted prior to April, 1991, to evaluate the applicability of the MLSPs and other measuring devices. They showed that the MLSPs were able to yield distinctive drawdown data for different depths at specific radial distances. A pair of straddle packers (YEP-4.75/6.00 by ROCTEST) was used in some of these pumping tests. The deflated outside diameter of the packer is 12 cm, and the length of the inflatable gland is 1 m. This pair of straddle packers can be used to separate a well in three sections, one above the top packer, one below the bottom packer, and one in between. For this project, however, the packers were used as a single packer by separating them by only 0.44 m, resulting in a total length of 2.44 m for this pair of straddle packers. When it was used, the pair was placed at different depths inside Well A to generate different partially penetrating effects on the MLSPs. It was found that the MLSPs properly responded to various partially penetrating conditions.

Drawdown data collected from these tests showed two interesting conditions:

(1) Without the packers set in Well A, drawdowns measured at depths above 14 m were noticeably smaller than those taken below 14 m. This indicates that the hydraulic conductivities of the saturated thickness above 14m are larger than those below 14 m. This fact is generally in agreement with the vertical hydraulic conductivity distributions shown in Figure 2-10. When the packers were placed inside Well A at about 13 m to 14 m, drawdowns measured at depths below 14 m were negligibly small relative to those taken above 14 m, provided pumping took place above the packers. If pumping took place below the packers set at 13 m to 14 m inside Well A, however, drawdowns measured at depths above 14 m became negligibly small relative to those taken below 14 m. This observation indicates that a low-permeability layer possibly exists at about 13 m to 14 m in the neighborhood of Well A. Existence and thickness of this low-permeability layer was not discernable from the soil samples possibly due to the fact that soil sampling missed this layer.

(2) An anomalous drawdown pattern was noted in the vertically-averaged drawdown data taken from these 5.08 cm observation wells. When water was pumped from below the packers set any depths inside Well A, drawdowns at farther Wells W15 and SE15 were greater than drawdowns at nearer wells W10 and SE10, respectively. This anomaly still existed for pumping tests where no packers were used in Well A. The anomaly disappeared only when water was pumped above the packers wherever they were placed inside Well A. As shown in Figure 2-3, W15, NE15, and Well A are deeper than 24 m and W10, SE10, NE10, and N15 are shallower than 24 m. Therefore, a possible explanation for the anomalous drawdown is that a high-permeability zone exists below 24 m in the neighborhood

of Well A. When water was pumped from Well A below or without the packers, this high-permeability zone transmitted most water to Well A and hence more drawdown appeared in W15 and SE15 which cut into this zone. When water was pumped above the packers inside Well A, yield of Well A was primarily contributed from the flow regime above this possible high-permeability zone, and thereby it has little impact on drawdown in W15 and SE15.

The hydrogeological conditions surrounding Well A is rather complicated. To simplify the groundwater flow field in the neighborhood of Well A, it was decided that the straddle packers be placed between 12.19 m to 14.63 m inside Well A for long-term pumping and tracer tests conducted later, considering the Sevilleta aquifer is separated into a lower and upper stratum by a low-permeability layer approximately located in between 12 to 14 m. In so doing, pumping from above the packers has little influence on the lower stratum and investigation can be focused on the upper one only. It should be noted also that Well A is a partially penetrating well because the top of the well screen is always below the groundwater table before and during any pumping tests.

3.2 DEPTH-SPECIFIC PUMPING TEST DATA

Twelve pumping/tracer tests of longer durations were performed from April 1992 to March 1993. Pertinent test conditions of them are listed in Table 3-1. A converging test means groundwater is withdrawn from the aquifer through Well A such that groundwater movement is converging toward Well A during the test. A diverging test means groundwater is injected into the aquifer through Well A such that groundwater movement is diverging from Well A during the test. In a diverging test, Well B was used as a water supply well for the injection at Well A. Groundwater pumped from Well B was delivered through the

Table 3–1. Test Conditions of Pumping/Tracer Tests

Test No. date; time	Pumping Conditions				Notes
	type of test	flow rate (m^3/s)	packer location (BGS)	pumping duration (hours)	
1 5/9/92; 10:00–18:01	converging	3.785×10^{-3}	none	8.02	Both vertically averaged and depth specific drawdown was measured.
2 5/15/92; 10:30–18:00	converging	3.343×10^{-3}	none	7.50	Both vertically averaged and depth specific drawdown was measured.
3 5/21/92; 08:22–17:18	converging	3.974×10^{-3}	12.19 to 14.63 m	8.93	Both vertically averaged and depth specific drawdown was measured.
4 6/12/92; 09:52–16:40	diverging	4.731×10^{-3}	none	6.80	Bromide with a concentration of 25000 mg/l was injected at well A for 10 minutes, from 10:00 to 10:10.
5 6/18/92; 11:27 to 6/21/92; 11:30	diverging	5.047×10^{-3}	none	72.15	Both vertically averaged and depth specific drawdown was measured.
6 6/29/92; 08:40–22:42	diverging	4.668×10^{-3}	12.19 to 14.63 m	14.03	Both vertically averaged and depth specific drawdown was measured.
7 6/30/92; 13:08 to 7/3/92; 01:16	diverging	4.246×10^{-3}	12.19 to 14.63 m	60.13	Bromide with a concentration of 268000 mg/l was injected at well A for 10 minutes, from 07:40 to 07:50 on 7/1/92.
8 8/6/92; 19:20 to 8/10/92; 18:00	diverging	3.722×10^{-3}	12.19 to 14.63 m	95.33	Bromide with a concentration of 268000 mg/l was injected at well A for 83 minutes, from 08:41 to 10:04 on 8/7/92.
9 9/17/92; 17:34 to 9/20/92; 17:30	converging	3.949×10^{-3}	12.19 to 14.63 m	71.90	Only vertically averaged drawdown was measured.
10 10/15/92; 17:42 to 10/17/92; 03:07	converging	3.432×10^{-3}	12.19 to 14.63 m	32.42	Only depth specific drawdown was measured.
11 2/27/93; 09:50 to 2/28/93; 16:35	converging	6.310×10^{-3}	12.19 to 14.63 m	31.75	Only vertically averaged drawdown was measured.
12 3/26/93; 10:21 to 3/27/93; 16:00	converging	6.120×10^{-3}	12.19 to 14.63 m	29.66	Only vertically averaged drawdown was measured.

water conveyance pipe and reinjected into the aquifer through Well A. The first four pumping tests only lasted several hours. They were performed as preliminary tests to further evaluate the efficiency of every piece of equipment and the appropriateness of the procedure for long-term pumping/tracer tests.

The first long-term test, Test No. 5, was conducted for 72.15 hours without packers set in Well A. This was a diverging test, and pressure buildup at different depths of MLSP SE3, W3, and NE6 are presented in Figures 3-1, 3-2 and 3-3; respectively. Noticeable buildups began to show in these three MLSPs from about 100 seconds after injection started. Distinctive buildups are demonstrated at different depths, indicating that the MLSPs give depth-specific measurement. From Figure 3-1, it is seen that the vertical flow at SE3 is consistently upward from 20.75 m to 5.55 m below the ground surface. The vertical flow in W3 and NE6, however, is not consistently upward (see Figures 3-2 and 3-3). For W3, buildups at 17.72 m are the largest among the seven depths where data were collected. Downward vertical flow existed from 17.72 m through 23.82 m, and upward vertical flow existed from 17.72 m through 11.60 m. In the shallower depths above 11.60 m, downward vertical flow took place from 5.51 m to 8.56 m, and upward vertical flow was from 11.60 m to 8.56 m. For NE6, flow is almost horizontal at 20.53 m and 23.57 m as evidenced by the almost equal buildups measured at these two depths. There is a downward hydraulic gradient from 17.76 m to 20.53 m, and an upward one from 17.76 m to 14.7 m. These inconsistent vertical flow patterns indicate that significant layering effects exist and influence groundwater movement at depths approximately below 14 m. Above 14 m, small vertical flow exists at depths between 5.28 m to 11.38 m. At the three locations, it is interesting to

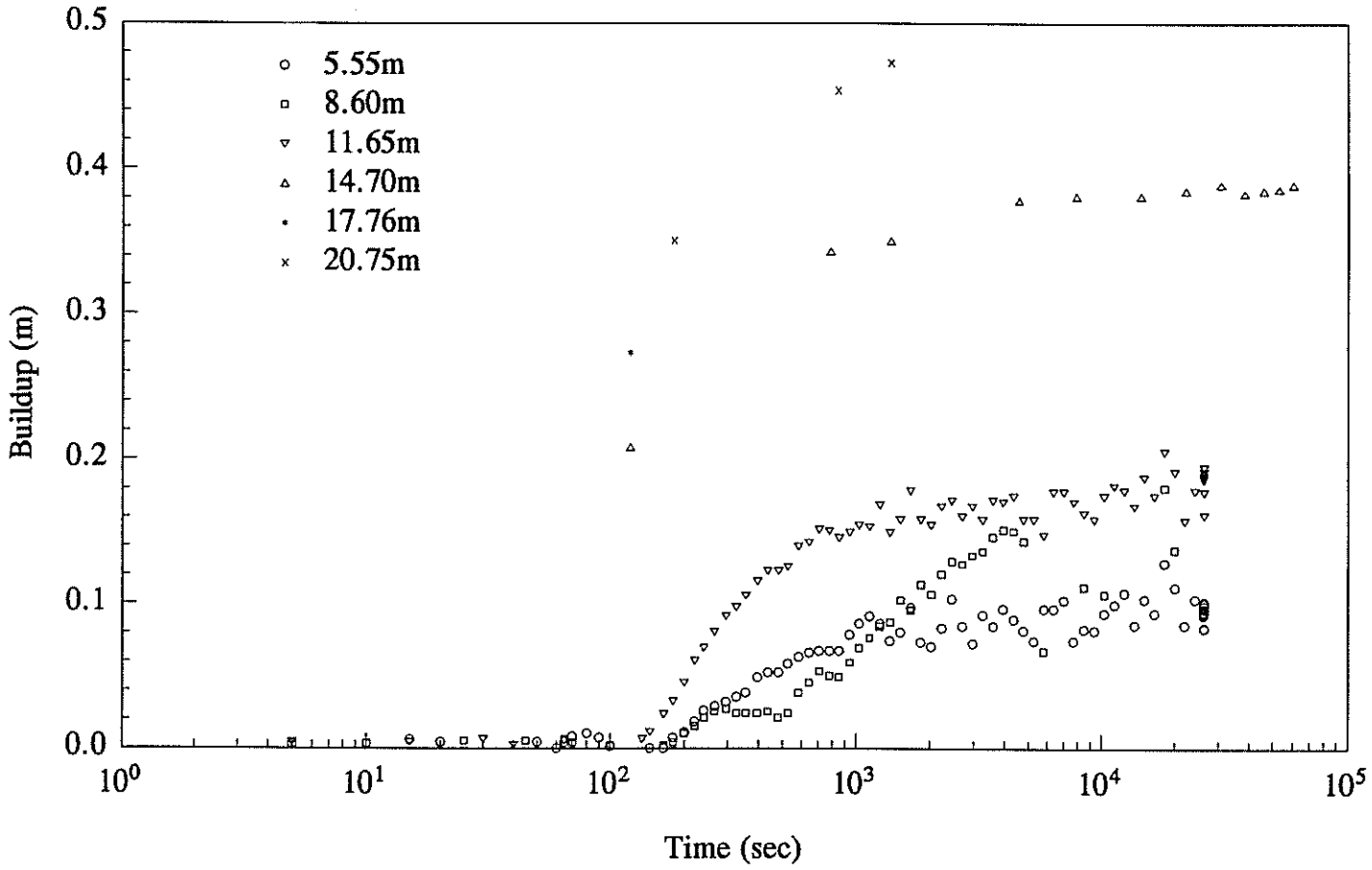

Figure 3-1. Depth-specific buildup measured at different depths of SE3 during Test No. 5.

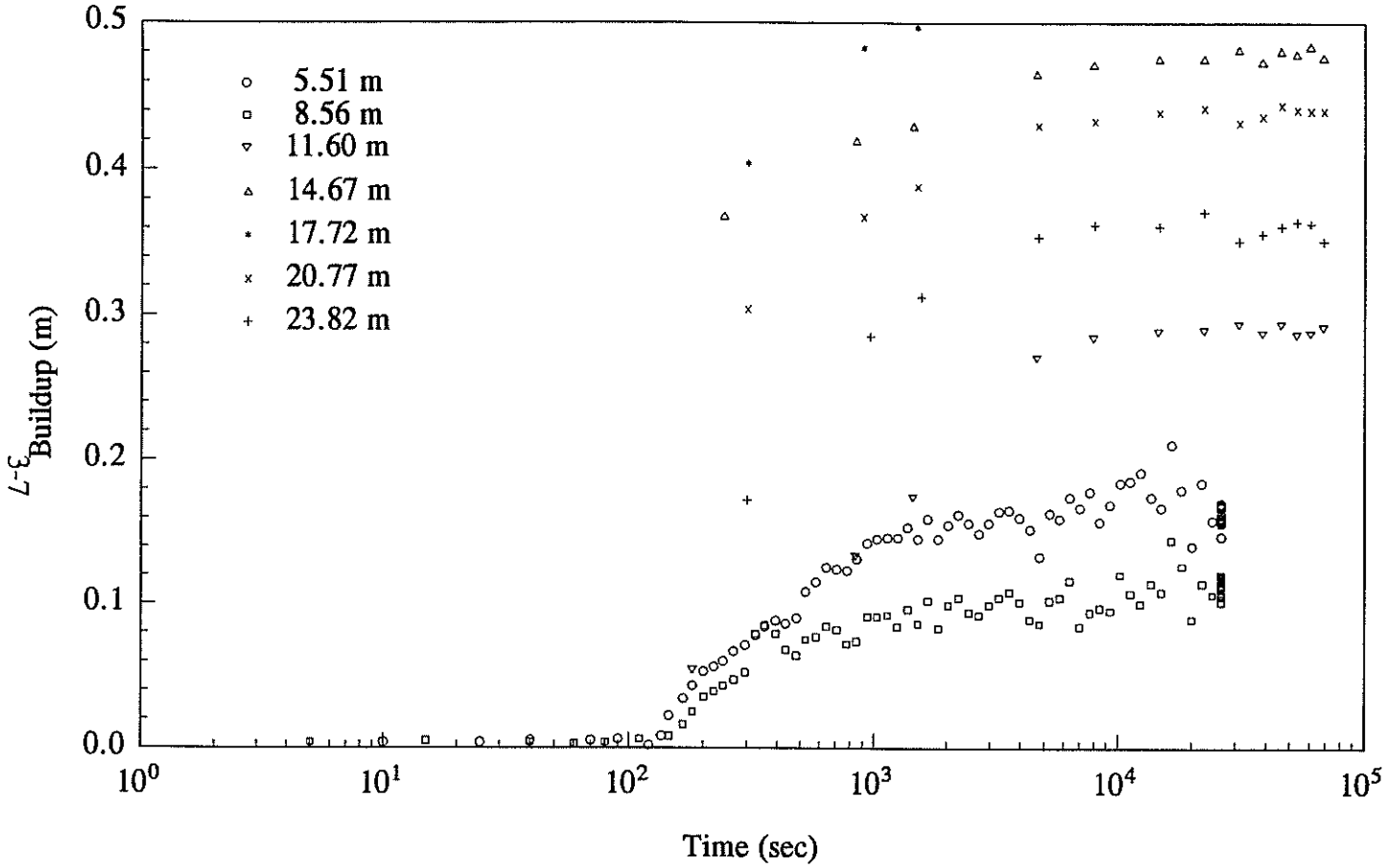

Figure 3-2. Depth-specific buildup measured at different depths of W3 during Test No. 5.

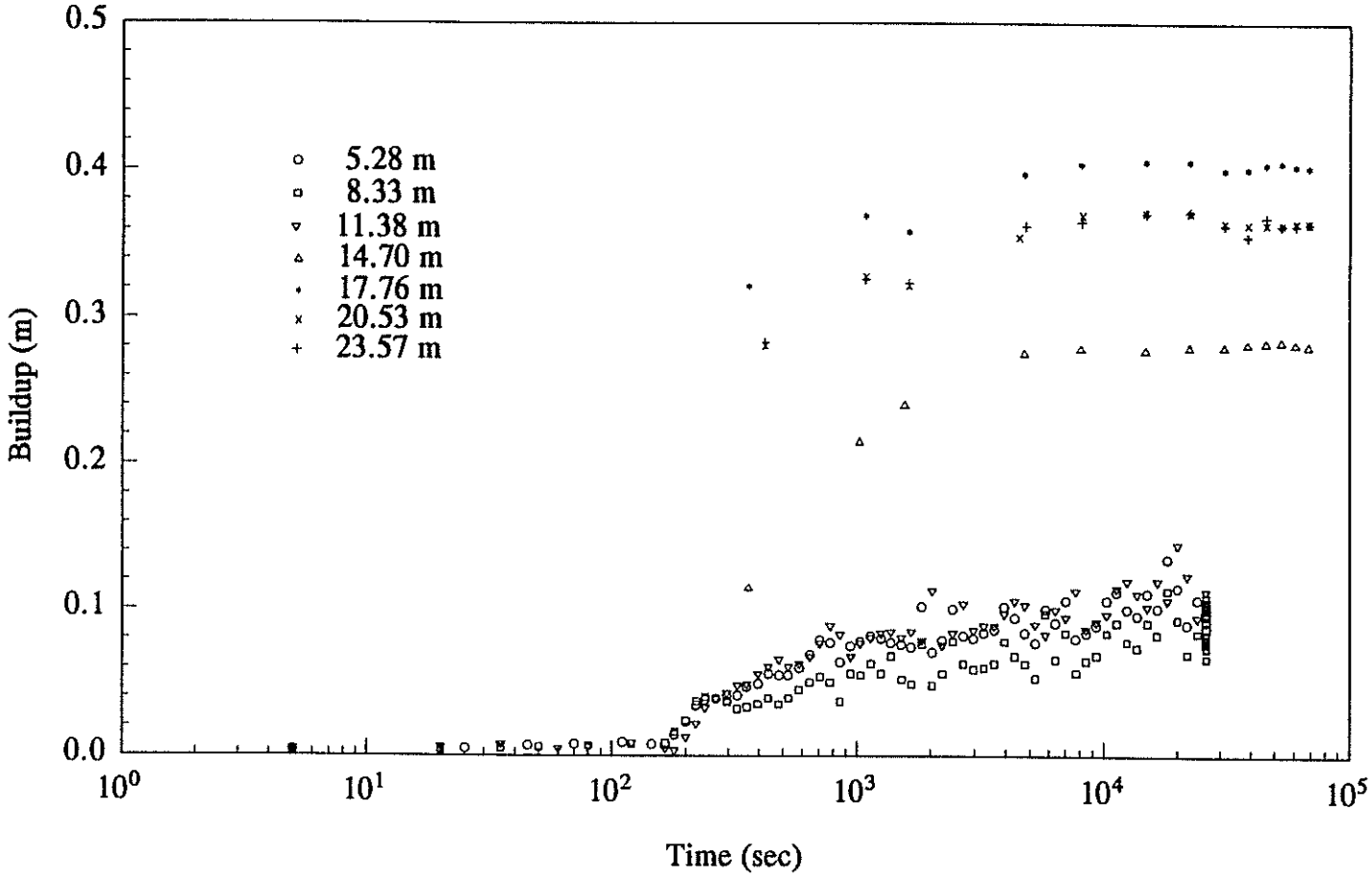

Figure 3-3. Depth-specific buildup measured at different depths of NE6 during Test No. 5.

note that buildups at depths below 14 m are generally greater than those at depths above 14 m, confirming that the hydraulic conductivities of the geological materials above 14 m are lower than those below 14 m.

It was observed from Figures 3-1 through 3-3 that at large times (approximately greater than $2x10^4$ seconds) the buildup measured at different depths became almost parallel straight lines on the semilog plot. Since the Theis solution can be well approximated by a logarithm function, this trend implies that the large-time buildup/drawdown data at specific depths can be accounted for using the Theis solution. This field observation was further confirmed in other pumping tests conducted later; drawdown data from Test No. 10 as discussed below give the most unambiguous proof. It is also known that the "pseudo-steady-state" condition is reached when the Theis solution can be approximated by its logarithm function substitute. The pseudo-steady-state condition means that the drawdown/buildup is transient while its gradients are under steady-state conditions. Information gathered from Test No. 6 and 7, in which the packers were placed inside Well A from 12.19 m to 14.63 m, showed that the pseudo-steady-state for the diverging tests with packers took place about 12 hours after pumping and injection started. Thus, it was decided that the tracer injection start at least 12 hours after the commencement of water injection.

Test No. 8 was run for about 96 hours with the packers placed between 12.19 m to 14.63 m inside Well A. Groundwater was injected into the aquifer through the upper section above the packers. Depth-specific buildup data at SE3, W3 and NE6 are demonstrated in Figures 3-4, 3-5 and 3-6, respectively. Clearly, buildups at depths below 14 m are indeed much smaller than those at depths above 14 m, giving evidence to the existence of

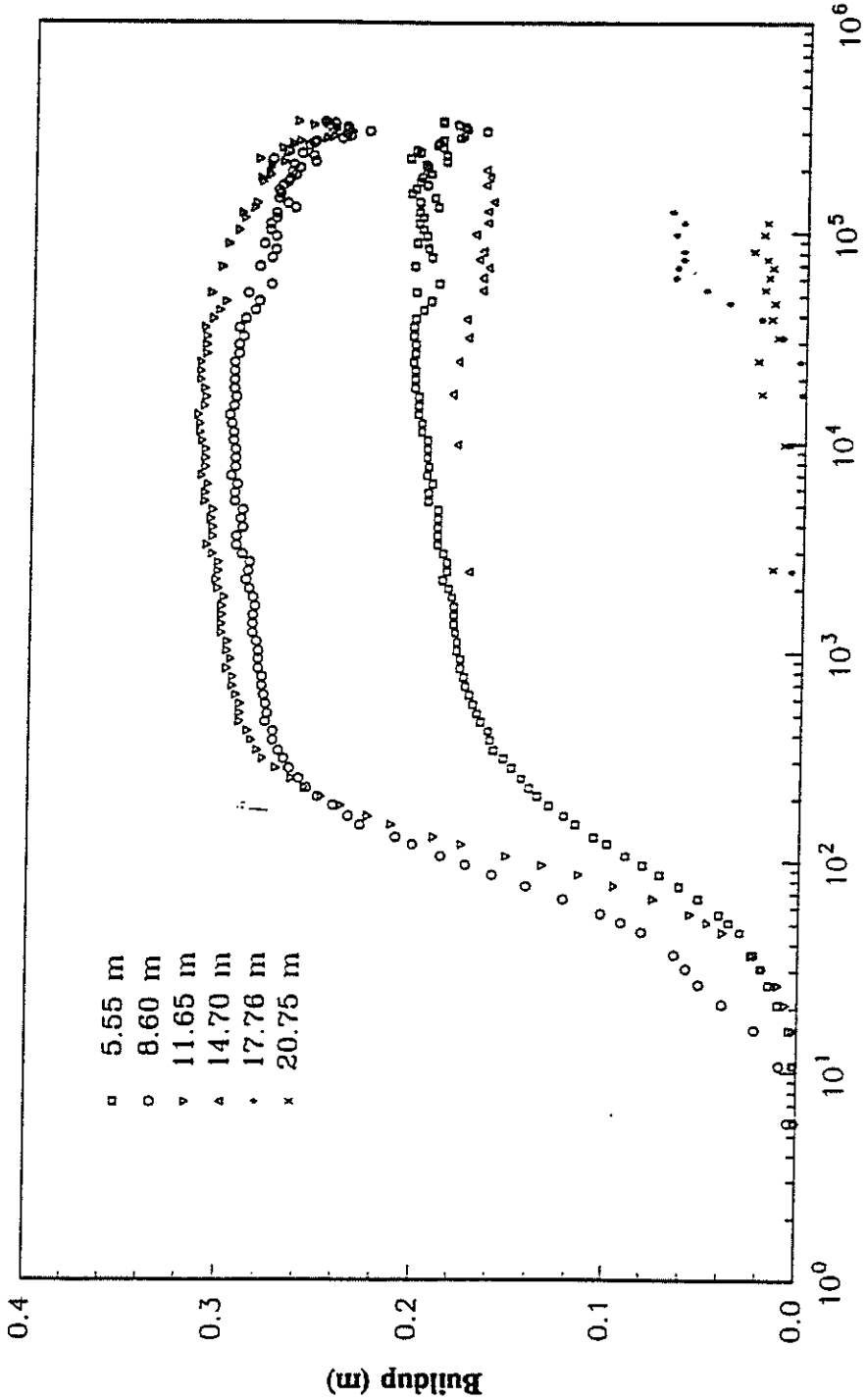

Figure 3-4. Depth-specific buildup measured at different depths of SE3 during Test No. 8.

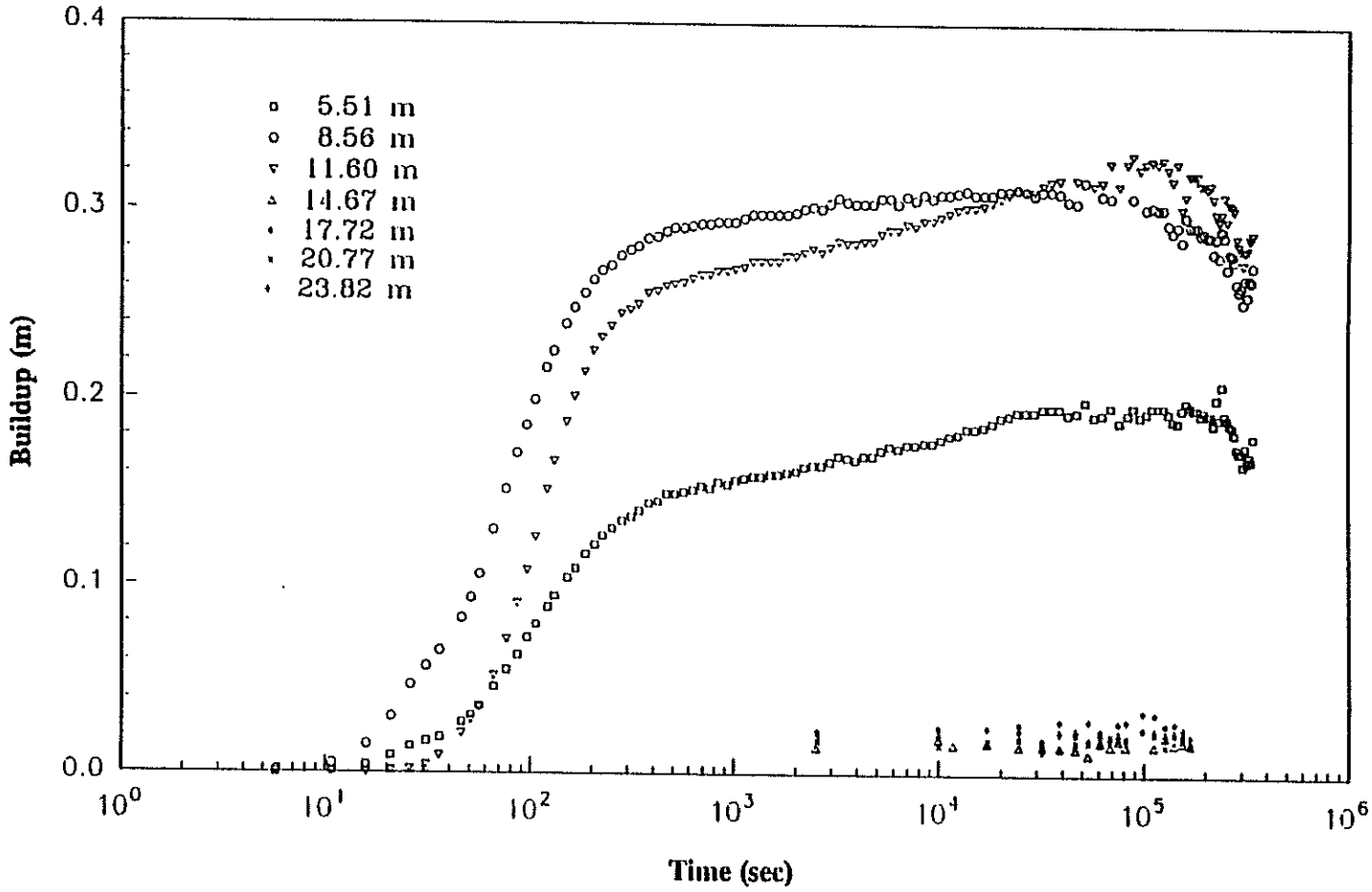

Figure 3-5. Depth-specific buildup measured at different depths of W3 during Test No. 8.

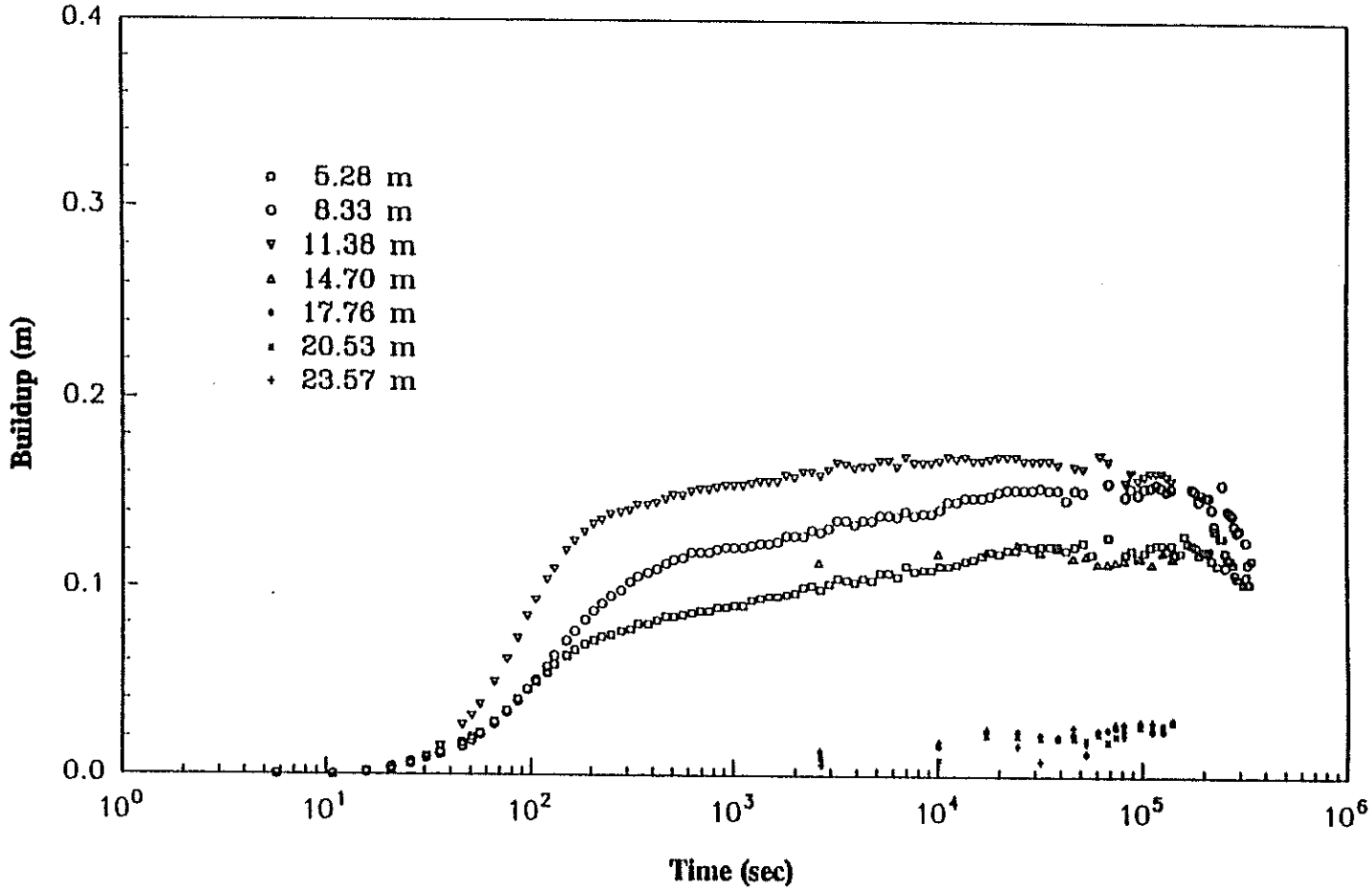

Figure 3-6. Depth-specific buildip measured at different depths of NE6 during Test No. 8.

a low-permeability layer approximately located between 12.19 m and 14.63 m. Tails of these depth-specific buildup curves dropped at large times after about 14 hours to 24 hours of injection. This phenomenon had not appeared in the earlier diverging tests. It could have been caused by (1) the buildup surrounding Well A was interfered with by the cone of drawdown created by pumping at Well B, or (2) the pump failed to maintain a constant pumping rate at large times. Considering that only a few tens of centimeters of buildup/drawdown were noted at distances up to 15m from Well A pumping tests, it is doubtful that the drop of buildup was caused by the interference of cone of drawdown. On the other hand, this problem existed in converging Test No. 10, where no pumping or injection took place at Well B. Therefore, it is more reasonable to attribute this undesired phenomenon to the fact that the pumping rate actually decreased at large times.

At NE6, vertical flow is consistently upward from 11.38 m through 5.28 m. At SE3, downward vertical flow from 8.16 m to 11.65 m prevailed for about 200 seconds. After this, vertical flow became consistently upward from 11.65 m through 5.5 m. However, the vertical hydraulic gradient between 11.65 m and 8.60 m was very small; the head difference between the two depths was less than about 2 cm. This implies the flow was primarily horizontal in between these two depths. At W3, the vertical flow was downward from 8.56 m to 11.60 m and upward from 8.56 m to 5.51 m, before the interference of the cone of drawdown took place. The upward and downward vertical flow conditions at the three MLSP's were due to the partially penetrating effects and the possible layering influence. At large times before the buildups drop, the buildup data at different depths indeed exhibit parallel straight lines at the three MLSP's. Tests No. 9 through 12 were conducted under

the converging condition, where pumping took place only at Well A and the groundwater from pumping was discharged to a ditch about 80 m east of Well A. In Test No. 9, 11, and 12, only vertically-averaged drawdown was taken and their data are shown in 3.3. In Test No. 10, however, only depth-specific drawdown data were taken from different depths of SE3, W3 and NE6. This test had run for about 32.5 hours. Groundwater was withdrawn from above the packers, which were placed between 12.19 m and 14.63 m inside Well A.

Depth-specific drawdown data taken at SE3, W3, and NE6 are shown in Figures 3-7, 3-8, and 3-9, respectively. The drawdowns started to drop at around $7x10^4$ seconds. Since the possibility of interference by buildup did not exist, this drop was more likely caused by pumping rate change. Again, the drawdown data at NE6 shows a consistently downward vertical flow, which is the reversed trend shown in the diverging Test No. 8. The vertical flow conditions at SE3 and W3 are the reversed conditions noted in Test No. 8. This further demonstrates that the MLSP's did correctly respond to pumping and injection occurring in Well A. Also, it can be seen very clearly in Figures 3-7 through 3-9 that the large-time drawdown data at different depths for a fixed MLSP indeed become parallel straight lines on the semilog plots. This feature formed the backbone of the method developed to estimate the planar anisotropy for the saturated thickness above 14 m in the Sevilleta Site. Hereafter, the term "aquifer" is referring to the saturated thickness above 14 m of the Sevilleta Site since most important pumping and tracer tests had been performed with the packers placed in between 12.19 m and 14.63 m and data had been collected for depths above 14 m.

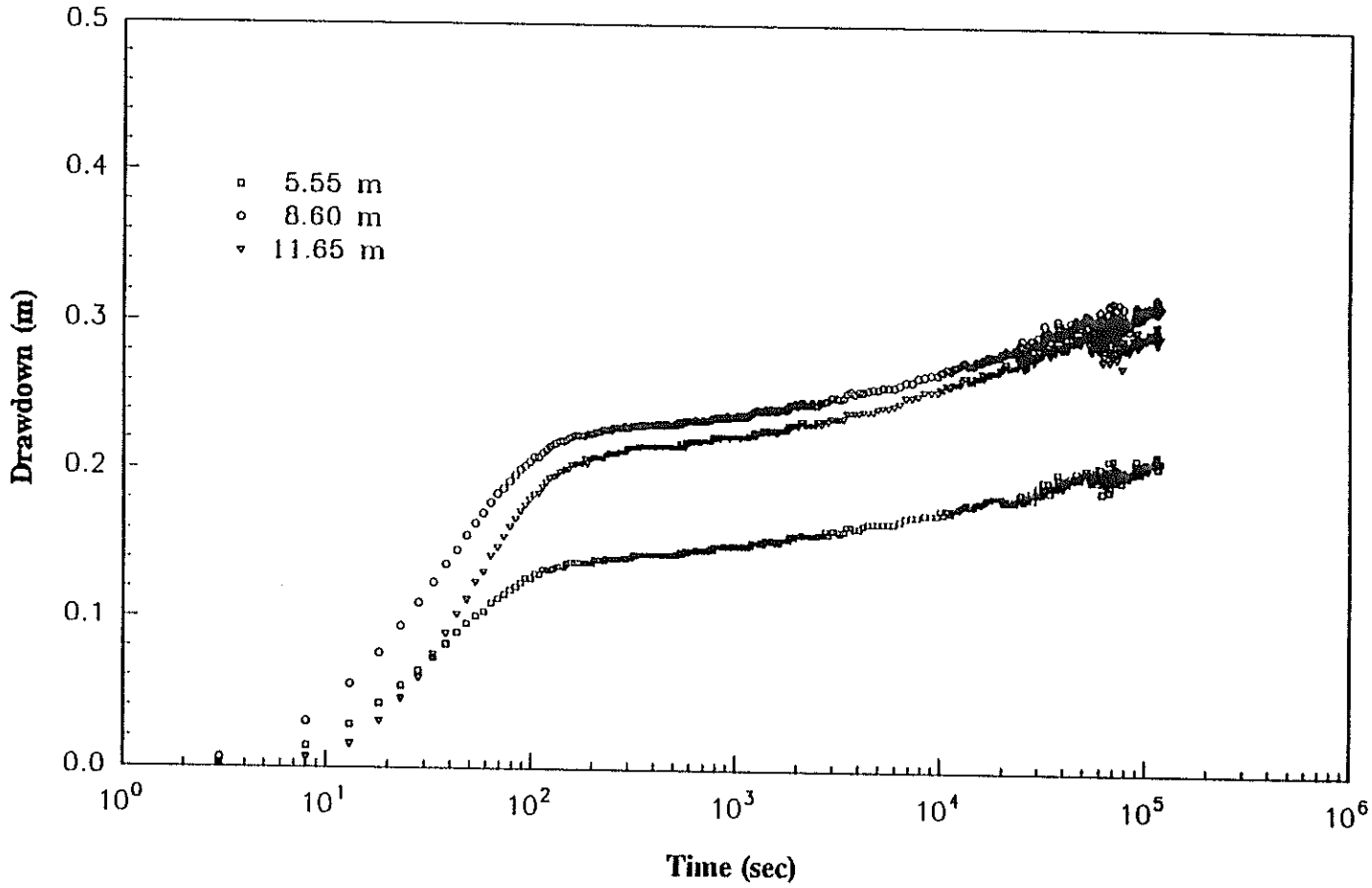

Figure 3-7. Depth-specific drawdown measured at different depths of SE3 during Test No. 10.

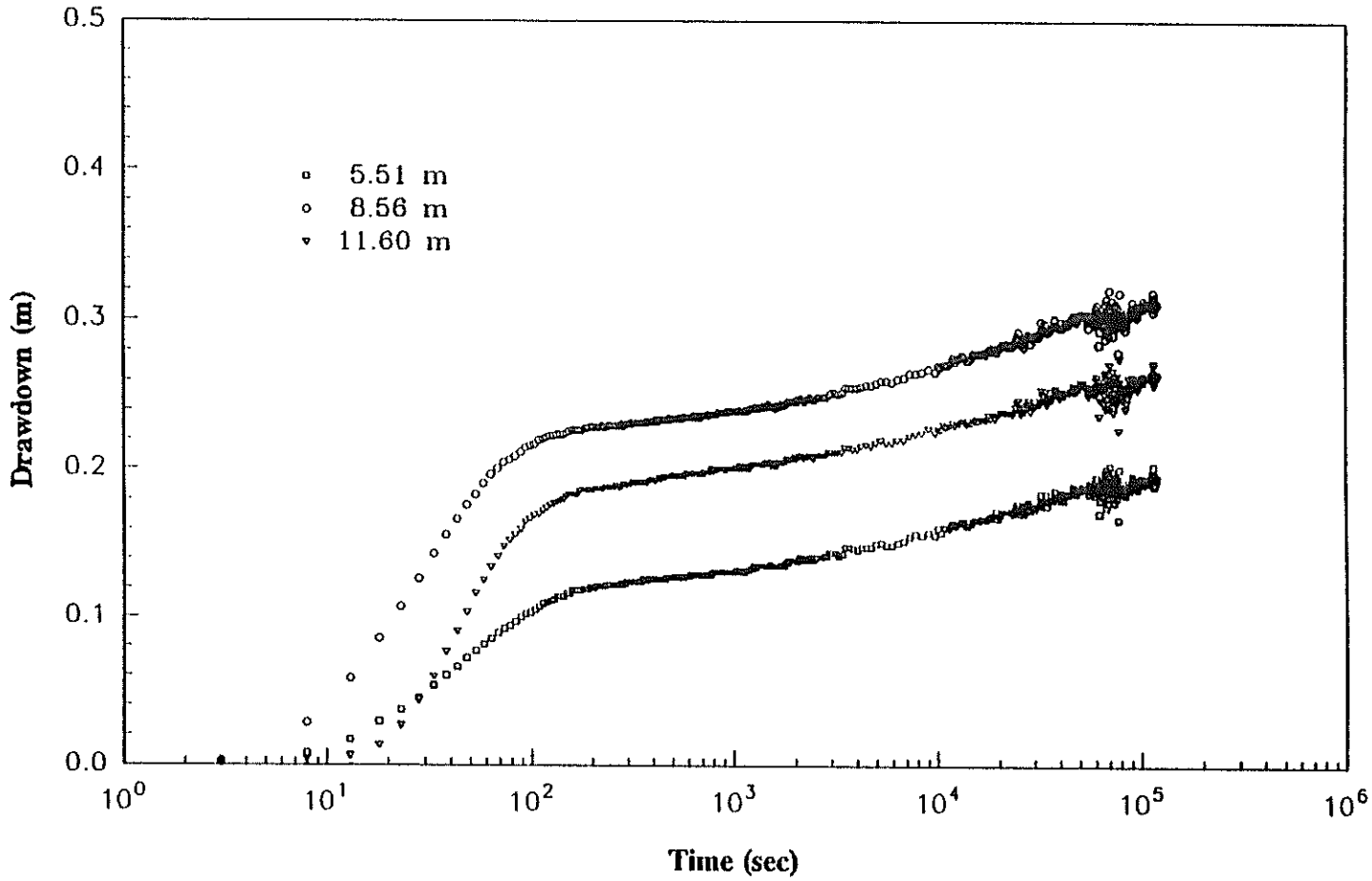

Figure 3-8. Depth-specific drawdown measured at different depths of W3 during Test No. 10.

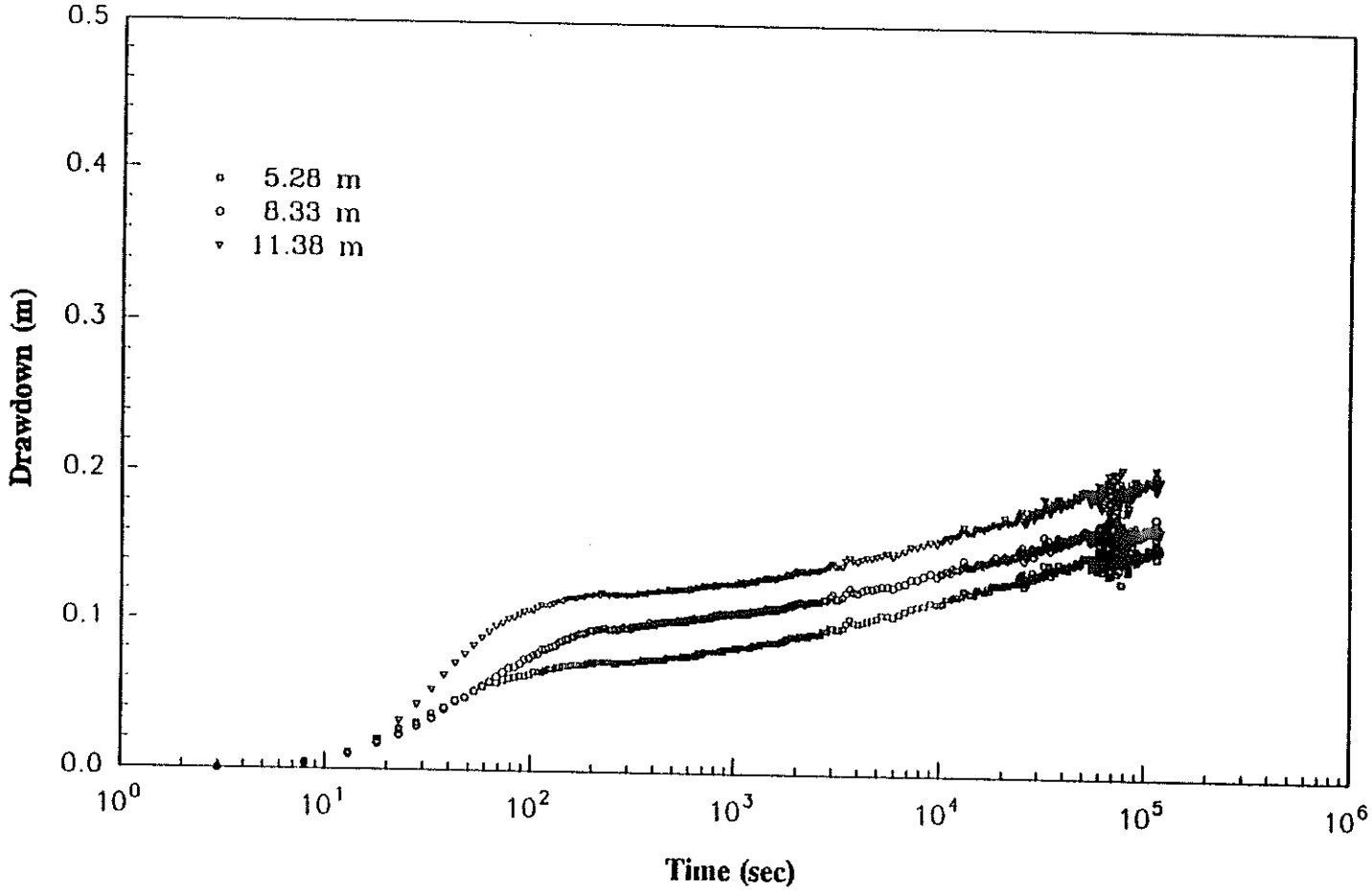

Figure 3-9. Depth-specific drawdown measured at different depths of NE6 during Test No. 10.

3.3 VERTICALLY AVERAGED PUMPING TEST DATA

Vertically averaged drawdown data were measured in the observation wells during Test No. 9, 11 and 12. These data are considered vertically averaged because the observation wells have long well screens (see Figure 2-3) over which the possible head differentials due to layering or vertical anisotropy are averaged out by mixing. Unfortunately, the vertically averaged drawdown data had considerable noise, the best quality data for the three tests are presented from Figures 3-10 through 3-12. In addition to the noise, all of the drawdown data show that they decreased instead of increasing approximately between 200 and 1,000 seconds after pumping started. This means that the aquifer had been "replenished" during these periods of pumping, which is difficult to account for under the given conditions. These drawdown data do not demonstrate the typical three-section trend either. Due to these concerns, the vertically averaged drawdown data were not analyzed for aquifer anisotropy estimation or other parameter identification.

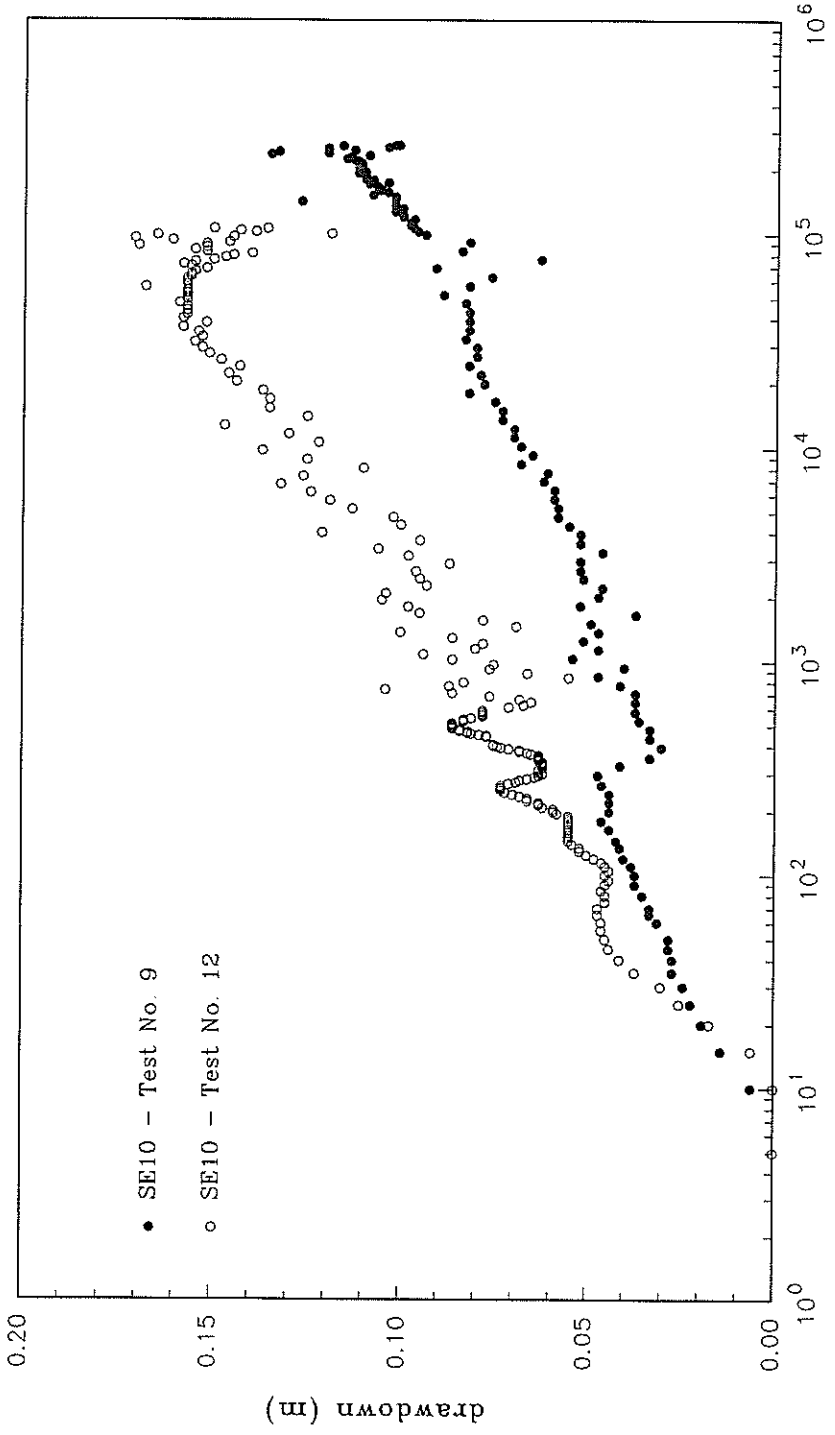

Figure 3-10. Vertically averaged drawdown measured at SE10 during Test No. 9 and No. 12.

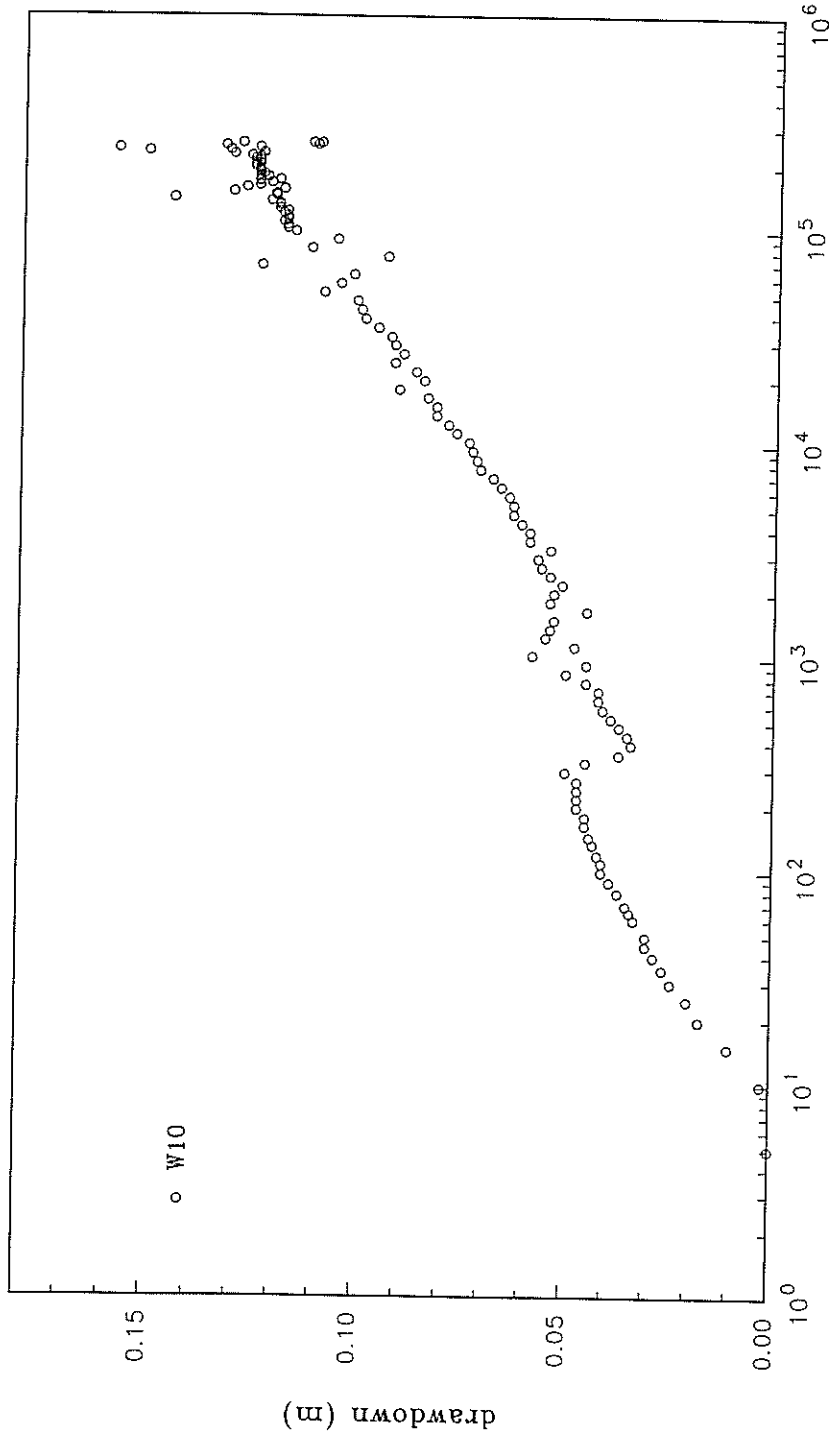

Figure 3-11. Vertically averaged drawdown measured at W10 during Test No. 9.

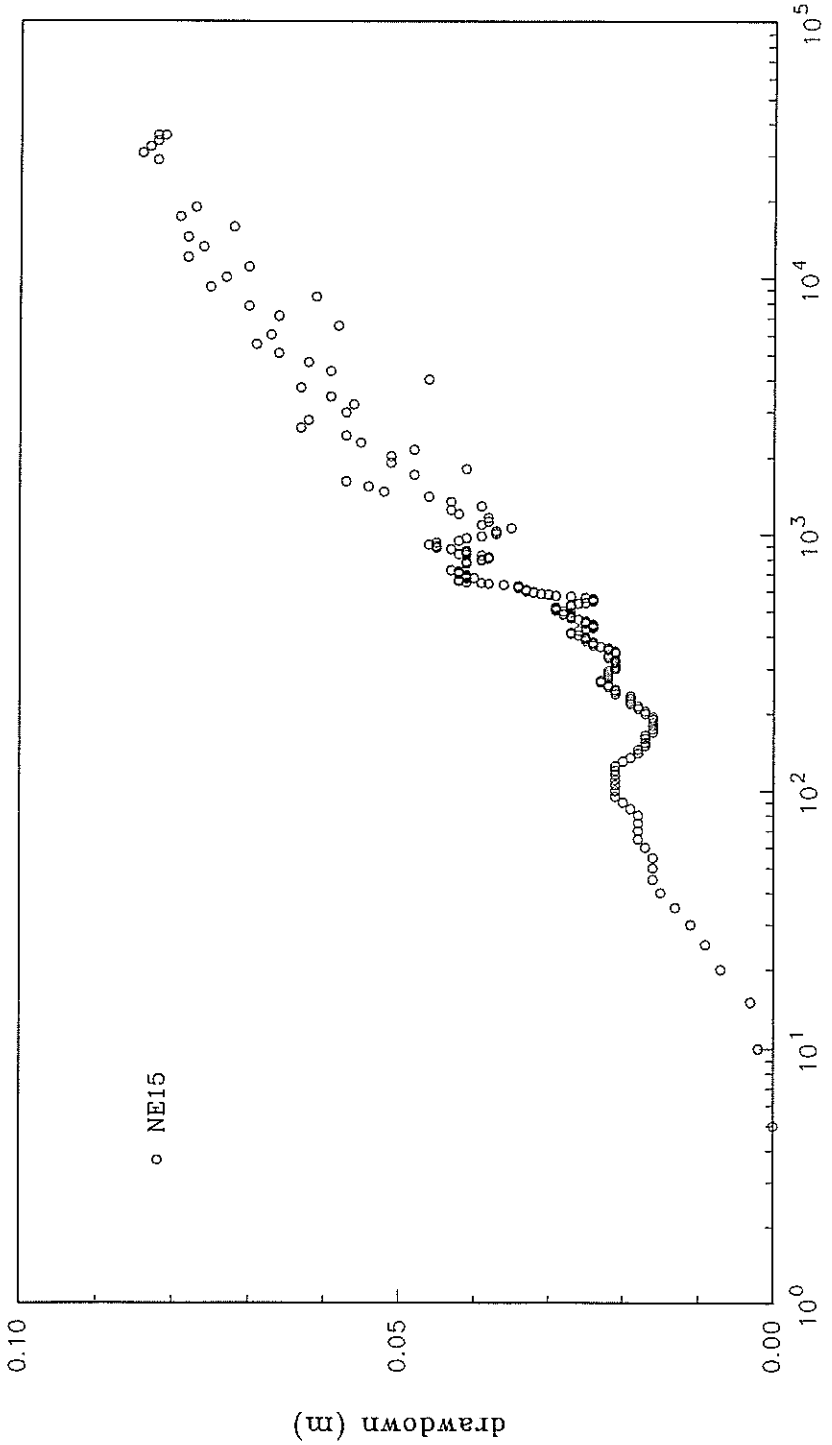

Figure 3-12. Vertically averaged drawdown measured at NE15 during Test No. 11.

4. LAPLACE-HANKEL DOMAIN CALCULATION OF UNCONFINED WELL HYDRAULICS

Analysis of the pumping test data from the Sevilleta aquifer requires solutions of well hydraulics for unconfined aquifers. The three-dimensional analytical solution given by Neuman [1974] was selected to analyze the drawdown data. This solution is suitable for the condition where groundwater flow is generated by a partially penetrating well in an unconfined, vertically anisotropic aquifer. It is complicated in mathematics, involving an integral consisting of an oscillatory Bessel function, $J_o(x)$, and an infinite series. Rolfes [1980] gave an improved numerical method over that employed in the DELAY2 program to handle the calculation of this solution. Both Rolfes's and Neuman's DELAY2 methods are cumbersome in programming and time-consuming in computation, not very ideal for handling large amounts of data. Here, we developed a new method to calculate the solution. This method calls for the use of the Laplace-Hankel domain counterpart of the original solution given by Neuman [1974].

Both the Laplace and Hankel transforms are the integral transform technique [Sneddon, 1972]. The Laplace transform uses the exponential function as its transform kernel. The Hankel transform uses the Bessel function, $J_0(x)$, for its transform kernel. Here, the Laplace transform is applied to time and p is the transform parameter of t. The Hankel transform is applied to the radial distance and a is the transform parameter of r. Advantages of this Laplace-Hankel domain calculation method are: (1) the Hankel inverse is handled numerically through the Fast Hankel transform (FHT) technique and the Laplace inverse is calculated with the Stehfest [1970] numerical method. Thus, the difficult integration and calculation encountered in dealing with the original solution are avoided or

minimized, and (2) the Laplace-Hankel domain solution is linearly composed of three terms (g_1, g_2 and g_3 as shown below). Each term represents a specific, physically meaningful condition; i.e., g_1 represents the "base condition" where the aquifer is confined and the pumping well is fully penetrating, g_2 represents the water table effects and g_3 represents the partial penetration effects. Different solutions thus can be derived from the linear combination of g_1, g_2 and g_3. One computer program for calculating g_1, g_2 and g_3 can give solutions for different problems, not only the unconfined flow due to a partially penetrating pumping well.

The Stehfest method is easy to use and has been frequently employed to numerically inverse many Laplace-domain solutions of groundwater problems (e.g., Moench, 1984a; and others). The FHT method, however, has been commonly used in geophysics and it has not been recognized in hydrogeology. This method uses digital convolution instead of direct numerical quadrature to evaluate the Hankel transform integral. In general, digital convolution is an order of magnitude faster than direct numerical integration, primarily because the Bessel function evaluation is avoided. Anderson [1979] gave detailed discussion on the FHT method. The FORTRAN program, DHANKL, developed by Anderson [1982] is employed to handle the Hankel inverse.

The Laplace and Hankel inverse of g_1 gives the Theis solution, indicating that g_1 represents the "base condition" of a confined aquifer and a fully penetrating pumping well. In this sense, g_2 and g_3 give the deviation, due to the existence of a water table and of a partially penetrating pumping well, from the base condition. Linear combination of g_1, and g_2, and/or g_3 gives solutions for different problems. For example, neglecting g_2 gives the

solution for a confined aquifer subject to a partially penetrating pumping well as given by Hantush [1961]. Neglecting g_3 leads to the solution for unconfined flow due to a fully penetrating pumping well as given by Neuman [1972]. Of course, when neither g_2 nor g_3 is ignored, the combination of the three terms gives the solution for unconfined flow subject to a partially penetrating pumping well given by Neuman [1974]. In addition, for a specific condition, not only the drawdown of interest is determined, but any influences from the water table condition and/or a partially penetrating well, if exists, are explicitly evaluated. This is very helpful in understanding the problem of interest.

4.1 LAPLACE-HANKEL DOMAIN SOLUTION AND CALCULATION

The problem of interest is schematized in Figure 4-1, where the pumping well partially penetrates the aquifer from d to l. Before pumping starts, the water table is assumed to be horizontal. It is assumed that drawdown everywhere is small during pumping as compared to the saturated thickness, b, and the aquifer thickness is assumed to be constant. The pumping well can partially penetrate the aquifer. The solid well casing has a length of d as measured from the water table to the top of the well screen. The well screen has a length of l-d, where l is measured from the water table to the bottom of the well screen. When the pumping well is fully penetrating, d is equal to zero and l is equal to b. The observation well can be partially penetrating as well. Measured from the water table to the top of the observation well screen, d_0 is the total length of the solid casing. The total screened interval of an observation well is l_0 - d_0, where l_0 is measured from the water table to the bottom of the observation well. Drawdown or groundwater samples collected from an observation well are considered vertically-averaged over the screened interval, l_0 - d_0. If the

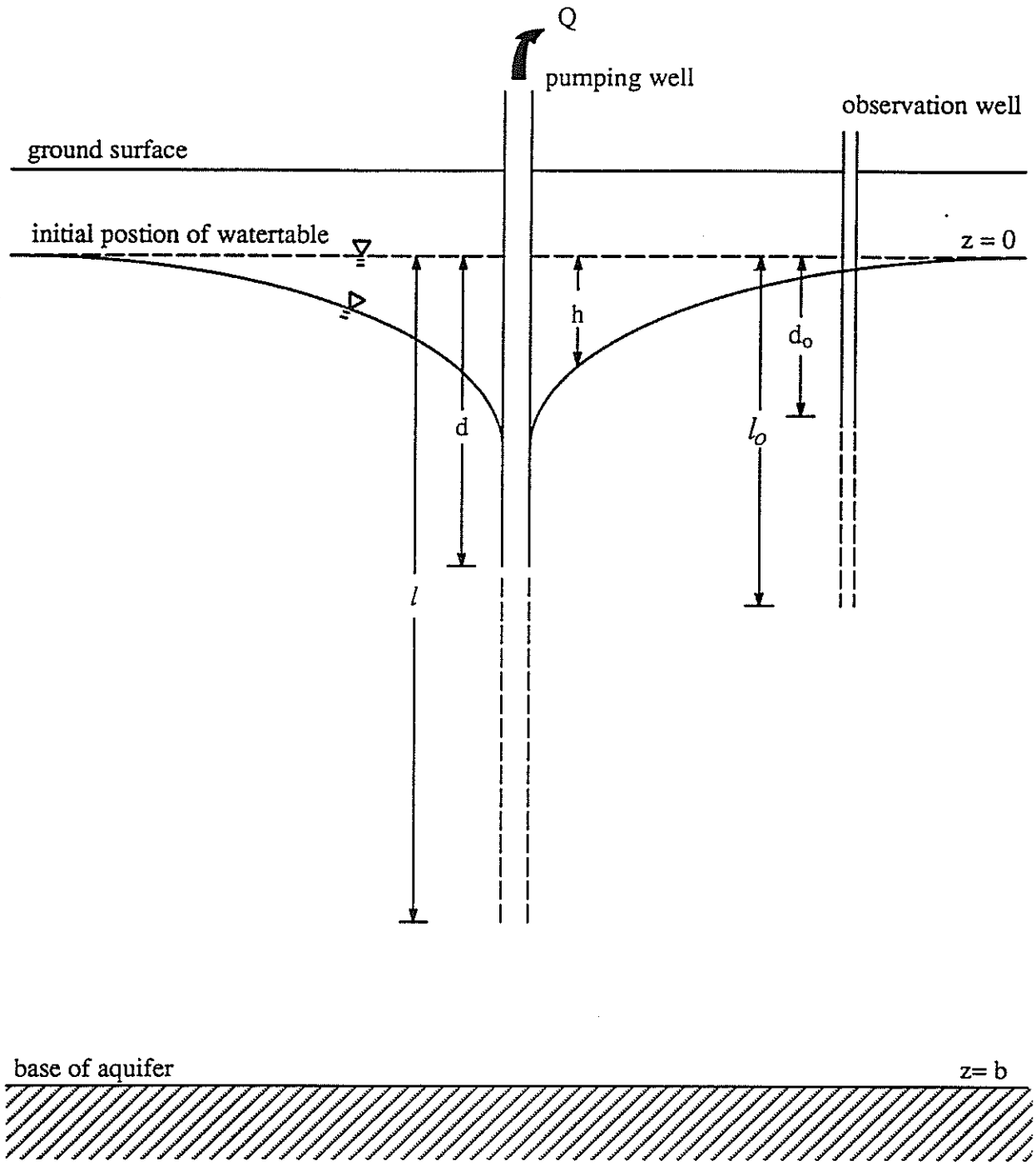

Figure 4–1. Schematic for an unconfined aquifer pumped by a partially penetrating well.

screened interval is small (i.e., $l_0 = d_0$) as for a piezometer, the data measured are called depth-specific at a fixed depth of $z = d_0 = l_0$. The observation well can be fully penetrating (i.e., $d_0 = 0$ and $l_0 = b$). Data collected from a fully penetrating observation well are vertically averaged across the whole aquifer thickness.

Based on equation A.14 of Neuman (1974) and writing the partially penetrating effects in appropriate form, the Laplace-Hankel domain solution for the depth-specific drawdown for the current study can be written as

$$g(a,z,p) = g_1 - g_2 + g_3 \tag{4-1}$$

where

$$g_1 = \frac{Q}{2\pi Tp}\,(a^2 + pS/T)^{-1} \tag{4-2}$$

$$g_2 = \frac{Q}{2\pi bK_z}\,(F_p F_w) \tag{4-3}$$

$$g_3 = \frac{Q}{\pi^2 K_r (l-d)} \sum_{n=1}^{\infty} F_n \,(a^2 + p\frac{S}{T} + \frac{n^2\pi^2}{b^2}\,\frac{K_z}{K_r})^{-1} \tag{4-4}$$

$$F_p = \frac{b}{l-d}\,\frac{\sinh[\eta(b-d)] - \sinh[\eta(b-l)]}{\sinh(\eta b)} \tag{4-5}$$

$$F_w = \frac{\cosh[\eta(b-z)]}{[\alpha_y \eta \sinh(\eta b) + p \cosh(\eta b)]\eta^2} \tag{4-6}$$

$$F_n = \frac{1}{n} \cos\left[\frac{n\pi z}{b}\right] \left[\sin\left[\frac{n\pi l}{b}\right] - \sin\left[\frac{n\pi d}{b}\right]\right] \tag{4-7}$$

and

$$\alpha_y = K_z/S_y \quad , \quad \eta^2 = \frac{K_r}{K_z}(a^2 + pS/T)$$

The Laplace and Hankel inverse of (4-1) gives the results of interest in the r and t domain. By equation 6.532.4 of Gradshteyn and Ryzhik (1980; p.678), the Hankel inverse of g_1 is found to be

$$H^{-1}\left[\frac{Q}{2\pi Tp}(a^2 + pS/T)^{-1}\right] = \frac{Q}{2\pi Tp}\int_0^\infty \frac{aJ_0(ar)}{a^2 + pS/T}da = \frac{Q}{2\pi Tp}K_o(r\sqrt{pS/T}) \tag{4-8}$$

The Laplace inverse of (4-8), by equation 13.41 of Oberhettinger and Badii (1973; p. 338), gives the Theis solution, or

$$h_1(r,t) = L^{-1}H^{-1}(g_1) = \frac{Q}{4\pi T}W(u) \qquad \textbf{(4-9)}$$

where W(u) is the exponential integral which can be evaluated with the formulae given by Abramowitz and Stegun (1970; p. 231). The function, F_W, contributes to drawdown the water table effects because the specific yield, accounting for drainage of water table decline, is only involved in F_W. Based on this fact, S_y can be used to indicate whether the aquifer is confined (i.e., $S_y = 0$) or unconfined ($S_y \neq 0$) in the computer program. The Laplace and Hankel inverse of g_2 gives the water table effects on drawdown,

$$h_2(r,z,t) = \frac{Q}{2\pi bK_z} L^{-1}H^{-1}(F_pF_w) \qquad \textbf{(4-10)}$$

where the FHT and the Stehfest methods are used to numerically invert the Hankel and Laplace transforms, respectively.

The condition of a fully penetrating pumping well is recognized in calculation by setting d equal to zero and *l* equal to b (i.e., d = 0 and *l* = b for a fully penetrating pumping well). When this happens, g_3 is zero and F_p is unity. Thus, drawdown due to a fully penetrating pumping well can be determined by

$$h(r,z,t) = h_1 - h_{21} \qquad \textbf{(4-11a)}$$

where

$$h_{21} = \frac{Q}{2\pi b K_z} L^{-1}H^{-1}(F_w) \qquad \textbf{(4-11b)}$$

As given in (4-4), the Hankel transform part of g_3 (i.e., $a^2 + pS/T + n^2\pi^2K_z/(b^2K_r)$) can be exactly inverted using (4-8). Completion of this leaves only the Laplace transform in the remaining part of g_3 and the effects of a partially penetrating pumping well thus can be determined by

$$h_3(r,z,t) = L^{-1}H^{-1}(g_3) = \frac{Q}{\pi^2 K_r(l-d)} \sum_{n=1}^{\infty} F_n L^{-1}\left[\frac{K_o(r^2 p \frac{S}{T} + n^2\pi^2\beta)^{1/2}}{p}\right] \qquad \textbf{(4-12)}$$

where $\beta = (K_z r^2)/(K_r b^2)$. As shown in Hantush (1961), analytical inverse of the Laplace transform in (4-12) is an integral function that is difficult to evaluate. Thus, the Stehfest method is used to numerically calculate the Laplace inverse in (4-12).

As a result, drawdown subject to a partially penetrating pumping well condition (i.e., $d \neq 0$ and/or $l \neq b$) can be determined by

$$h(r,z,t) = h_1 - h_2 + h_3 \qquad \textbf{(4-13)}$$

where h_1, h_2 and h_3 are determined using (4-9), (4-10), and (4-12), respectively. If drawdown is measured from an observation well screened from d_o to l_o, (4-13) should be "vertically averaged" to yield the vertically averaged drawdown,

$$\bar{h}(r,t) = \frac{1}{l_o - d_o} \int_{d_o}^{l_o} (h_1 - h_2 + h_3)\, dz = h_1 - \bar{h}_2 + \bar{h}_3 \qquad \textbf{(4-14)}$$

where

$$\bar{h}_2 = \frac{Q}{2\pi b K_z} \; L^{-1}H^{-1}(F_p \bar{F}_w) \qquad \textbf{(4-15a)}$$

$$\textit{with} \quad \bar{F}_w = \frac{\sinh\,[\eta(b-d_o)] - \sinh\,[\eta(b-l_o)]}{\eta^3(l_o-d_o)[\alpha_y \eta \sinh\,(\eta b) + p\,\cosh\,(\eta b)]} \qquad \textbf{(4-15b)}$$

and

$$\bar{h}_3 = \frac{Qb}{\pi^3 K_r (l-d)} \sum_{n=1}^{\infty} \bar{F}_n \, L^{-1}\left[\frac{K_o}{p}\,(r^2 p \frac{S}{T} + n^2\pi^2\beta)^{1/2}\right] \qquad \textbf{(4-15c)}$$

$$\textit{with} \quad \bar{F}_n = \frac{1}{n^2(l_o-d_o)}\left[\sin\left(\frac{n\pi l_o}{b}\right) - \sin\left(\frac{n\pi d_o}{b}\right)\right]\left[\sin\left(\frac{n\pi l}{b}\right) - \sin\left(\frac{n\pi d}{b}\right)\right] \qquad (4\text{-}15d)$$

If the pumping well is fully penetrating (i.e., d=0 and l=b) while the observation well is partially penetrating from d_o to l_o, the drawdown can be calculated using

$$\bar{h}(r,t) = h_1 - \bar{h}_{21} \tag{4-16a}$$

where

$$\bar{h}_{21} = \frac{Q}{2\pi b K_z} L^{-1}H^{-1}(\bar{F}_w) \tag{4-16b}$$

in which $\bar{F}_w$ is defined by (4-15b).

It is noted that $\bar{F}_n$ (and thus $\bar{h}_3$) is zero if the observation well fully penetrates the unconfined aquifer (i.e., $d_o = 0$ and $l_o = b$). This indicates effects of a partially penetrating pumping well on drawdown disappear in a fully penetrating observation well. A total of seven cases can be derived from (4-1) through the combination of h_1, h_2, h_{21}, h_3, $\bar{h}_2$, $\bar{h}_{21}$, and $\bar{h}_3$. In computer programming, solutions for these seven cases can be selected by controlling S_y, l_o, d_o, l and d as shown in the flowchart of Figure 4-2. Each of the seven cases is specifically explained in Table 4-1. Drawdowns calculated using the FHT and the Stehfest Laplace inverse are compared with results given by Rolfes (1980) and from the

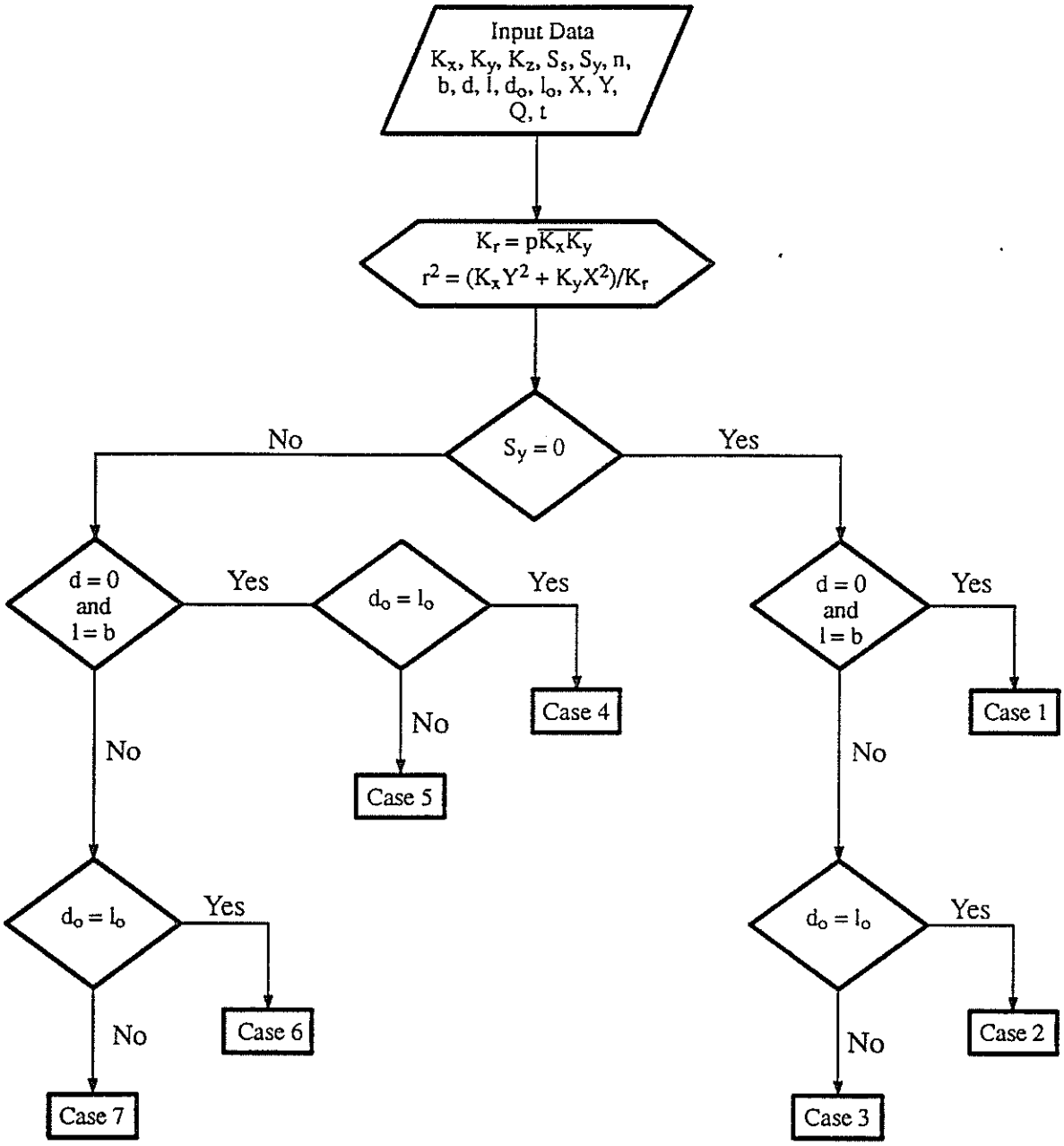

Figure 4–2. Flow chart describing calculation of different solutions in the Laplace–Hankel domain.

Table 4-1. Seven cases associated with the Laplace-Hankel Domain Calculation

Case No.	Aquifer Condition	Pumping Well	Observation Well	Formula
1	Confined	Fully Penetrating	Point observation at d_o or screened from d_o to l_o	h_1
2	Confined	Partially Penetrating	Point observatin at $z=d_o$	$h_1 + h_3$
3	Confined	Partially Penetrating	Screened from d_o to l_o	$h_1 + \bar{h}_3$
4	Unconfined	Fully Penetrating	Point observation at $z=d_o$	$h_1 - h_{21}$
5	Unconfined	Fully Penetrating	Screened from d_o to l_o	$h_1 - \bar{h}_{21}$
6	Unconfined	Partially Penetrating	Point observation at $z=d_o$	$h_1 - h_2 + h_3$
7	Unconfined	Partially Penetrating	Screened from d_o to l_o	$h_1 - \bar{h}_2 + \bar{h}_3$

DELAY2 program in Tables 4-2 and 4-3. It is seen that this method yields very accurate results.

4.2 DISCUSSIONS AND RESULTS

The Laplace transform parameter, p, is inversely related to t. The asymptotic nature of drawdown at large t thus can be understood by evaluating the Laplace-domain counterpart at small p. For p = 0 as for t approaching infinity, both F_W and g_3 become independent of p and still remain finite. This indicates that for large times, the water table effects and the partially penetrating well effects can reach steady state. The Theis solution or h_1, however, never reaches steady state. Thus at large times, depth-specific drawdown for an unconfined aquifer subject to a partially penetrating well is

$$h(r,z,t) = \frac{Q}{4\pi T}[W(u) - h_w(r,z) + h_p(r,z)] \qquad \textbf{(4-17)}$$

where $h_w(r,z)$ and $h_p(r,z)$ represent the steady-state water table effects and partially penetrating effects, respectively. Specifically, h_w and h_p are

$$h_w = H^{-1}\left(\frac{2K_r}{K_z} F_p \hat{F}_w\right) \qquad \textbf{(4-18)}$$

and

Table 4–2. Comparison of Dimensionless Drawdown Calculated by the Laplace–Hankel Method and Other Methods; the Pumping Well is Fully Penetrating and the Drawdown is Vertically Averaged.

	Current Method	Rolfes [1980]	DELAY2
$S/S_y = 10^{-9}$			
$\beta = 10^{-13}$			
$(4u)^{-1}$	h	h	h
10^{-1}	0.2491×10^{-1}	0.2492×10^{-1}	0.2478×10^{-1}
1	0.1044x10	0.1044x10	0.1038x10
10^{2}	0.5417x10	0.5417x10	0.5392x10
10^{5}	0.1232×10^{2}	0.1232×10^{2}	0.1226×10^{2}
10^{10}	0.2376×10^{2}	0.2387×10^{2}	0.2367×10^{2}
$\beta = 10^{-6}$			
10^{-1}	0.2491×10^{-1}	0.2492×10^{-1}	0.2478×10^{-1}
1	0.1043x10	0.1044x10	0.1038x10
10^{2}	0.5396x10	0.5397x10	0.5385x10
10^{5}	0.1161×10^{2}	0.1161×10^{2}	0.1160×10^{2}
10^{10}	0.1247×10^{2}	0.1247×10^{2}	0.1245×10^{2}
$\beta = 10^{-3}$			
10^{-1}	0.2467×10^{-1}	0.2465×10^{-1}	0.2465×10^{-1}
1	0.1019x10	0.1019x10	0.1017x10
10^{2}	0.4765x10	0.4765x10	0.4766x10
10^{5}	0.5622x10	0.5622x10	0.5623x10
10^{10}	0.5694x10	0.5694x10	0.5696x10
$\beta = 10^{-1}$			
10^{-1}	0.1703×10^{-1}	0.1703×10^{-1}	0.1702×10^{-1}
1	0.3000	0.3000	0..3001
10^{2}	0.3173	0.3173	0.3174
10^{5}	0.3174	0.3174	0.3175
10^{10}	0.3138x10	0.3138x10	0.3140x10
$S/S_y = 10^{-1}$			
$\beta = 10^{-13}$			
10^{-1}	0.2491×10^{-1}	0.2492×10^{-1}	0.2478×10^{-1}
1	0.1044x10	0.1044x10	0.1038x10
10^{2}	0.5417x10	0.5417x10	0.5392x10
10^{5}	0.1232×10^{2}	0.1232×10^{2}	0.1226×10^{2}
10^{10}	0.2376×10^{2}	0.2388×10^{2}	0.2367×10^{2}
$\beta = 10^{-6}$			
10^{-1}	0.2491×10^{-1}	0.2492×10^{-1}	0.2478×10^{-1}
1	0.1043x10	0.1044x10	0.1038x10
10^{2}	0.5396x10	0.5397x10	0.5385x10
10^{5}	0.1168×10^{2}	0.1168×10^{2}	0.1167×10^{2}
10^{10}	0.2144×10^{2}	0.2141×10^{2}	0.2142×10^{2}
$\beta = 10^{-3}$			
10^{-1}	0.2467×10^{-1}	0.2465×10^{-1}	0.2465×10^{-1}
1	0.1019x10	0.1019x10	0.1017x10
10^{2}	0.4806x10	0.4806x10	0.4807x10
10^{5}	0.9924x10	0.9924x10	0.9925x10
10^{10}	0.2144×10^{2}	0.2141×10^{2}	0.2144×10^{2}
$\beta = 10^{-1}$			
10^{-1}	0.1709×10^{-1}	0.1708×10^{-1}	$0..1708 \times 10^{-1}$
1	0.3452	0.3452	0.3453
10^{2}	0.3045x10	0.3045x10	0.3047x10
10^{5}	0.9924x10	0.9924x10	0.9927x10
10^{10}	0.2144×10^{2}	0.2141×10^{2}	0.2144×10^{2}

Table 4–3. Comparison of dimensionless drawdown calculated by the Laplace–Hankel method and by DELAY2; the pumping well is fully penetrating and drawdown is depth–specific.

$S/Sy = 10^{-9}$						
$(4u)^{-1}$	z/b = 0.1		z/b = 0.5		z/b = 1.0	
	current	DELAY2	current	DELAY2	current	DELAY2
$\beta = 10^{-3}$						
10^{-1}	0.2491×10^{-1}	0.2418×10^{-1}	0.2491×10^{-1}	0.2446×10^{-1}	0.2491×10^{-1}	0.2461×10^{-1}
10^{1}	0.1039×10	0.1037×10	0.1044×10	0.1043×10	0.1044×10	0.1043×10
10^{2}	0.3382×10	0.3384×10	0.5238×10	0.5241×10	0.5403×10	0.5405×10
10^{5}	0.3598×10	0.3601×10	0.6197×10	0.6201×10	0.6729×10	0.6732×10
$\beta = 10^{-1}$						
10^{-1}	0.1440×10^{-1}	0.1421×10^{-1}	0.2491×10^{-1}	0.2492×10^{-1}	0.2491×10^{-1}	0.2489×10^{-1}
10^{1}	0.2490	0.2493	0.9282	0.9270	0.1034×10	0.1033×10
10^{2}	0.4859	0.4846	0.1778×10	0.1780×10	0.2211×10	0.2213×10
10^{5}	0.4859	0.4847	0.1778×10	0.1780×10	0.2211×10	0.2213×10
$\beta = 1$						
10^{-1}	0.5026×10^{-2}	0.5140×10^{-2}	0.1976×10^{-1}	0.1976×10^{-1}	0.2425×10^{-1}	0.2424×10^{-1}
10^{1}	0.7553×10^{-1}	0.7560×10^{-1}	0.3351	0.3353	0.4655	0.4652
10^{2}	0.7982×10^{-1}	0.7988×10^{-1}	0.3544	0.3545	0.4927	0.4923
10^{5}	0.7990×10^{-1}	0.7996×10^{-1}	0.3545	0.3546	0.4928	0.4924

$$h_p = \sum_{n=1}^{\infty} \frac{4b}{\pi(l-d)} F_n K_o (n^2\pi^2\beta)^{1/2} \qquad \textbf{(4-19)}$$

where F'_W is derived from F_W by setting p to zero and by changing η^2 to a^2K_r/K_z. Note that no Laplace inverse exists in (4-18) and (4-19) because p has been dropped for the large time approximation.

According to (4-17), drawdown at a specific r and z for large times is the Theis solution offset by a constant composed of h_w and h_p. When z changes, h_w and h_p varies as well, indicating drawdown curves for different z at a fixed r are parallel Theis curves. Each of these curves can be fitted by the Theis solution using a constant T and a value different from S for the storage coefficient. This "fitted storage coefficient" actually represents the sum of S, S_y and the partially penetrating effects, and thus it is more appropriately termed as an effective storage coefficient. This effective storage coefficient changes with depth at a fixed r, since the offset of h_w and h_p varies with z. As r is large, h_p diminishes, indicating that the partially penetrating effects vanish at large distances and large times.

If the pumping well is fully penetrating, the offset is only due to the water table effects. Again, large-time drawdown curves at different depths for a fixed r are parallel Theis curves. Each of these curves can be fitted by the Theis solution using a value larger than S for the storage coefficient. This fitted storage coefficient normally is deemed to be the sum of S and S_y. Regardless of whether the pumping well is partially penetrating or not, large-time drawdown curves at different depths of a fixed r are parallel Theis curves; Figure 4-3 gives quantitative illustration. Depth-specific conditions subject to a fully-penetrating

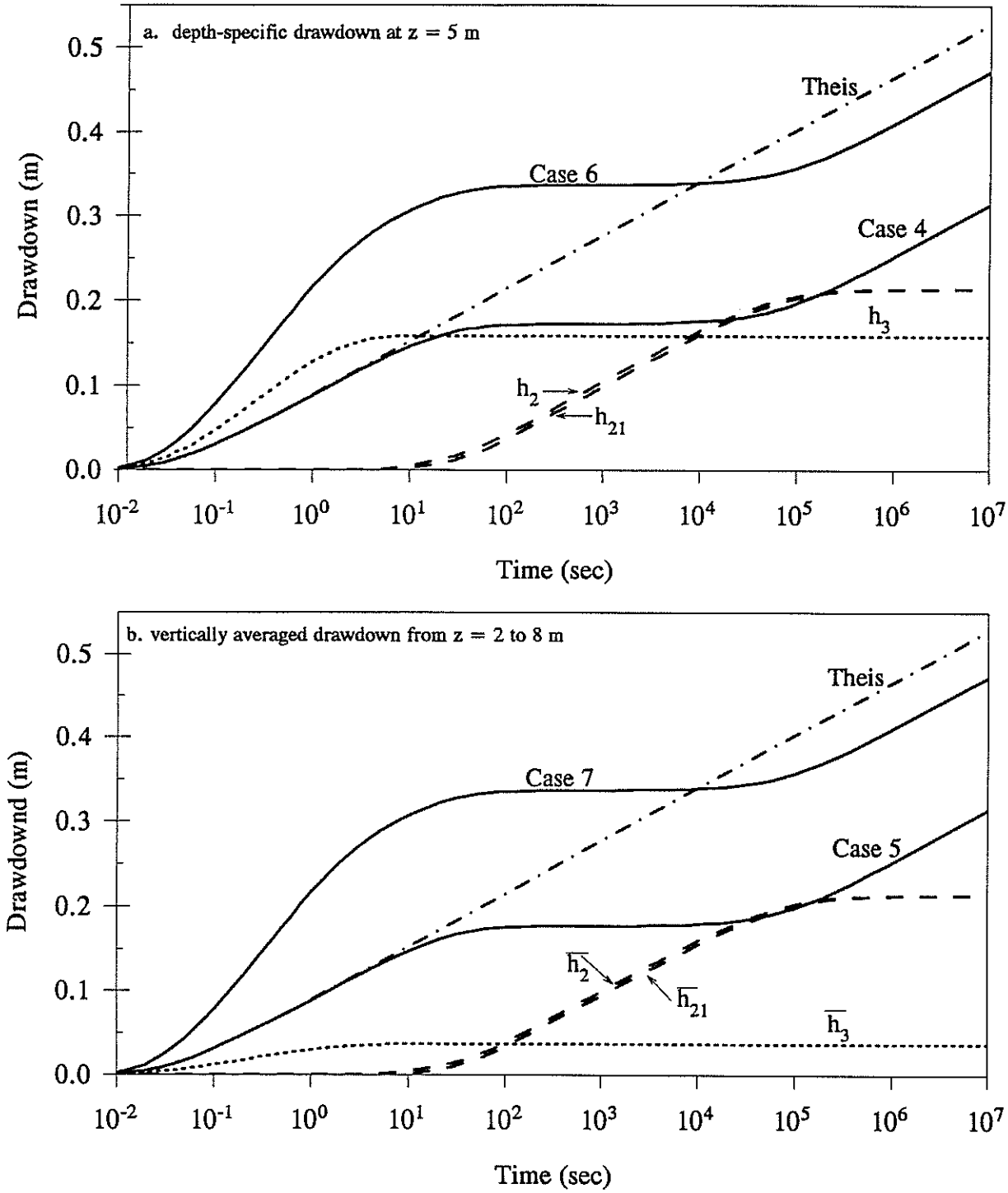

Figure 4-3 Drawdown expressed as the sum of Theis solution, water table effect, and partial penetration effect.

pumping well (Case 4) and to a partially-penetrating pumping well (Case 6) are shown in Figure 4-3a. Vertically-averaged conditions subject to a fully-penetrating pumping well (Case 5) and to a partially penetrating pumping well (Case 7) are displayed in Figure 4-3b. It can be seen that (1) at large times, the water table effect and the partial penetration effect are constant for the four cases, and the time-drawdown relationships for the four cases are indeed straight lines parallel to the Theis solution, (2) at small times, the water table effect is negligible relative to the partial penetration effect. Thus, drawdown variations of Case 4 and Case 5, where pumping well is fully penetrating, are coincident with the Theis solution. Drawdown variation of Case 6 and Case 7, where pumping well is partially penetrating, are larger than the Theis solution due to the partial penetrating effect only, and (3) at any times, the water table effects of h_2, h_{21}, $\bar{h}_2$ and $\bar{h}_{21}$ are not significantly different whereas the partial penetration effects of h_3 and $\bar{h}_3$ show noticeable difference.

In Figure 4-4, the water table effect and the partially penetrating well effect are separately demonstrated. As shown in Figure 4-4a, the water table effect is the largest at the water table (i.e., $z=0$) and continuously decreases as the depth increases. This vertical variation of water table effect diminishes as r increases; e.g., at $r=150$ m the water table effect at the water table and at the bottom of the aquifer is insignificantly different. At large times, the water table effect reaches a stable condition for all r and z. This indicates that h_w in (4-17) actually is constant for a given aquifer condition. In Figure 4-4b, it is seen that the partial penetration effect disappears at large r. At small r, this effect changes with z. The drawdown due to the partial penetrating effect is positive for depths within the screened interval (i.e., $d \leq z \leq l$. Note that in this particular example d is 3 m below the water table

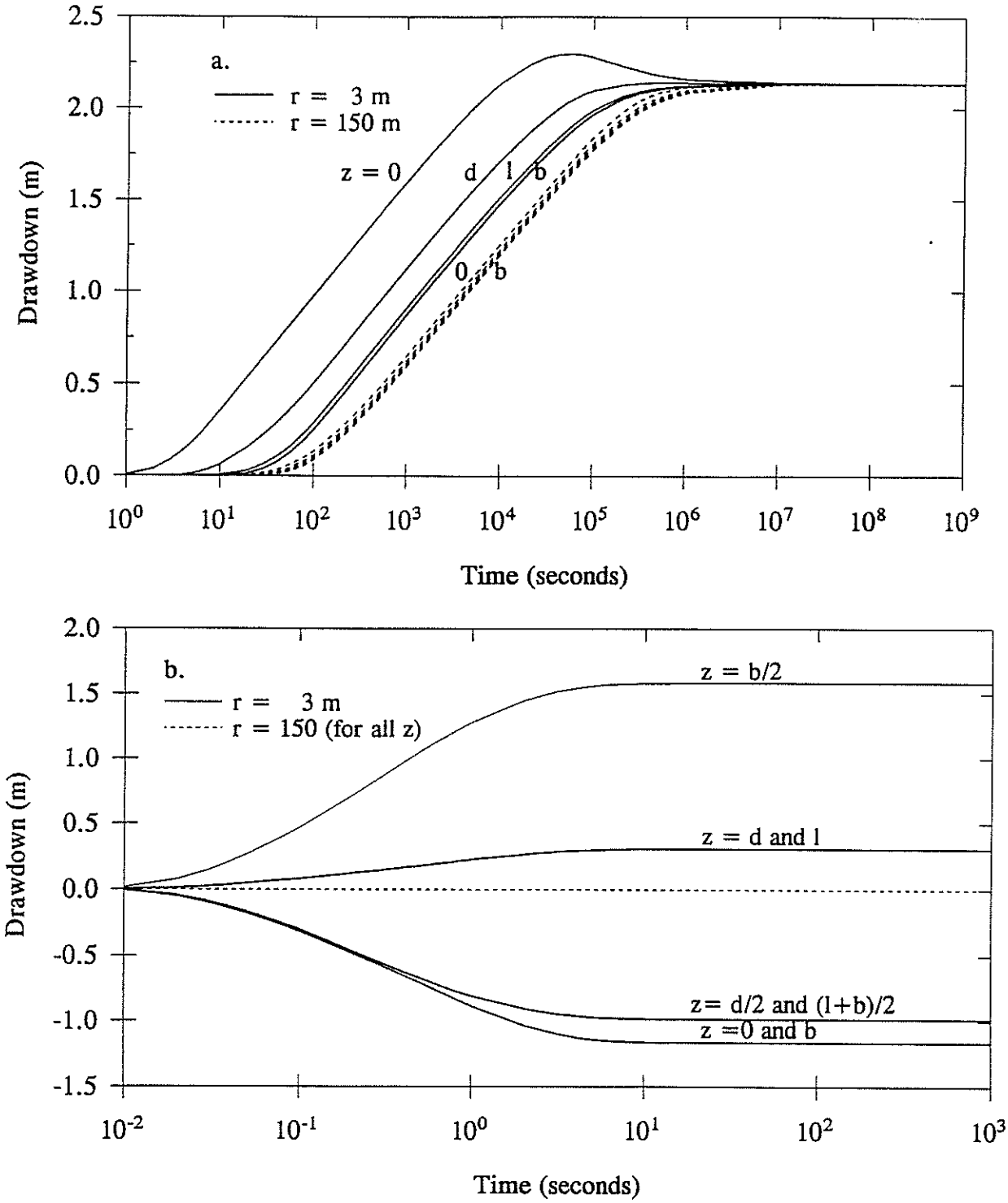

Figure 4-4 Drawdown at different depths due to (a) the water table effect and (b) the partially penetrating pumping effect.

and l is 3 m above the bottom of the aquifer such that the groundwater flow field is vertically symmetrical with respect to the center depth, b/2. In this event, the maximum drawdown due to the partial penetration effect occurs at b/2, and drawdown variations at d and l, at 0 and b, at d/2 and (l+b)/2 are the same, respectively, reflecting the vertical symmetry. At large times, the partial penetration effect at different depths is of different steady-state values. If the groundwater flow field is not vertically symmetrical, the drawdown due to the partially penetrating effect is still positive within the screened interval but the maximum drawdown does not necessarily occur at b/2. Other symmetrical conditions no longer exist.

5. AQUIFER ANISOTROPY ESTIMATION

Well hydraulics theories for unconfined conditions have been developed by various investigators. Boulton [1954, 1963] developed analytical solutions for unconfined well hydraulics where an empirical constant called the delay index was involved to account for the delayed yield due to water table decline. Neuman [1972, 1974], however, emphasized on the three-dimensional nature of unconfined flow and gave three-dimensional analytical solutions. Recently, Akindunni and Gillham [1992] and Nwankwor et al. [1992] have pointed out that the yield due to water table decline is time-dependent as influenced by the slow drainage occurring in the vadose zone and significant vertical flow exists in the saturated zone.

Assuming the aquifer is horizontally isotropic and both the pumping and observation wells fully penetrate the saturated thickness, Prickett [1965] and Neuman [1975] developed curve-matching methods to estimate S, S_y, K_r, and K_z (or the delay index). It is very difficult to generate appropriate type curves for the full range of times. These authors employed the asymptotic solutions for small- and large-time to prepare types curves only valid for drawdown data measured at early and late times. Dagan [1967] and Lakshminarayana and Rajagopalan [1978] gave curve-matching methods for the condition where the pumping well was partially penetrating. For other aquifer conditions, determination of aquifer anisotropy has been studied by various investigators. Hsieh and Neuman [1985a,b] developed theories and methods to estimate the three-dimensional anisotropy tensor for a fractured formation, where any of the three principal directions is unknown as a priori. Way and McKee [1982] presented a method to estimate the three-dimensional anisotropy of a leaky aquifer. Other aquifer anisotropy studies can be found in

Hantush [1964, 1966a,b], Papodopulos [1965], Neuman et al. [1984], Stoner [1981], Miller [1984], nd others. All of these aforementioned methods are not applicable for the current study, where the drawdown data are depth-specific, the aquifer is unconfined with a three-dimensional anisotropy, and the pumping well is partially penetrating.

The linear or nonlinear least-square fitting method, which avoids using type curves, has been frequently used to estimate aquifer parameters [e.g., Johns et al., 1992; Chandler et al., 1981, and others]. This method becomes ineffective when the number of unknown parameters is greater than three or four.

Since the mathematical model developed to analyze the tracer test data assumes that the three-dimensional groundwater flow field reaches the pseudo-steady-state condition (i.e., drawdown is transient while the hydraulic gradient is steady-state), the storage coefficient and the specific yield are not of primary concern. What is important is the planar anisotropy tensor for the horizontal flow. Here, a method of estimating the planar anisotropy tensor is developed based on the discussion in Chapter 4 and the drawdown curve patterns at large times. The depth-specific drawdown data taken from test No. 10 are used to characterize the anisotropy tensor.

5.1 METHOD DEVELOPMENT AND RESULTS

Since the vertical direction normally is a principal direction for alluvium aquifers, the anisotropy tensor can be written as

$$\underline{\underline{K}} = \begin{bmatrix} K_{xx} & K_{xy} & 0 \\ K_{xy} & K_{yy} & 0 \\ 0 & 0 & K_z \end{bmatrix} \tag{5-1}$$

where K_{xx}, K_{xy} and K_{yy} are elements of horizontal anisotropy.

Using cylindrical coordinates, the three-dimensional groundwater flow field due to pumping can be expressed as

$$\begin{Bmatrix} v_r \\ v_\theta \\ v_z \end{Bmatrix} = - \begin{bmatrix} K_{rr} & K_{r\theta} & 0 \\ K_{r\theta} & K_{\theta\theta} & 0 \\ 0 & 0 & K_z \end{bmatrix} \begin{Bmatrix} \partial h/\partial r \\ \frac{1}{r}\,\partial h/\partial \theta \\ \partial h/\partial z \end{Bmatrix} \tag{5-2}$$

which can be reduced to

$$\begin{Bmatrix} v_r \\ v_\theta \end{Bmatrix} = - \begin{bmatrix} K_{rr} & K_{r\theta} \\ K_{r\theta} & K_{\theta\theta} \end{bmatrix} \begin{Bmatrix} \partial h/\partial r \\ \frac{1}{r}\partial h/\partial \theta \end{Bmatrix} \tag{5-3}$$

and

$$v_z = - K_z\, \partial h/\partial z \tag{5-4}$$

where

$$K_{rr} = K_{xx}\cos^2\theta + K_{xy}\sin 2\theta + K_{yy}\sin^2\theta$$

$$K_{\theta\theta} = K_{xx}\sin^2\theta - K_{xy}\sin 2\theta + K_{yy}\cos^2\theta$$

$$K_{r\theta} = \frac{(K_{yy} - K_{xx})}{2}\sin 2\theta + K_{xy}\cos 2\theta$$

$$\theta = \tan^{-1}(y/x)$$

In light of (5-3) and (5-4), the horizontal and vertical flow components are separately related to the planar anisotropy characterized by K_{xx}, K_{xy} and K_{yy} and to the vertical principal hydraulic conductivity of K_z, respectively. This means that the vertical flow has no influence on the horizontal flow and the planar anisotropy can be estimated without involving K_z and v_z.

As shown in Figure 5-1, the depth-specific drawdowns at large times of SE3, W3, and NE6 for Test No. 10 are parallel straight lines on the semilog plots. This field evidence validates the theoretical discussions made in Chapter 4 that depth-specific drawdowns at large times follow the Theis solution. Using the logarithm approximation, each of the straight lines of large-time drawdown can be expressed as

$$h(x,y,z,t) = 0.183\frac{Q}{T_e}\left[\log(2.25\frac{T_e t}{r^2 S}) + h_p(r,z) - h_w\right] \qquad \textbf{(5-5)}$$

where

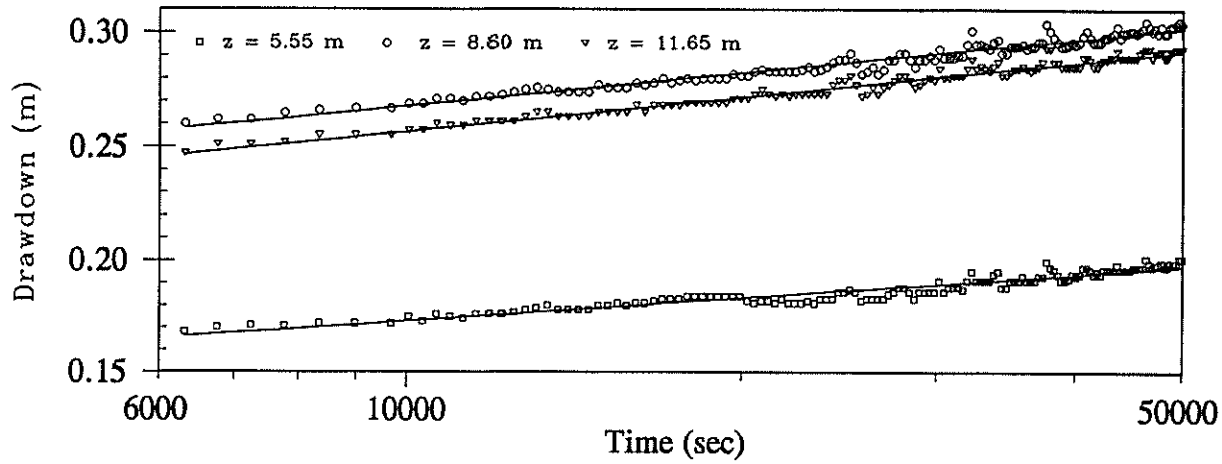

a. SE3; x = 1.60 m, y = -2.41 m, average slope = 0.049

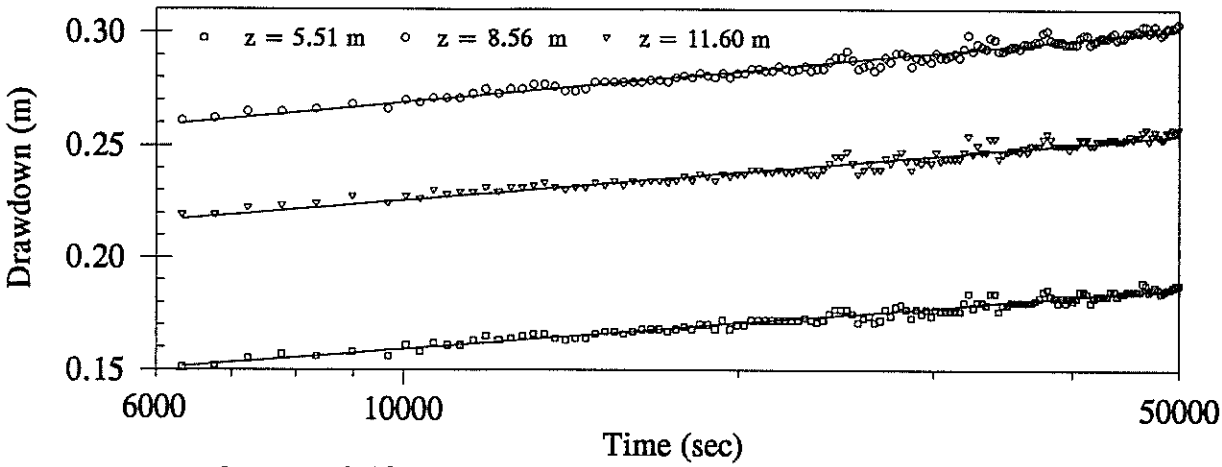

b. W3; x = -3.12 m, y = 0.08 m, average slope = 0.042

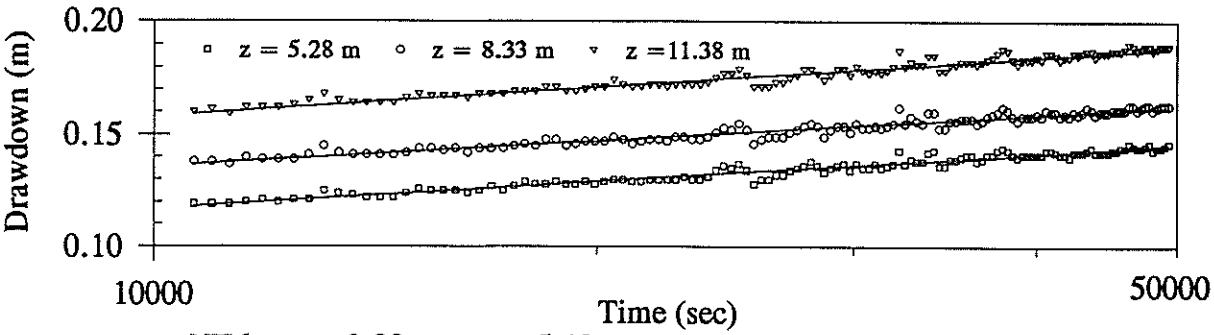

c. NE6; x = 3.29 m, y = 5.12 m, average slope = 0.041

Figure 5-1 Large-time drawdown at different depths of SE3, W3, and NE6 during Test No. 10 showing parallel straight lines on semilog plots.

$$T_e = (T_{xx}T_{yy} - T_{xy}^2)^{1/2} \tag{5-6}$$

$$r^2 = (T_{xx}y^2 + T_{yy}x^2 - 2T_{xy}xy) / T_e \tag{5-7}$$

Since transmissivity is the product of the hydraulic conductivity and the constant aquifer thickness (e.g., $T_{xx} = bK_{xx}$), the nature of $\underline{\underline{K}}$ is identical to that of $\underline{\underline{T}}$ and the planar anisotropy can be characterized by T_{xx}, T_{xy} and T_{yy} without the loss of generality.

It needs to be reemphasized that the water table effect, h_W, is constant in (5-5) as revealed by Figure 4-4a. Thus, the source of vertical dependence in (5-5) is h_p, which can be calculated with (4-19), provided $\underline{\underline{K}}$ is known. The constant h_W can be determined with (4-18) if S, S_y, and $\underline{\underline{K}}$ are known. These parameters are to be determined, and h_p and h_w cannot be known a priori. However, this does not create problems in estimating $\underline{\underline{T}}$ using (5-5) because h_p and h_w are constant for a specific r and a specific z when the large-time conditions are concerned. These two constants can be easily incorporated into the logarithm function appearing in (5-5) by using the relationship of $x = \log(10^x)$. As a result, (5-5) is rewritten as

$$h(x,y,z,t) = 0.183\frac{Q}{T_e}\log(2.25\frac{T_e t}{r^2 S_e}) \tag{5-8}$$

where S_e is the product of S and the appropriate logarithmic conversion of h_p and h_w. As a lumped parameter combining the effects of storage, water table and partial penetration, S_e is termed the effective storage coefficient, which is dependent on r and z. At a fixed r, S_e changes with z and each straight line of large-time drawdown thus has a different S_e. The "directional transmissivity" evaluated at a fixed r of each MLSP is constant due to the fact that the straight lines of large-time drawdown are parallel and subject to a constant slope.

The method of estimating $\underline{\underline{T}}$ using the large-time drawdown data is:

(1) Determine the directional transmissivity for each set of the large-time data collected from SE3, W3 and NE6 using the relationship

$$T_i = 0.183\frac{Q}{m_i} \quad , \quad i = 1,2,3$$

where m_i is the constant slope associated with the parallel straight lines of large-time drawdown at ith MLSP. Here, the subindex, i, equal to 1, 2 and 3 represents SE3, W3, and NE6, respectively. As indicated in Figure 5-1, m_1 is 0.049 m/s, m_2 is 0.042 m/s/ and m_3 is 0.041 m/s. Using 3.43 x 10^{-3} m^3/s for Q, T_1 is determined to be $1.27x10^{-2}$ m^2/s, T_2 is $1.49x10^{-2}$ m^2/s and T_3 is $1.54x10^{-2}$ m^2/s. These three directional transmissivities are not significantly different in magnitude, implying the aquifer is not significantly anisotropic in the horizontal plane.

(2) Denote t_0 as the time at which the extrapolated straight line of large-time drawdown intercepts the horizontal axis of h being zero. The different S_e can be estimated with the

associated t_0, at a specific depth. However, this calculation is not necessary since the ratios of t_0/S_e at different depths subject to a constant T_i are constant. Recalling that t_0 is associated with h being zero, the argument of the logarithm function in (5-8) must be equal to unity for t being t_0, that is;

$$2.25\frac{T_i}{r_i^2}\left[\frac{t_0}{S_e}\right]_z = 1$$

which defines the constant ratio of $(t_0/S_e)_z$ as

$$\left[\frac{t_0}{S_e}\right]_z = \frac{r_i^2}{2.25T_i} \qquad \textbf{(5-9)}$$

where $(t_0/S_e)_z$ is the ratio of t_0 to S_e for a specific z, and r_i is the actual distance from the ith MLSP to Well A.

(3) Since (5-8) should be applicable to any straight lines of large-time drawdowns, the argument of its logarithm function under the true anisotropic conditions where T_e and r are defined by (5-6) and (5-7) must be unity for h being zero. Therefore, the following relationships must be true

$$2.25\frac{T_e}{r^2}\left[\frac{t_0}{S_e}\right]_z = 1$$

to which introducing (5-9) yields

$$\frac{T_e}{r^2} = \frac{T_i}{r_i^2} \quad , \quad i = 1,2,3, \tag{5-10}$$

(4) Three simultaneous equations of three unknowns, T_{xx}, T_{xy} and T_{xy}, can be derived from (5-10) after replacing T_e and r by their definitions given in (5-6) and (5-7) as

$$\frac{T_{xx}y_i^2 + T_{yy}x_i^2 - 2T_{xy}x_iy_i}{T_{xx}T_{yy} - T_{xy}^2} = \frac{r_i^2}{T_i} \quad , \quad i = 1,2,3, \tag{5-11}$$

where (x_i, y_i) refers to the coordinates of the ith MLSP, and $r_i^2 = x_i^2 + y_i^2$. The solution of the three simultaneous equations can be determined using either the linear approximation method or nonlinear methods. The linear approximation method linearizes (5-11) by using $(T_1 + T_2 + T_3)/3$ for $(T_{xx}T_{yy} - T_{xy}^2)^{1/2}$. The three unknowns of T_{xy}, T_{xy} and T_{yy} left in the three linearized algebraic equations can be determined without difficulty. The nonlinear method deals with the original form of (5-11) without replacing the term $(T_{xx}\,T_{yy} - T_{xy}^2)$ by the arithmetic mean of T_1, T_2 and T_3. The solution of the three simultaneous nonlinear equations can be determined using minimization functions/subroutines available in software packages (e.g., the function "fmins" in MATLAB). Surprisingly, the solutions determined with the linear and nonlinear methods for the current case are almost identical, namely, T_{xx} is $1.52\text{x}10^{-2}$ m^2/s, T_{yy} is $1.37\text{x}10^{-2}$ m^2/s and T_{xy} is $1.57\text{x}10^{-3}$ m^2/s. Accordingly, the principal transmissivity of T_x is $1.62\text{x}10^{-2}$ m^2/s in the direction of N58°E, and the principal transmissivity of T_y is $1.27\text{x}10^{-2}$ m^2/s in the direction of N32°W. The planar anisotropy ellipse is demonstrated in Figure 5-2, where the eccentricity is 1.13. The eccentricity is

defined by $(T_x/T_y)^{1/2}$ or $(K_x/K_y)^{1/2}$. The average saturated thickness between the initial water table and the low-permeability layer ranges from 9.14 to 11.58 m, depending on the actual depth where the low-permeability layer locates. Using 10 m for the average saturated thickness, the principal hydraulic conductivity of K_x is 1.62×10^{-3} m/s, and the principal hydraulic conductivity of K_y is 1.27×10^{-3} m/s. They serve the upper and lower bound for any directional hydraulic conductivity at a specific direction in between the two principal directions. In general, the hydraulic conductivities are of the magnitude of about 10^{-3} m/s, which is representative of the hydraulic conductivity for sand and gravel [Table 2.2; Freeze and Cherry, 1979]. This is also in agreement with the soil classification results discussed in Chapter 2.3.

Considering that anisotropy is intrinsic to the aquifer and it cannot change with time, the planar anisotropy condition shown in Figure 5-2 is deemed to be correct for the aquifer. To prove that this anisotropy condition is accurate, it is used in (5-8) to calculate the large-time drawdowns at different depths of SE3, W3 and NE6. The comparison of the measured and calculated large-time drawdowns is shown in Figure 5-3. It is seen that the field data indeed can be reproduced by (5-8) using the anisotropy condition obtained, supporting the validity of the method and its results developed here for estimating the planar anisotropy.

After the planar anisotroply is determined, the vertical hydraulic conductivity, K_z, can be estimated based on the fact that at large times the vertical drawdown variation is mainly caused by the partial penetration effect, h_p. For a fixed r, the drawdown difference at z_1 and z_2 thus can be calculated by

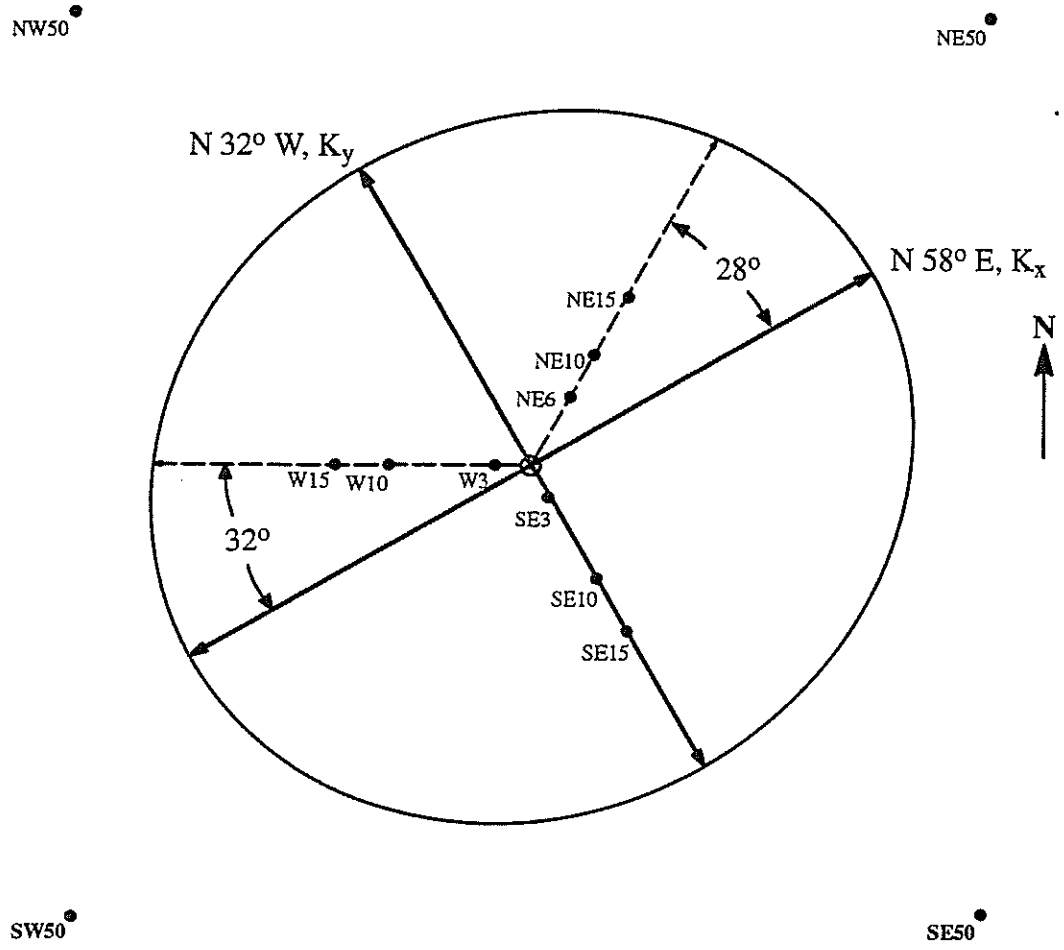

$K_x = 1.62 \times 10^{-3}$ m/s
$K_y = 1.27 \times 10^{-3}$ m/s

Figure 5–2. The Planar Anisotropy Ellipse Estimated From Large–Time Drawdown Data.

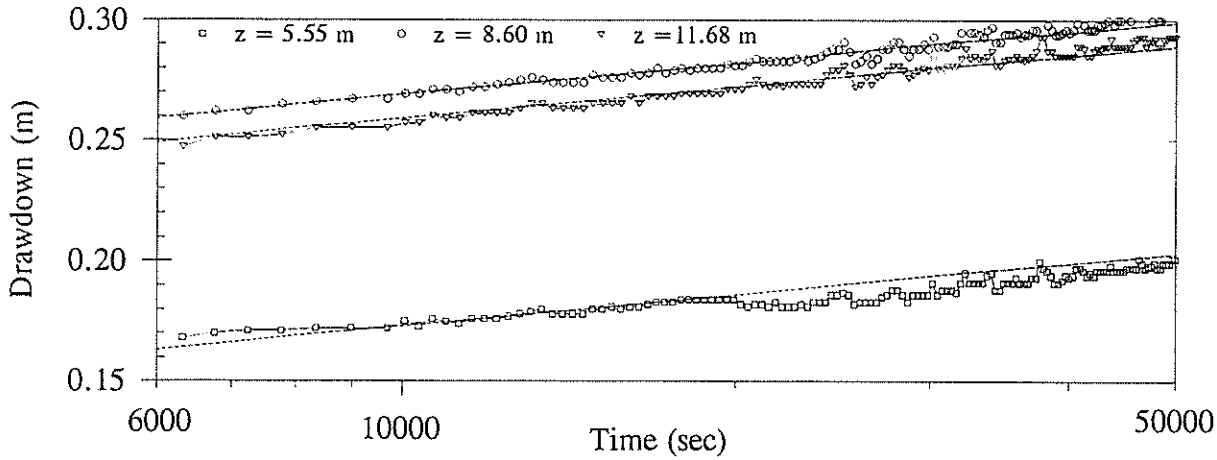

a. SE3; $S_e(5.55) = 4.34 \times 10^{-3}$, $S_e(8.60) = 2.78 \times 10^{-5}$, $S_e(11.65) = 4.70 \times 10^{-5}$

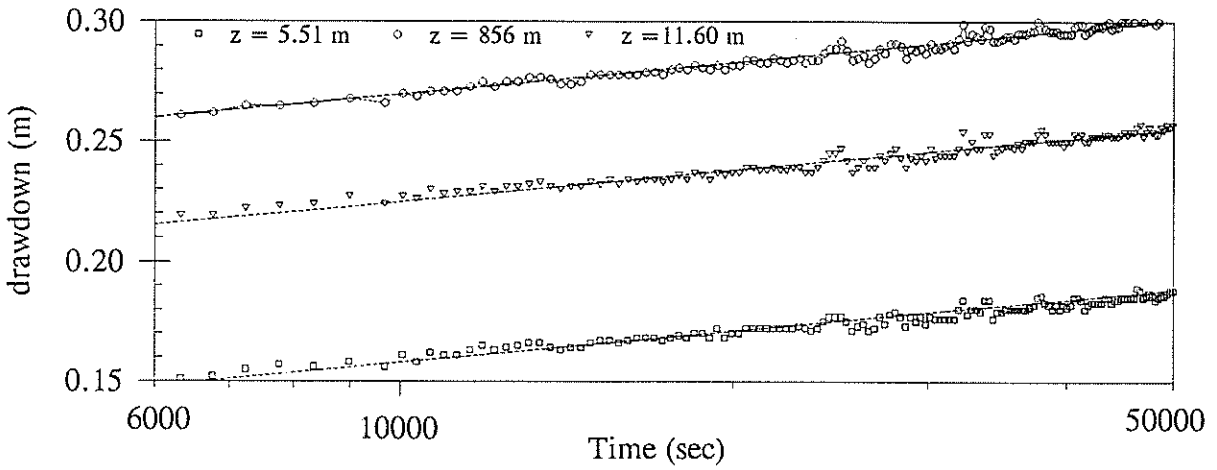

b. W3; $S_e(5.51) = 8.11 \times 10^{-3}$, $S_e(8.56) = 2.24 \times 10^{-5}$, $S_e(11.60) = 2.39 \times 10^{-4}$

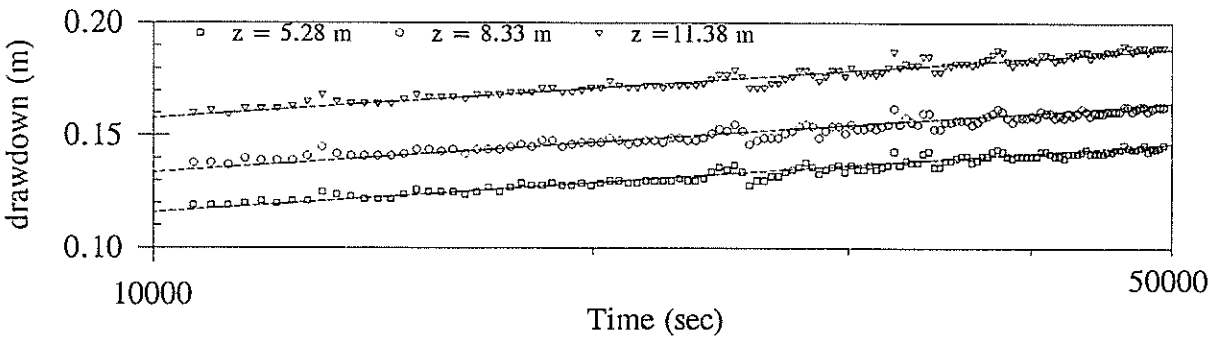

c. NE6; $S_e(5.28) = 1.92 \times 10^{-3}$, $S_e(8.33) = 7.45 \times 10^{-3}$, $S_e(11.60) = 2.11 \times 10^{-3}$

Figure 5-3. Comparison of measured (symbols) with calculated (lines) drawdown at large time for Test No. 10.

$$\Delta h = h_p(r,z_1) - h_p(r,z_2) \tag{5-12}$$

where Δh can be estimated by measuring the vertical difference between any two parallellarge-time drawdown lines associated with z_1 and z_2, respectively. The large-time partial penetration effect, h_p, is given in (4-19). The only unknown in (5-12) is the parameter, β, which is defined as

$$\beta = \frac{K_z}{K_r}\frac{r^2}{b^2} \tag{5-13}$$

Therefore, β can be uniquely determined from (5-12) for a known Δh. Then, K_z can be determined from (5-13) for the β value obtained. As shown in Figure 5-4, the large-time partial penetration effect, h_p, at the three depths of SE3 is plotted against different β's. Reading from Figure 5-1a, Δh between z = 5.55 m and 11.65 m is about 0.1 m, which is related to about 0.0038 for β as indicated by Figure 5-4. The large-time drawdown difference, Δh, between z=8.6 m and 11.65 m measured from Figure 5-1a is about 0.01 m, which refers to a β value approximately equal to 0.0032. These two β's determined are close and their average, 0.0035, is chosen to estimate K_z by means of (5-13). Now, K_r and r in (5-13) have to be calculated with the appropriate anisotropic conditions determined already using (5-6) and (5-7). As a result, K_z is calculated to be $5.74\text{x}10^{-5}$ m/s, which is about two order of magnitude smaller than K_x or K_y, being typical for an alluvium aquifer.

The same procedure was applied to W3 and NE6 to find K_z. However, the β values estimated for different depths in each individual data set are not close, as may be caused by the vertical heterogeneous conditions. Therefore, K_z was not further evaluated using these two sets of data, and its value is considered to be 5.74×10^{-5} m/s.

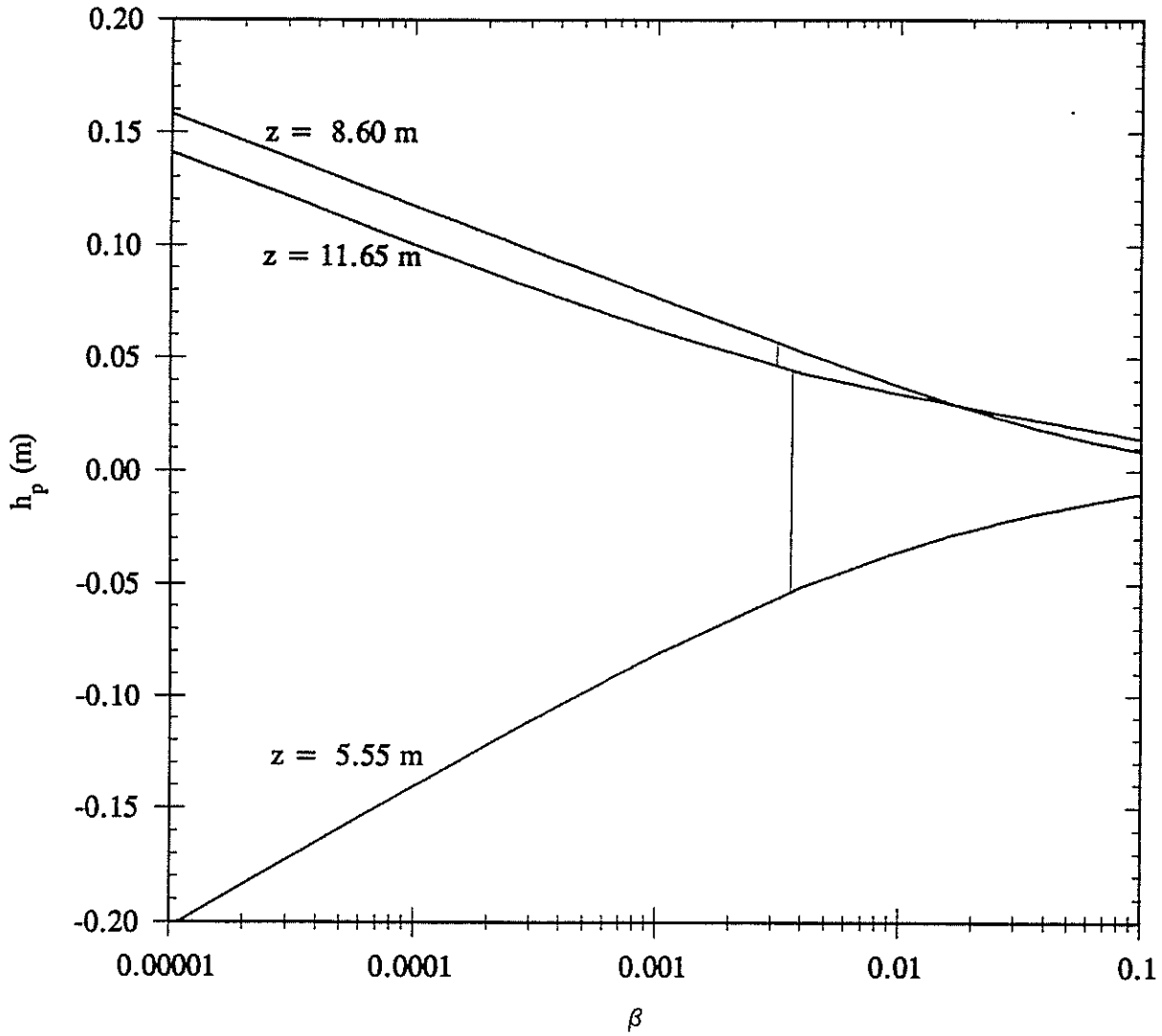

Figure 5-4 Determination of β from vertical variation of the partial penetration effect at SE3.

6. A NEW TECHNIQUE FOR USING THE MAPPING FUNCTION

As measures of the aquifer response to pumping, drawdowns are usually observed for various pumping times at observation wells or piezometers during a pumping test. Analysis of these drawdown histories with appropriate methods can reveal the hydrogeological conditions of the aquifer being tested. If the aquifer type (i.e., confined, unconfined, leaky or fractured) for a set of drawdown data is known, and appropriate well hydraulics theories are available for interpreting them, model parameters involved in these theories can be estimated by practical means such as graphic techniques. For example, Theis (1935) provided the logarithmic type-curve matching method to estimate the transmissivity and the storage coefficient of an infinitely large confined aquifer. The type-curve is the dimensionless log-log plot of the Theis (1935) solution. Cooper and Jacob (1946), however, presented a semilogarithmic method to estimate these two parameters without needing a type curve, thereby avoided curve matching. For unconfined aquifer conditions, Prickett (1965) developed a curve-matching method based on the unconfined well hydraulics theory given by Boulton (1963) to determine the hydrogeological parameters used in that theory. This was followed by Neuman's (1975) curve-matching method for determining the parameters involved in his unconfined well hydraulics theory (Neuman, 1973). Relatively comprehensive discussions on graphic methods for various problems (e.g., those related to confined, unconfined, leaky and fractured aquifers, to the determination of aquifer anisotropy or hydrogeological boundaries, and others) can be found in Kruseman and deRidder (1990), and Streltsova (1987).

In recent years, petroleum reservoir engineers have developed the so-called pressure

derivative method to characterize aquifers (Tiab and Kumar, 1980; Gringarten, 1987; Bourdet et al., 1983 and 1989; Bourdet and Gringarten, 1980; Clarke and van Golf-Racht, 1985). The pressure derivative is referred to as the derivative of drawdown with respect to the logarithmic pumping time, $\partial h/\partial(\log t)$. It has been found empirically that plots of the pressure derivatives against pumping times on logarithmic paper can yield four curve characteristics, namely, a maximum, a minimum, a stabilization and an upward/downward trend. If they exist, these characteristics appear at different pumping times and can disclose certain hydrogeological features of the reservoirs. A maximum, usually occurring at early stages of pumping, indicates wellbore storage and skin effects. A minimum, usually occurring at the intermediate pumping times, indicates replenishment through confining layers. An upward or a downward trend at late pumping times indicates an impervious hydrogeological boundary or a constant-head (recharge) hydrogeological boundary, respectively. A stabilization indicates radial flow under confined conditions without hydrogeological boundary effects. The pressure derivatives are generated without the use of any well hydraulics solutions. Thus, they are used not so much to quantitatively determine the model parameters as to qualitatively understand the pertinent hydrogeological conditions. The pressure-derivative method is useful, as a screening tool, in selecting the well hydraulics theories appropriate for the drawdown data of interest.

It has long been recognized (e.g., Wenzel, 1942; Walton, 1960; Prickett, 1965; Neuman, 1975; Streltsova, 1987) that drawdown histories from unconfined, leaky or fractured aquifers typically have three distinct sections as compared with the Theis solution. The early- and late-time sections can be fitted by the Theis solution with different values for

the storage coefficient. It is also understood that the Theis solution yields larger drawdowns for smaller storage coefficients and vice versa, provided all other conditions remain the same. These two facts suggest that a three-section (or even multiple-section) drawdown history can possibly be reproduced by the Theis solution where different values of the storage coefficient are needed to fit different sections of the drawdown history . In fact, it is formally proven below that the set of these different "pseudo-storage coefficients" forms a mapping function in time, which effectively accounts for drawdown variation caused by hydrogeological conditions not recognized by the Theis solution. To investigate the feasibility of using this "mapping function" to diagnose the hydrogeological conditions involved in drawdown data, a mathematical model is developed in an intuitive manner as

$$\frac{\partial^2 h}{\partial r^2} + \frac{1}{r}\frac{\partial h}{\partial r} = \frac{\omega(t)}{T}\frac{\partial h}{\partial t} \tag{6-1}$$

$$h(r,o) = 0 \tag{6-2}$$

$$\lim_{r\to 0}\left(r\frac{\partial h}{\partial r}\right) = \frac{-Q}{2\pi T} \tag{6-3}$$

$$\lim_{r\to\infty} h = 0 \tag{6-4}$$

where $\omega(t)$ is the mapping function. Other terms are defined at the end of the paper.

Here the analytical solution for (6-1) through (6-4) is determined, the method of finding $\omega(t)$ is established, the usefulness of employing $\omega(t)$ in interpreting drawdown data in terms of aquifer hydrogeologic conditions is evaluated, and the mapping function is used to estimate important hydrogeological parameters such as the storage coefficient and the specific yield. The new analytical solution is identical to the Theis solution on a scaled time frame, which mathematically incorporates the mapping function. Of course, the mapping function, $\omega(t)$, is problem-specific; that is, $\omega(t)$ changes with the hydrogeology. For a confined aquifer satisfying only the assumptions invoked in the Theis solution, $\omega(t)$ becomes a constant equal to the storage coefficient of the aquifer. Under this circumstance, the new analytical solution reduces to the Theis solution as expected. A robust and self-contained method was developed to determine $\omega(t)$ from field data. Through a few case studies, it was noted that a plot of $\omega(t)$ versus time exhibits distinctive characteristics that are pertinent to specific hydrogeological conditions imbedded in the drawdown data. This suggests that these plots can be used to diagnose the hydrogeology conditions. In addition, $\omega(t)$ can be employed to estimate the storage coefficient of a granular aquifer, a fracture or a porous matrix, and the specific yield of an unconfined aquifer, depending on the type of aquifer being investigated. Analytical definitions for $\omega(t)$ derived herein show that the pressure-derivative method is inversely related to $\omega(t)$, thereby theoretically justifying the empirical pressure-derivative method. They are also useful in finding quantitative information associated with the curve characteristics of $\omega(t)$.

6.1 THE ANALYTICAL SOLUTION

By making use of a new time,

$$t_s = \int_o^t \frac{dx}{\omega(x)} , \qquad \textbf{(6-5)}$$

the right-hand side term in (6-1) is changed to (1/T) $\partial h/\partial t_s$ while other terms and conditions in (6-1) through (6-4) are not altered. In terms of t_s, therefore, the new model becomes equivalent to the Theis model with a fictitious storage coefficient being equal to unity. As a result, the new solution must be mathematically identical to the Theis solution written in terms of t_s, or

$$h(r,t) = \frac{Q}{4\pi T} \int_u^\infty \frac{e^{-x}}{x} dx \; ; \quad u = \frac{r^2}{4Tt_s} \qquad \textbf{(6-6)}$$

where t_s is defined by (6-5). If $\omega(t)$ is constant (say, equal to the storage coefficient S), t_s defined by (6-5) reduces to t/S and (6-6) becomes identical to the Theis solution. Thus, the Theis solution is a special case of the new solution.

6.2 DETERMINATION OF THE MAPPING FUNCTION FROM FIELD DATA

For a given set of observed drawdown data, (h_i, t_i) with i = 1,2, ...N, the mapping function $\omega(t)$ can be estimated by the following four steps.

1. The value of the constant T is needed for the determination of $\omega(t)$. By making use

of the early-time (the first section) data with the Theis solution through curve-matching techniques or other appropriate methods, T can be estimated.

2. Once T is known, the only unknown in (6-6) is t_s (without recourse to the integral definition). Since (6-6) is a monotonically increasing function, there is a single corresponding t_{si} for each given observation h_i. By treating t_s as the root of (6-6) for the given h, each t_{si} can be determined by applying Newton-Raphson or other search methods to (6-6) and the corresponding h_i. Thus the one-to-one relationship of (h_i, t_{si}) can be determined without difficulty.

3. The one-to-one relationship of (t_{Si}, t_i) can be uniquely derived from the (h_i, t_{Si}) obtained in step 2 and the given field data of (h_i, t_i). These three relationships, (h_i, t_i), (h_i, t_{Si}), and (t_{Si}, t_i) are used to determine $\omega(t)$.

4. Differentation of t_s given by (6-5) with respect to t gives

$$\frac{dt_s}{dt} = \frac{d}{dt}\int_0^t \frac{dx}{\omega(x)} = \frac{1}{\omega(t)}$$

which yields the first functional definition for $\omega(t)$ as

$$\omega(t) = \frac{dt}{dt_S} \tag{6-7}$$

Since (t_{si}, t_i) have been determined in step 3, the derivative in (6-7) can be calculated numerically to obtain $\omega(t)$. Without contradicting (6-7), another way of mathematically defining $\omega(t)$ is

$$\frac{\partial h}{\partial t_s} = \frac{\partial h}{\partial t}\frac{dt}{dt_s} = \frac{\partial h}{\partial t}\,\omega(t)$$

which results in a second functional definition for $\omega(t)$ as

$$\omega(t) = \frac{\partial h/\partial t_S}{\partial h/\partial t} \tag{6-8}$$

In (6-8), the derivatives can be numerically calculated from (h_i, t_{si}) and (h_i, t_i). Since $\partial h/\partial t_S$ can also be analytically determined from (6-6), using the Liebniz rule for differentiation of integrals, a third functional definition for $\omega(t)$ can be derived from (6-8) by replacing the numerator with its analytical expression as

$$\omega(t) = \frac{Q}{4\pi T}\,\frac{1}{t_s}\frac{e^{-u}}{\partial h/\partial t} \quad ; \; u = \frac{r^2}{4Tt_S} \tag{6-9}$$

where, again $\partial h/\partial t$, is estimated numerically.

Equations (6-7), (6-8) and (6-9) give three different legitimate ways of calculating the mapping function $\omega(t)$. They do not contradict one another yet they may lead to different accuracy calculations, depending on the data frequency, noise and the profiles (i.e., the

curvatures) embedded in (h_i, t_i), (h_i, t_{si}) and (t_{si}, t_i). The derivatives involved in (6-7), (6-8) and (6-9) can be calculated with finite-difference schemes of uneven increments or the weighted difference method as used for calculating pressure derivatives.

Since discrete data points are included in (h_i, t_i), (h_i, t_{si}) or (t_{si}, t_i), the mapping function $\omega(t)$ is obtained in a discrete fashion as well; that is, for each t_i there is a corresponding $\omega(t_i)$. The discrete $\omega(t_i)$ can be expressed in certain fitted functions by cubic spline, polynominal approximation or some other regression analysis. This is discouraged because the fitted functions are nonunique for the given $\omega(t_i)$, do not necessarily provide more detailed information than the characteristics shown by the discrete $\omega(t_i)$ itself, and may render the integration of (6-5) difficult.

It is understood that drawdowns in the scaled-time domain must follow the Theis solution with a fictitious storage coefficient equal to unity. Thus, plotting measured drawdowns against the obtained t_s on logarithmic paper should be matchable by a logarithmic Theis curve with S equal to one and the transmissivity equal to the value of T used in step 1. When the plot is made on semilogarithmic paper, Jacob's method can be used to verify the T and fictitious S values. These practices can reveal the accuracy of t_s values obtained.

The accuracy of the estimated mapping function $\omega(t_i)$ can be checked by the following procedure. The discrete function $\omega(t_i)$ is treated as a piece-wise continuous function

$$\omega(t_i) = \omega_i, \quad t_{i-1} \le t \le t_i, i = 1,2,....N, t_o = 0 \qquad \textbf{(6-10)}$$

Integration of (6-10) in accordance with (6-5) yields a new set of scaled times, denoted by

t'_{si}, as

$$t'_{Si} = \int_0^{t_i} \frac{dx}{\omega(x_i)} = \frac{t_1}{\omega_1} + \frac{t_2 - t_1}{\omega_2} + ... + \frac{t_i - t_n}{\omega_n} \; ; \; n \leq N \qquad \textbf{(6-11)}$$

Now it is seen that the piece-wise continuous expression of $\omega(t_i)$ renders the integration of (6-5) a simple algebraic function, significantly simplifying the calculation of t'_{si}. If $\omega(t_i)$ is exactly estimated from field data, t'_{si} should be identical to t_{si} as calculated in step 2. Numerical computation of derivatives across discrete field data, as required in determining $\omega(t_i)$, is sensitive to data noise. Therefore, t'_{si} is never identical to t_{si}, which is determined without the involvement of $\omega(t)$. In general, t_{si} is more accurate than t'_{si}, and thus the comparison of them indicates the accuracy of the estimated mapping function $\omega(t_i)$. It should be noted that the accuracy of numerical search for t_{si} can also be checked by the method given above; additional improvement of this accuracy as needed can be achieved through the searching schemes without difficulty.

There are three relationships, (6-7), (6-8) and (6-9), that can be used to determine $\omega(t)$. They yield different degrees of accuracy for $\omega(t)$ for the same set of given data. It seems that (6-9) should give the best estimation for $\omega(t)$ as the term of $\partial h/\partial t_s$ is analytically determined in it. However, this is not the case, and no general rules are available for guiding the selection of these three equations for the most accurate estimation of $\omega(t)$. It is thus suggested that all of them be used to obtain three sets of $\omega(t_i)$, which can then be used to generate three sets of t'_{si}, respectively. Comparing each set of t'_{si} with t_{si} gives information on the most accurate set of $\omega(t_i)$.

The set of t'_{si} associated with the most accurate $\omega(t_i)$ is used in (6-6) to determine the "calculated drawdowns" for known Q, r and T. The comparison of calculated and measured drawdowns indicates the reproducibility of the field data behavior by (6-6) and the proposed modelling approach. Although being more accurate than t'_{si}, t_{si} is not employed to determine the calculated drawdown because its estimation is independent of the essential element in the new solution, the mapping function $\omega(t)$. Specifically, t_{si} is developed as ad hoc information for completing the estimation of $\omega(t)$ and the calculated drawdown. It has been found that this mapping function is not very sensitive to the value of T in the sense that no significant changes in magnitudes and curve characteristics of $\omega(t)$ are noted by varying T up to about fifteen percent of the difference. However, if the T value used is incorrect, the calculated drawdowns will not converge to the observed. In this event, T needs to be redetermined with more care.

The method of determining the mapping function $\omega(t)$ developed here is robust. The completeness of this self-contained method is ensured by the fact that only the field data and mathematical relationships rigorously derived from the solution of interest are used.

In (6-8), the numerator of $\partial h/\partial t_s$ actually represents the drawdown rate for the Theis solution. The denominator of $\partial h/\partial t$ represents the actual drawdown rate, which is a function of the field hydrogeological conditions. Thus, the logarithmic $\omega(t)$ demonstrates the difference between the hydrogeological conditions involved in actual drawdown data and those in the Theis solution, as shown by

$$\log\ \omega(t)\ =\ \log\frac{\partial h}{\partial t_s}\ -\ \log\ \frac{\partial h}{\partial t} \qquad \textbf{(6-12)}$$

This suggests that for diagnostic purposes, the mapping function $\omega(t)$ should be plotted on log-log paper. It also proves that the mapping function indeed involves information on hydrogeological conditions not set forth in the Theis solution.

6.3 APPLICATION AND DISCUSSIONS

To demonstrate the usefulness of this new approach in diagnosing the hydrogeological conditions embedded in drawdown data, (6-6) is first employed to analyze a set of hypothetical data prepared with the Theis solution using Q = 1.74 m^3/min, T= 0.77 m^2/min and S = $2x10^{-4}$. The observation well, where the hypothetical drawdown is calculated, is 60 m from the pumping well (i.e., r = 60 m). The mapping function $\omega(t)$ obtained using the method discussed above with an input T of 0.77 m^2/min is indeed a constant, of which the magnitude is $2x10^{-4}$ as shown in Figure 6-1.

To understand the effects of boundary conditions on the mapping function, (6-6) is employed to analyze another two sets of hypothetical data prepared with the Theis solution and image wells for a recharge or an impervious boundary. The recharge or the impervious boundary is 300 m from the pumping well in a direction normal to that formed by the pumping and observation wells. Thus, in the calculation, the image well substituting the impermeable or the recharge boundary is 540 m from the observation well (i.e., r_i = 540 m). For comparison purposes, the analysis results are also shown in Figure 6-1.

At large pumping times, an upward trend of $\omega(t)$ is associated with a recharge boundary and a downward trend with an impermeable boundary. These trends can be formally verified in light of (6-8). After the recharge boundary influences the drawdown, the actual drawdown rate ($\partial h/\partial t$) becomes smaller than that without the boundary influences (i.e., $\partial h/\partial t_s$). Accordingly, under the influence of a recharge boundary, $\omega(t)$ continuously increases with time. The mapping function $\omega(t)$ will increase to infinity when the steady-state condition is established because $\partial h/\partial t$ is zero under such a condition. The influence of an impermeable boundary is that the drawdown rate ($\partial h/\partial t$) becomes large relative to $\partial h/\partial t_s$. As a result, $\omega(t)$ continuously decreases under the influence of an impermeable boundary.

As a matter of fact, quantitative information on the large-time trend of $\omega(t)$ can be found by calibrating (6-8) against the theoretical $\partial h/\partial t$. For large times, the drawdown function in t_s can be written, using the logarithmic approximation of the Theis well function, as

$$h(r,t_S) = -C \ln(\frac{\delta r^2}{4Tt_S}); \qquad C = \frac{Q}{4\pi T} \tag{6-13}$$

where $\delta = \exp(0.5772) = 1.78$. The following two relationships can be derived from (6-13)

$$\frac{\partial h}{\partial t_S} = \frac{C}{t_S} \tag{6-14a}$$

and

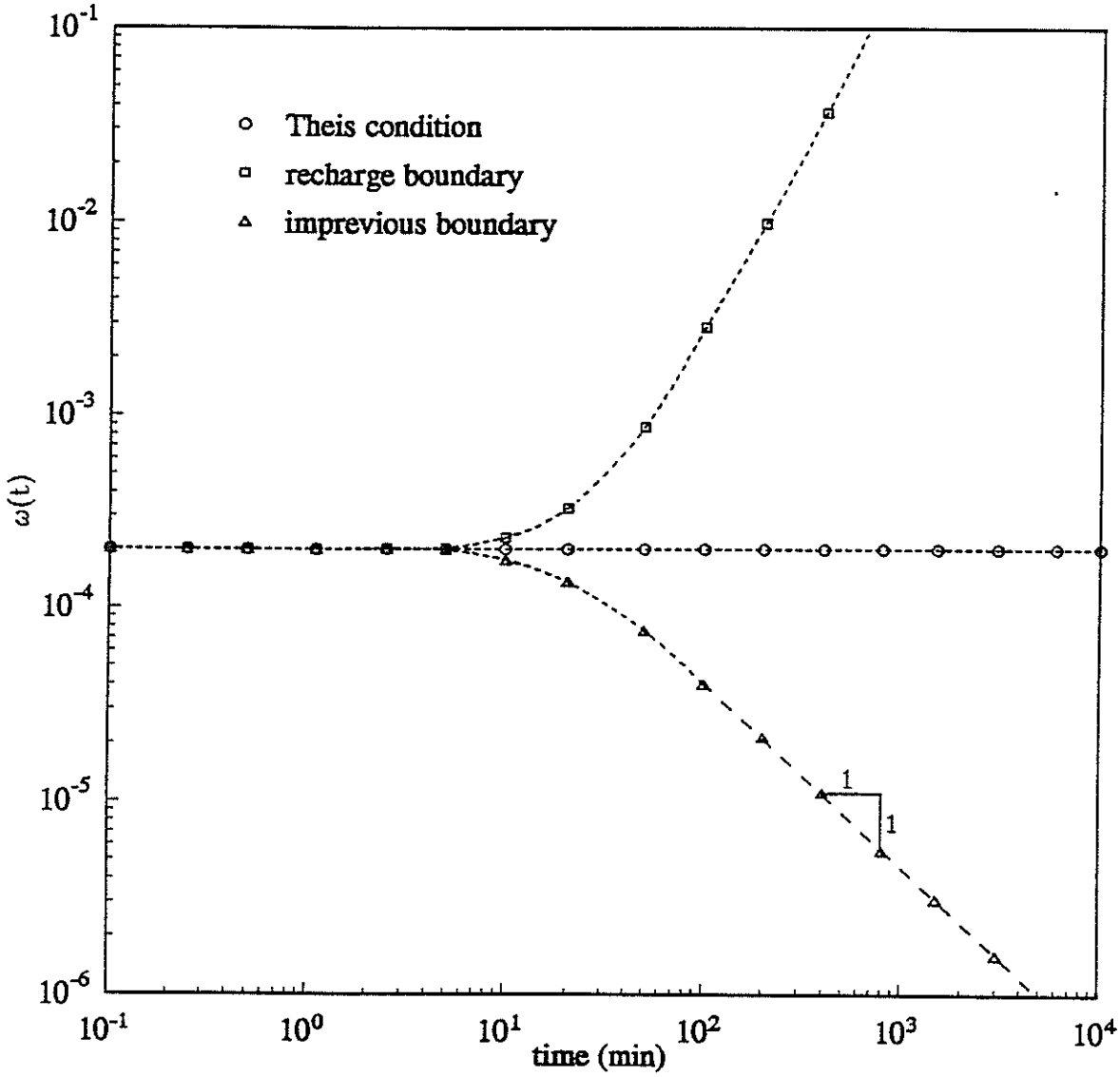

Figure 6-1 Mapping function analysis of hypothetical data with influence of an impermeable or a recharge boundary.

$$t_S = \frac{\delta r^2}{4T} \exp\ [h(r,t_s)/C] \qquad \textbf{(6-14b)}$$

The hypothetical drawdown subject to an impervious boundary for large times can be determined as

$$h(r,t) = -C[\ln(u_r) + \ln(u_i)] \qquad \textbf{(6-15a)}$$

or

$$\frac{\partial h}{\partial t} = \frac{2C}{t} \qquad \textbf{(6-15b)}$$

where

$$u_r = \frac{\delta r^2 S}{4Tt}$$

$$u_i = \frac{\delta r_i^2 S}{4Tt}$$

It is important to note that at the appropriate scaled time t_s, h(r,t) equals $h(r,t_s)$. Therefore,

the substitution of (6-15a) into (6-14b) gives

$$t_S = t^2/C_1 \tag{6-16}$$

where

$$C_1 = \frac{\delta r_i^2 S^2}{4T}$$

Substituting (6-16) into (6-14a) gives

$$\frac{\partial h}{\partial t_S} = \frac{CC_1}{t^2} \tag{6-17}$$

By introducing (6-17) and (6-15b) to (6-8), the mapping function ω(t) at large time is

$$\omega(t) = \frac{C_1}{2}\frac{1}{t} \tag{6-18a}$$

or

$$\log\ \omega(t) = \log\frac{C_1}{2} - \log\ t \tag{6-18b}$$

Therefore, when subject to an impervious boundary, the downward trend of $\omega(t)$ at large times has a slope equal to -1 on a log-log plot of $\omega(t)$ versus t. This negative unity slope is clearly shown in Figure 6-1.

For a recharge boundary, the hypothetical drawdown at large times can be calculated with (6-15a) where a negative sign instead of a plus sign is used between the two logarithmic functions. As a result, the drawdown becomes independent of time (the steady-state condition), and $\partial h/\partial t$ is zero. This proves that the upward trend of $\omega(t)$ for a recharge boundary increases to infinity on a log-log plot of $\omega(t)$ versus t.

This analysis shows that the mapping function $\omega(t)$ reflect the existence of a nearby impervious or recharge boundary condition, in spite of the assumption of an infinite flow domain for the new model. In a log-log plot of $\omega(t)$ versus t, the downward trend for an impervious boundary has a slope equal to -1 at large time, and the upward trend for a recharge boundary increases rapidly to infinity at large times. The analytical definitions of $\omega(t)$ are useful in interpreting the information contained in the empirical plots of $\omega(t)$.

Application of (6-6) to analyze field drawdown data is given below for three case studies. It will be shown that the mapping function is significantly different for each situation, and can be used to estimate the storage coefficients and the specific yields, depending on the type of aquifers involved.

Case Study 1: Tabulated field data from Walton (1987; Table 5.6)

This data set was taken from an unconfined aquifer where Q = 3.79 m^3/min (1000 gpm) and r = 61 m (200 ft). Using the method given by Neuman (1975), Walton (1987)

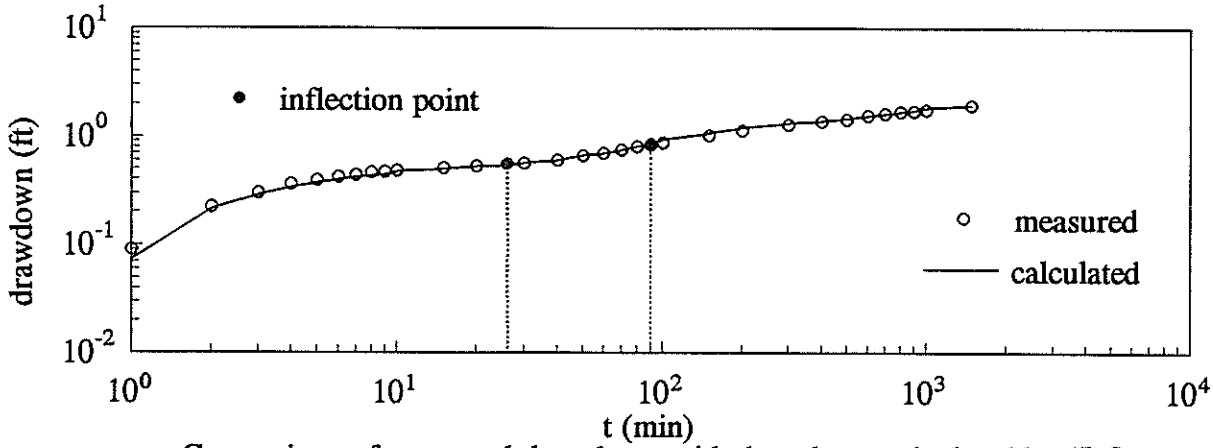

a. Comparison of measured drawdown with drawdown calculated by (5-6) using the estimated mapping function.

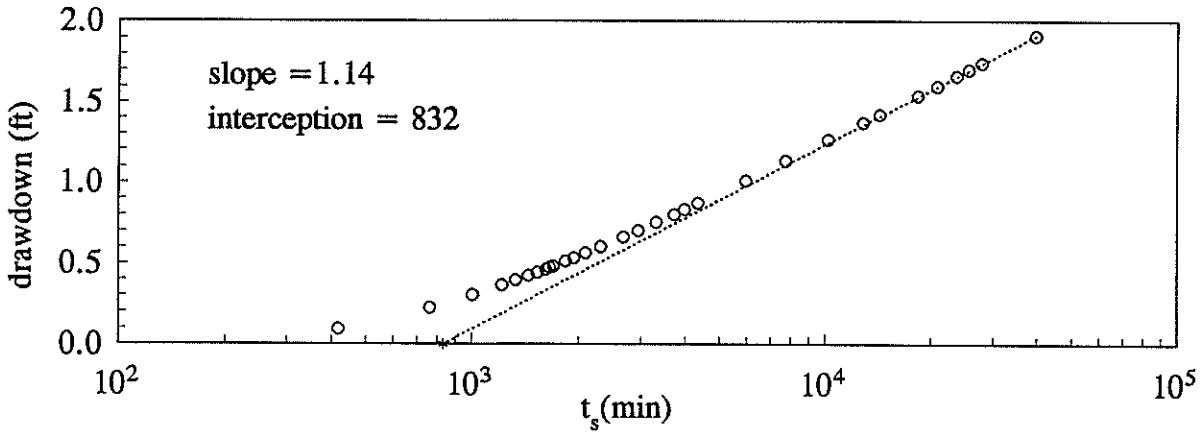

b. Semilogarithmic presentation of measured drawdown versus scaled time.

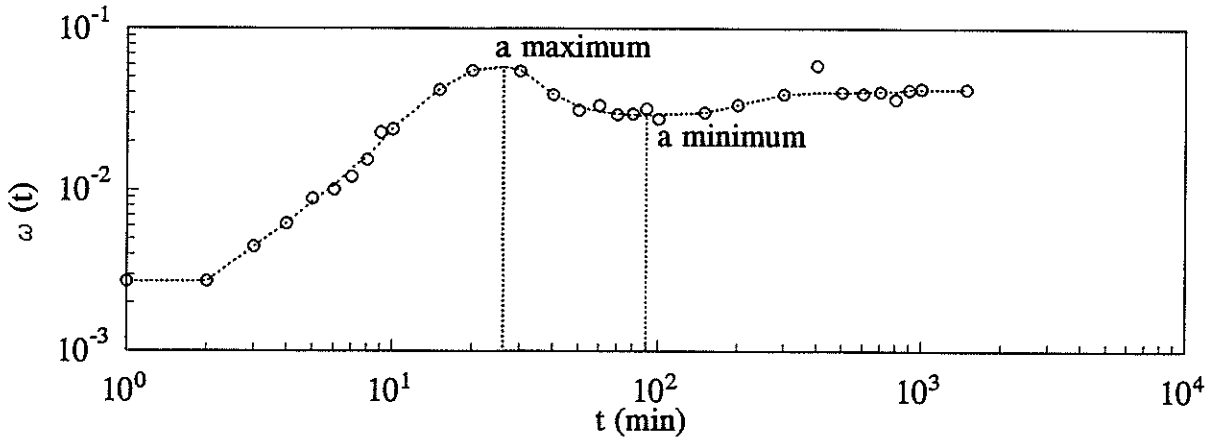

c. Logarithmic plot of the estimated mapping function.

Figure 6-2 Mapping function analysis of field data given by Walton [1987; Table 5.6].

obtained the following results: $S = 2.33 \times 10^{-3}$, $S_y = 3.17 \times 10^{-2}$ and the average $T = 2.35$ m^2/min.

Results from (6-6) with an input T of 2.01 m^2/min are presented in Figure 6-2. As shown by Figure 6-2a, good agreement is observed for the measured and calculated drawdowns, demonstrating the ability of (6-6) to reproduce field data. In Figure 6-2b measured drawdowns are plotted against the logarithmic scaled times t_s. As expected, a straight line is found at large scaled times. Its slope of about 1.14 leads to a value of 1.99 m^2/min for T, which is about one percent different from the input T. The intercept occurs at t_s equal to about 823 min, which yields a value of 1.02 for the fictitious storage coefficient, close to the desired value of 1. These results indicate that t_s and $\omega(t)$ are accurately estimated.

The estimated mapping function from the approach outlined above is shown in Figure 6-2c, where four sections can be noticed. The first section lasts for about two minutes after pumping starts. In the first section, $\omega(t)$ is nearly a constant approximately equal to 3.2×10^{-3}. This constant value is consistent with the storage coefficient of the unconfined aquifer, 2.33×10^{-3}, as estimated by Walton (1987). The second section is from 2 minutes to about 23 minutes; during this period $\omega(t)$ gradually increases to a maximum which occurs approximately around 23 minutes and equals 5.5×10^{-2}. The third section is from 23 minutes to around 95 minutes; during this period $\omega(t)$ gradually decreases from the maximum to a minimum which occurs approximately around 95 minutes and equals 3.6×10^{-2}. The fourth section is from 95 minutes to the end of pumping; during this period $\omega(t)$ increases from the minimum to a plateau which has a relatively constant $\omega(t)$ approximately equal to

about 4.2×10^{-2}. This temporal variation of $\omega(t)$ can be attributed to the water table decline effects on the drawdown data, which are initially negligible, change to a maximum and a minimum during the intermediate pumping period, and then are stabilized at large pumping times.

The relatively constant $\omega(t)$ in the first section indicates that at small pumping times unconfined groundwater flow can be approximated by the Theis solution using the aquifer storage coefficient instead of the specific yield; here S is estimated as 3.2×10^{-3} from the value of $\omega(t)$ obtained at early time. The stable $\omega(t)$ in the fourth section indicates that unconfined groundwater flow at large pumping times can also be approximated by the Theis solution where the sum of S and S_y is used in lieu of the storage coefficient; here the sum of S and S_y is 4.2×10^{-2} as determined from $\omega(t)$. As a result, S_y is calculated to be 3.88×10^{-2}, which is in reasonably good agreement with 3.17×10^{-2}, as determined by Walton (1987). Therefore, the mapping function $\omega(t)$ can also be used to estimate the storage coefficient and the specific yield of an unconfined aquifer.

Comparing $\omega(t)$ with the drawdown history shown in Figure 6-2a, it is interesting to note that the maximum and minimum points of $\omega(t)$ correspond with the two inflection points of the drawdown history. The maximum of $\omega(t)$ occurs at about 23 minutes, while the first inflection point of drawdown history is at about 25 minutes. The minimum of $\omega(t)$ occurs at about 95 minutes, while the second inflection point is at about 100 minutes. This correspondence is theoretically based, and can be mathematically verified. Differentiation of (6-8) with respect to t gives

$$\frac{\partial \omega}{\partial t} = \frac{\partial}{\partial t}\left[\frac{\partial h/\partial t_s}{\partial h/\partial t}\right] = -\frac{\partial h}{\partial t_s}\frac{\partial^2 h/\partial t^2}{(\partial h/\partial t)^2} \qquad \textbf{(6-19)}$$

where $\partial h/\partial t_s$ is independent of t.

The maximum or minimum of $\omega(t)$ occurs at the point which $\partial\omega/\partial t$ is zero. The right-hand side of (6-19) can be zero only if drawdown acceleration $\partial^2 h/\partial t^2$ is zero, since $\partial h/\partial t_s$ can never be zero and $\partial h/\partial t$ is always finite and nonzero for the conditions of interest. The points with $\partial^2 h/\partial t^2$ being zero are the inflection points of the drawdown history. Therefore, it is formally shown that the maximum or minimum of $\omega(t)$ corresponds to the inflection point in the drawdown history.

Case Study 2: <u>Tabulated field data from Kohlbeck and Alvarez (1991; Table 2.a)</u>

This data set has been inadequately analyzed with the leaky aquifer solution given by Hantush and Jacob (1955), as recognized in the original paper. When the measured drawdowns are plotted against the logarithmic pumping times as shown in Figure 6-3, a sigmoid curve appears, which is typical for drawdown data taken from a confined aquifer connected to a recharge (constant-head) boundary. The appropriate inflection-point graphic method developed by Hantush (1959) was used to analyze the data, where Q = 8.7 m^3/min and r = 105 m. Pertinent information for the graphic method is: the maximum drawdown is 2.16 m, the straight line passing through the inflection point has a slope of 1.05 m/min, and the inflection point occurs at h = 1.17 m and t = 52 minutes. As a result, T is estimated to be 1.44 m^2/min, and S is 1.34 x 10^{-3}.

The results obtained by (6-6) with an input T of 1.49 m^2/min are presented in Figure 6-4. Comparison of measured and calculated drawdowns is given in Figure 6-4a, where an

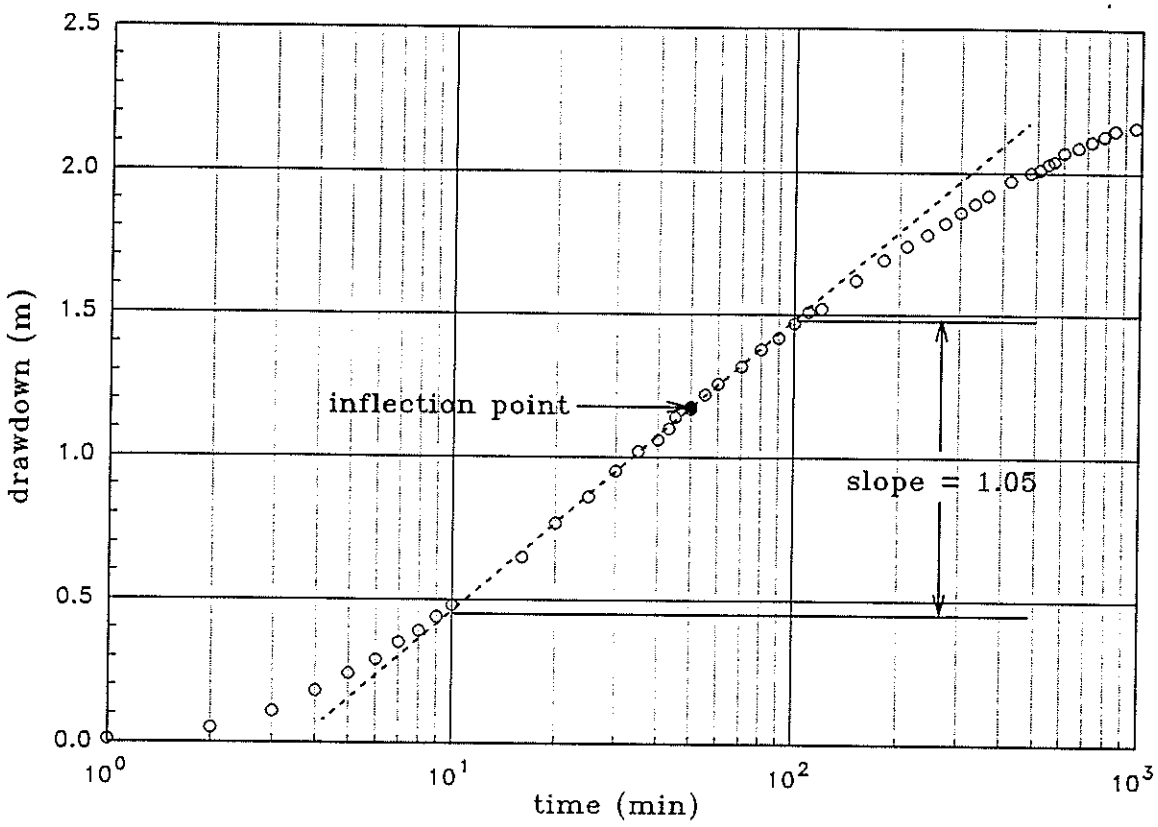

Figure 6-3 Semilogarithmic analysis of field data given by Kohlbeck and Alvarez [1991; Table 2a].

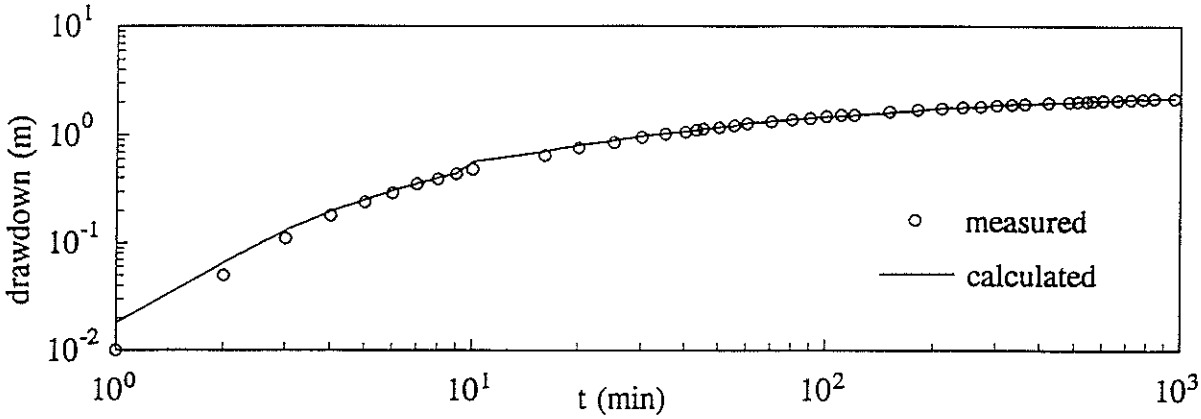

a. Comparison of measured drawdown with drawdown calculated by (5-6) using the estimated mapping function.

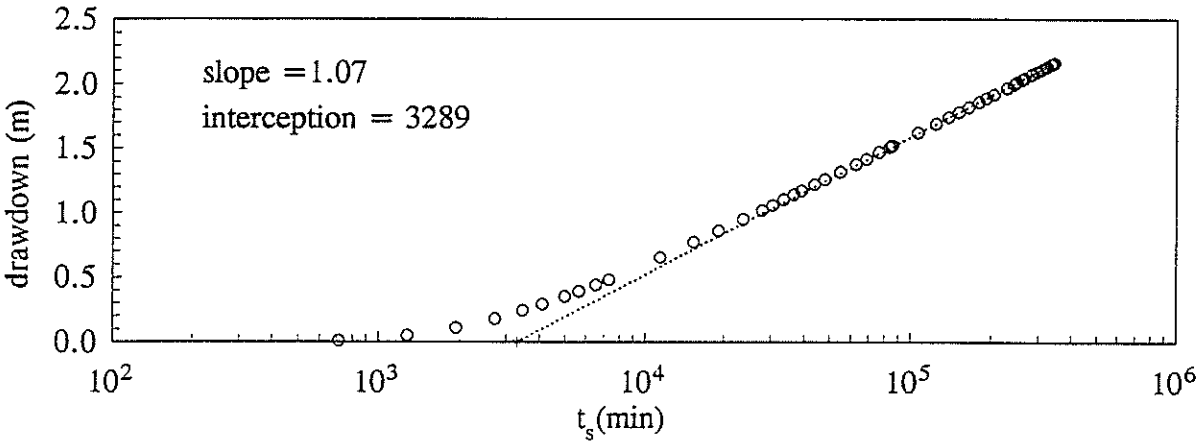

b. Semilogarithmic presentation of measured drawdown versus scaled time.

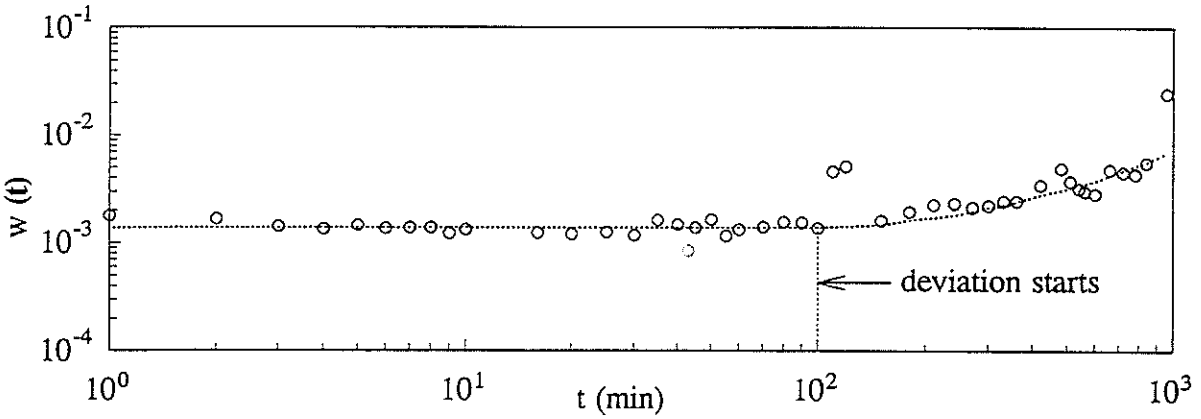

c. Logarithmic plot of the estimated mapping function.

Figure 6-4. Mapping function analysis of field data given by Kohlbeck and Alvarez [1991; Table 2a].

excellent agreement can be noted. The semilogarithmic plot of measured drawdowns against the scaled times from integration of $\omega(t)$ is shown in Figure 6-4b, from which T is estimated to be 1.49 m^2/min and the fictitious storage coefficient to be 1.01. Both of them are very close to their assumed values of 1.44 m^2/min and 1.0, respectively.

The mapping function obtained is shown in Figure 6-4c. A relatively constant value of about 1.3×10^{-3} prevails for approximately the first 50 minutes, and then $\omega(t)$ increases continuously to the end of pumping. This variation of $\omega(t)$ fits the finding discussed above. That is, the relatively long prevailing time for a constant $\omega(t)$ implies that the aquifer is under confined condition (at least for this time period), and the upward trend at the later pumping period is caused by recharge-boundary effects. The deviation time of 50 minutes coincides with the time of the inflection point on the drawdown data, the later increase in $\omega(t)$ indicates the boundary recharge.

Case Study 3: Tabulated field data from Moench (1984; Table 2)

The drawdown history of the observation well (UE-25a #1) was taken from the fractured formation in the vicinity of Yucca Mountain at the Nevada Test Site. According to Moench (1984b), the fractured formation has a thickness of about 400 m, and consists of five major zones of groundwater entry. The observation well is 110 m from the pumping well (UE-25b #1), which had a constant pumping rate of 2.15 m^3/min (35.8 l/s) for the pumping test of interest. Using a fracture skin model with consideration of wellbore storage, the hydraulic conductivity and the specific storage of the fissure system were estimated to be 6×10^{-4} m/min (1×10^{-5} m/s) and 1.5×10^{-6} m^{-1}, respectively.

For the current study, the early time scattered drawdown data from 0.5 minute through 1.4 minutes, and at 1.8 and 2.0 minutes are discarded. Also, data points showing the same measured drawdowns for sequential observation times are smoothed by assigning the drawdown values to the intermediate time. For example, 0.528 m reported for t = 800 and 900 minutes was assigned to t = 850 minutes, and the two data points of 800 and 900 minutes were discarded. Without doing this, the derivative of drawdown with respect to time between t = 800 and 900 minutes is infinity, leading to erroneous estimation of $\omega(t)$. The early time, first-section drawdown history covers data points from 1.6 minutes to about 20 minutes, from which the transmissivity and the storage coefficient of the fractures were estimated by the Theis curve matching method as 0.71 m^2/min and 9.5×10^{-4}, respectively. They are not converted to hydraulic conductivity and specific storage due to the lack of information on fracture apertures.

The results of the data analysis using (6-6) are demonstrated in Figure 6-5. Again, Figures 6-5a and 6-5b show the accuracy and reproducibility of (6-6) in dealing with this set of field data. In Figure 6-5c, the characteristics of $\omega(t)$ obtained are shown. Four distinct sections can be noted. The first section ends at t = 20 minutes and shows a constant $\omega(t)$ of about 10^{-3}, in good agreement with the storage coefficient value obtained from the Theis curve matching method. The second section starts at t = 20 minutes, linearly increases, and ends at about 140 minutes where $\omega(t)$ is equal to about 2.6×10^{-2}. In the second section, $\omega(t)$ has increased by about 26 times (i.e., from 10^{-3} to 2.6×10^{-2}) over a pumping period of about 120 minutes. This increase of $\omega(t)$ can be related to the replenishment effects generated by the fact that the porous matrix stores and then releases water to the fracture. Accordingly,

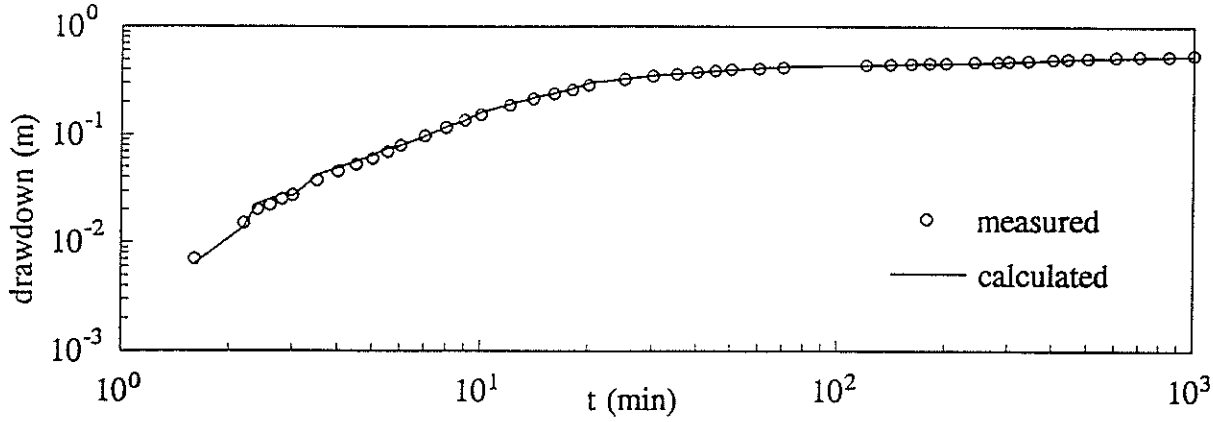

a. Comparison of measured drawdown with drawdown calculated by (5-6) using the estimated mapping function.

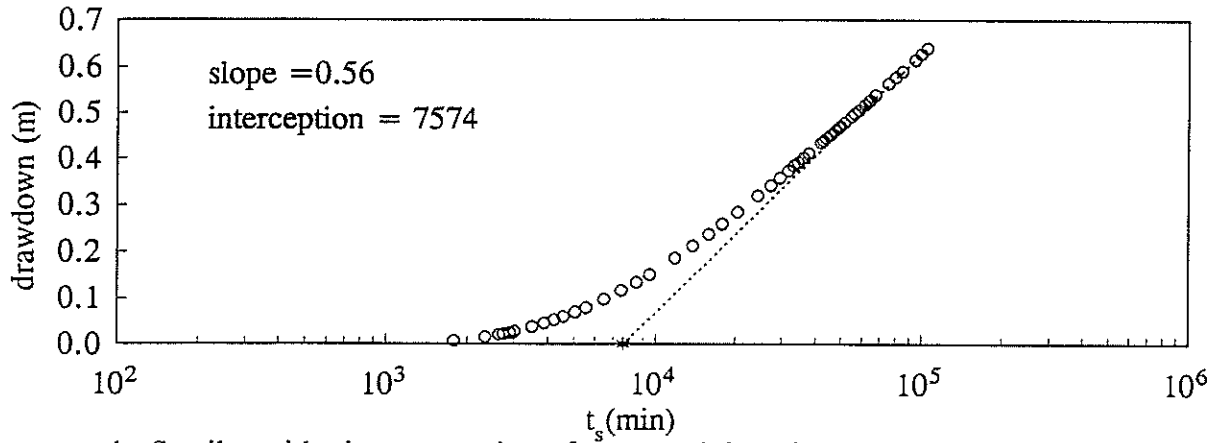

b. Semilogarithmic presentation of measured drawdown versus scaled time.

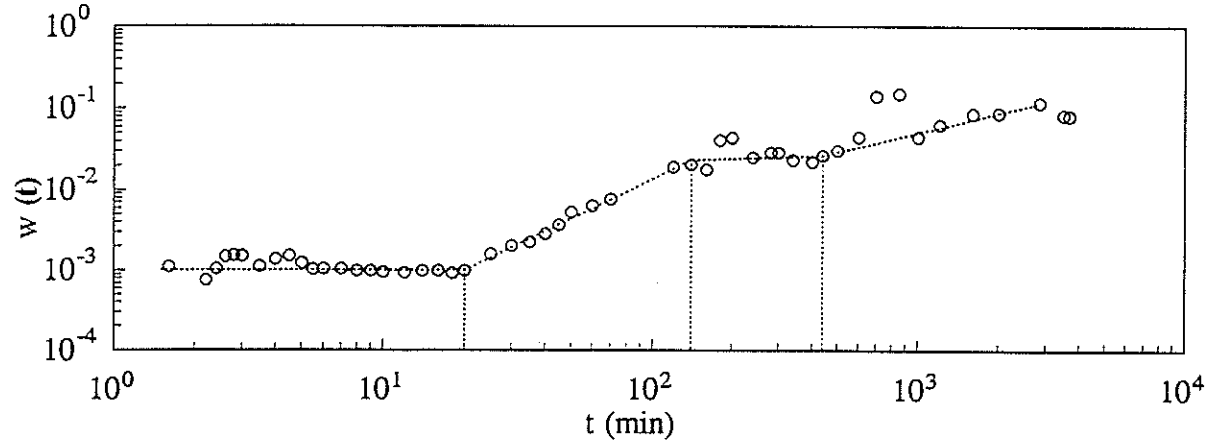

c. Logarithmic plot of the estimated mapping function.

Figure 6-5. Mapping function analysis of field data given by Moench [1984; Table 2].

the porous matrix starts to replenish the fractures at about t = 20 minutes, under a steadily increasing rate until about t = 120 minutes. After the end of the second section, $\omega(t)$ remains constant for about 360 minutes; that is, the third section has a constant $\omega(t)$ of 2.6×10^{-2} from t = 140 to about 500 minutes. For the stable $\omega(t)$ in the third section, one can consider that the vertical hydraulic gradients and thus the associated replenishing flow from the porous matrix to the fractures reaches a local equilibrium condition. If the stable $\omega(t)$ of 2.6×10^{-2} is considered to be the sum of the storage coefficient of fractures and porous matrices, S of the porous matrix is 2.5×10^{-2}. This converts to 3.13×10^{-4} m^{-1} for the specific storage using 80 m for the block thickness as suggested by Moench (1984b). This value is in agreement with the porous matrix specific storage, 3×10^{-4} m^{-1}, as obtained by Moench (1984b). Here, it is seen that the mapping function $\omega(t)$ is able to estimate the storage coefficient of the fracture and the matrix.

It is interesting to note that $\omega(t)$ starts to steadily increase again after 500 minutes. This steady increase does not resemble the rapid growth representing a recharge boundary as shown in Case Study 2. One possible explanation for the fourth section is that the fractured aquifer is a "penta-porosity" system consisting of five major zones of water entry. The inter-fracture porous blocks may replenish these water entry zones at different times and with different rates. These delayed influences may create the multiple sections of $\omega(t)$. Other additional drawdown/mapping function sections could have appeared if more data points had been available. Abdassah and Ershaghi (1986) demonstrate three sloped sections of triple-porosity fractured reservoirs in the semilogarithmic plot of drawdown versus pumping times. To verify further this penta-porosity phenomenon, more drawdown data from longer pumping

tests are needed. Nevertheless, it is of interest to know that the characteristic features of $\omega(t)$ for this fractured formation are distinctively different from those of granular aquifers as shown in Case Study 1. That is, multiple straight line sections appear in $\omega(t)$ for the fractured conditions while smooth, curved straight sections are shown in $\omega(t)$ for granular aquifers.

6.4 RELATION BETWEEN THE MAPPING FUNCTION AND PRESSURE-DERIVATIVE DATA

It is of interest to recognize that some of the pressure derivative characteristics are inversely related to those of $\omega(t)$. For example, replenishment to the aquifer leads to a maximum in $\omega(t)$ and a minimum in pressure derivative data. An impervious (or a recharge) boundary induces a downward (or an upward) trend at the end of $\omega(t)$ while an upward (or a downward) trend at the end of the pressure derivative data. This inverse relationship can be understood by noting that the denominator of (6-8) can be replaced by its equivalent form of $\partial h/\partial(\log t)$ (i.e. the pressure derivatives). As a result, $\omega(t)$ can be redefined as

$$\omega(t) = \frac{2.30t\ \partial h/\partial t_s}{\partial h/\partial\ (\log\ t)} \qquad \textbf{(6-20)}$$

Equation (6-20) mathematically demonstrates that the characteristic features of pressure derivative data are inversely exhibited by $\omega(t)$. This, however, does not mean that $\omega(t)$ is the inverse of the pressure derivative because they have completely different mathematical and practical significance. As a matter of fact, the characteristic features of $\omega(t)$ are more versatile than those shown by the pressure derivative data. For example, the

feature of multiple linear sections of $\omega(t)$ in Case Study 3 is not among the four curve characteristics of the pressure derivatives. The minimum of $\omega(t)$ as shown in Case Study 1 is not displayed as a maximum in the associated pressure derivative data. In pressure derivative data, a maximum, if it exists, always occurs at "early times", indicating the wellbore storage or skin effects. Our own studies and available literature never document that a maximum of pressure derivative data can occur in the same way as a minimum of $\omega(t)$ does. Also, the mapping function $\omega(t)$ can yield information on the estimation of important hydrogeological parameters such as the storage coefficient and the specific yield. This can not be done by the pressure-derivative method.

6.5 CONCLUSIONS

A mathematical model is developed to investigate the feasibility of using the mapping function in interpreting drawdown data. The analytical solution of this model and the method of determining the mapping function are obtained. The mapping function is problem-specific; i.e., different drawdown data yield different mapping functions. When plotting the mapping function on logarithmic paper, distinctive curve characteristics exhibited are related to specific hydrogeological conditions. For example, a maximum and a minimum stand for an unconfined aquifer, an upward trend at the end for a recharge boundary, a downward trend at the end for an impermeable boundary, multiple linear sections for fractured aquifers, and an stabilization (constant) for confined aquifers satisfying the assumptions of the Theis solution. Functional definitions for the mapping function are obtained. They prove that (1) the pressure-derivative data are inversely related to $\omega(t)$, thereby rendering some theoretical

justification of the pressure-derivative method which was developed empirically, (2) minima or maxima of $\omega(t)$ correspond to the inflection points on the drawdown-history curves, and (3) $\omega(t)$ indeed represents hydrogeological conditions not set forth in the Theis solution when plotted on logarithmic paper. The functional definitions are also useful in finding quantitative information contained in the curve characteristics of the mapping function. It has been demonstrated through a few case studies that the mapping function not only can reveal pertinent hydrogeological features influencing the drawdown data but also is capable of estimating the storage coefficients and the specific yields of aquifers. This method complements other available methods for interpreting pumping test data, and is useful in diagnostically understanding the hydrogeological conditions imbedded in drawdown data. This method is able to handle a broader spectrum of hydrogeological conditions than studied here. More research is needed to fully explore how to use the mapping function in diagnosing and determining the aquifer anisotropy, the partially penetrating pumping effects, the wellborne storage effects, the wellbore skin effects, and other practical concerns. It is also of great interest to find how to relate the mapping function to the hydrogeological conditions investigated by various available well hydraulics theories.

7. ISSUE OF ASYMPTOTIC CALCULATION OF WELL HYDRAULICS

The Laplace transform with respect to time has been normally used to find analytical solutions of well hydraulics problems. When the Laplace-domain counterparts are complicated, their Laplace inverse can be difficult and sometimes asymptotic solutions valid only for small or large times were determined. The relation that t is inversely related to p has been normally employed to determine the asymptotic solutions. Although this relation is correct, its application in finding asymptotic solutions can generate erroneous results. Chen and Stone [1993] investigated this issue and suggested that the Tauberian theorem be used to check the validity of asymptotic solutions obtained using this relationship. For the sake of conciseness, detailed discussions under the title of this section is referred to the paper given by Chen and Stone [1993], and a reprint of it is given in the appendix as a substitute of this section.

8. CONCLUSIONS

The following conclusions can be drawn from the studies:

(1) The Laplace-Hankel domain calculation method provides an effective means to evaluate complicated well hydraulics theories.

(2) The Laplace-Hankel domain solution for the three-dimensional well hydraulics theory given by Neuman (1974) separates the complicated hydraulic influences due to the water-table effect and the partially penetrating pumping effect into specific and individual terms. This separation makes detailed understanding of the problem easier.

(3) For an unconfined aquifer subject to partially penetrating pumping, the large-time drawdown histories at different depths of a fixed distance are parallel Theis curves. This indicates that the water-table effect and the partially penetrating pumping effect at large times are constant for a fixed distance.

(4) A method based on the large-time drawdown data and an appropriate well hydraulics theory in its Laplace-Hankel domain is developed to estimate the three-dimensional aquifer anisotropy tensor. For the Sevilleta aquifer, the aquifer anisotropy determined by this method has one principal transmissivity of 1.62×10^{-2} m^2/s in the direction of N58°E, and another of 1.27×10^{-2} m^2/s in the direction of N32°W. The eccentricity of the anisotropy ellipse is 1.13.

(5) The mapping function technique is useful in diagnosing the field drawdown data. This mapping function is mathematically derived from a new well hydraulics analytical solution and represents the difference between the hydrogeological conditions embedded in the field drawdown data and the assumed invoked in the Theis solution.

(6) In addition to diagnosing field drawdown data, the mapping function also offers some theoretical justification of the empirical pressure-derivative data method widely used by petroleum reservoir engineers.

(7) More research is needed to fully develop the applicability of the mapping function technique and the Laplace-Hankel domain calculation method because they have the potential to deal with appropriate problems not being investigated in this project.

(8) In finding the asymptotic well hydraulics solutions from the Laplace domain counterpart, the Tauberian theorem should be used to check the validity of the asymptotic solutions obtained.

REFERENCES

Abdassah, D., and I. Ershaghi, 1986. Triple-porosity systems for representing naturally fractured reservoirs, *Soc. Petrol. Eng.* (FE), April, 113-127.

Abramowitz, M., and I.A. Stegun, 1970. *Handbook of Mathematical Functions,* Dover Publication, 1046 pp.

Akindunni, F.F., and R.W. Gillham, 1992. Unsaturated and saturated flow in response to pumping of an unconfined aquifer: Numerical investigation of delayed drainage, *Ground Water*, 30:6:873-884.

American Society for Testing Materials, 1963. Grain size analysis of soils, D422-63, pp. 203-214, *In* 1967 Book of ASTM Standards, Pt. 11, Philadelphia.

Anderson, W.L., 1979. Numerical integration of related Hankel transforms of orders 0 and 1 by adaptive digital filtering, *Geophysics*, 44:7:1287-1305.

Anderson, W.L., 1982. Fast Hankel transforms using related and lagged convolutions, *ACM Transactions on Mathematical Software*, 8:4:344-368.

Boggs, S.B., Jr., 1987. *Principles of Sedimentology and Stratigraphy*, pp. 106-122, Merril Publishing Co., Columbus, Ohio.

Boulton, N.S., 1954. The drawdown of the water table under non-steady conditions near a pumped well in an unconfined formation, *Proc. Inst. Civil Engr.*, Part 3, 564-579.

Boulton, N.S., 1963. Analysis of data from non-equilibrium pumping tests allowing for the delayed yield from storage, *Proc. Inst. Civil Engrs.*, 26, 469-482.

Bourdet, D., T.M. Whittle, A.A. Douglas and Y.M. Pirard, 1983. A new set of time curves simplifies well test analysis, *World Oil*, May, 95-106.

Bourdet, D., J.A. Ayoub, and Y.M. Pirard, 1989. Use of pressure derivative in well-test interpretation, *Soc. Petrol. Eng. (FE)*, June, 293-302.

Bourdet, D. and A.C. Gringarten, 1980. Determination of fissure volume and block size in fractured reservoirs by type-curve analysis. Paper SPE 9293 presented at the 1980 SPE Annual Fall Techn. Conf. and Exhib., Dallas.

Chandler, S.P., N. Kapoor, and S.K. Goyal, 1981. Analysis of pumping test data using Marquardt algorithn, *Groundwater*, 19:3:225-227.

Chen, C.S. and W.D. Stone, 1993. Asymptotic calculation of Laplace inverse in groundwater problems, *Water Resour. Res.*, 29:1:207-209.

Clark, D.G., and T.D. Van Golf-Racht, 1985. Pressure-derivative approach to transient test analysis: A high-permeability North Sea reservoir example, *J.Petrol. Tech.*, November, 2023-2039.

Cooper, H.H. and C.E. Jacob, 1946. A generalized graphical method for evaluating formation constants and summarizing well field history, *Am. Geophys. Union Trans*, 27: 526-534.

Dagan, G., 1967. A method of determining the permeability and effective porosity of unconfined anisotropic aquifers, *Water Resour. Res.*, 3:4:1059-1071.

Freeze, R.A. and J.A. Cherry, 1979. *Groundwater*, Prentice-Hall, Inc., Englewood Cliffs, New Jersey.

Gradshteyn, I.S. and I.M. Ryzhik, 1980. *Tables of Integrals, Series, and Products*, Academic Press, 1160 pp.

Gringarten, A.C., 1987. Type-curve analysis: What it can and cannot do, *J. Petrol. Tech.*, January, 11-13.

Hantush, M.S. and C.E. Jacob, 1955. Non-steady radial flow in an infinite leaky aquifer, *Trans. Amer. Geophys. Union*, 36:95-100.

Hantush, M.S., 1959. Analysis of data from pumping wells near a river, *J. Geophys. Res.*, 64:1921-1932.

Hantush, M.S., 1961. Drawdown around a partially penetrating well, *Proc. Am. Soc. Civil Engrs.*, 87:(HY4):83-98.

Hantush, M.S., 1964. Hydraulics of Wells in *Advances in Hydrosci.*, edited by V.T. Chow, 1:281-432.

Hantush, M.S., 1966a. Wells in homogeneous anisotropic aquifers, *Water Resour. Res.*, 2:2:273-279.

Hantush, M.S., 1966b. Analysis of data from pumping tests in anisotropic aquifers, *J. Geophys. Res.* 71:2:421-426.

Hitchman, S.P., 1988. A collection manifold for multilevel ground-water sampling devices, *Ground Water*, 26:3:348-349.

Hsieh, P.A. and S.P. Neuman, 1985a. Field determination of the three-dimensional hydraulic conductivity tensor of anisotropic media, 1. Theory, *Water Resour. Res.* 21:11:1655-1665.

Hsieh, P.A. and S.P. Neuman, 1985b. Field determination of the three-dimensional hydraulic conductivity tensor of anisotropic media, 2. Methodology and application to fractured rocks, *Water Resour. Res.* 21:11:1667-1676.

Johns, R.A., L. Semprini, and P.A. Roberts, 1992. Estimating aquifer properties by nonlinear least-squares analysis of pump test response, *Ground Water*, 30:1:68-77.

Kohlbeck, F., and A. Alvarez, 1991. A method to determine the formation constants of leaky aquifers, and its application to pumping test data, *Ground Water*, 29:3:425-429.

Kruseman, G.P. and N.A. deRidder, 1990. Analysis and evaluation of pumping test data, 2nd Ed., *ILRI*, Wageningen, Netherlands, 377 pp.

Lakshminarayana, V., and S.P. Rajagopalan, 1978. Type-curve analysis of time-drawdown data for partially penetrating wells in unconfined anisotropic aquifers, *Ground Water*, 16:5:328-333.

Miller, R.T., 1984. Anisotropy in the Irontan and Galesville sandstones near a thermal-energy-storage well, St. Paul, Minnesota, *Ground Water* 22:5:532-537.

Moench, A.F., 1984a. Analysis of constant discharge wells by numerical inversion of Laplace transform solutions, in *Groundwater Hydraulics*, edited by J.S. Rosenshein and G.D. Bennett. Water Resources Monograph Series 9, AGU, Washington, D.C., 146-170.

Moench, A.F., 1984b. Double-porosity models for a fissured groundwater reservoir with fracture skin. *Water Resour. Res.*, 20:831-846.

Neuman, S.P., 1972. Theory of flow in unconfined aquifers considering delayed response of the water table, *Water Resour. Res.*, 8:4:1031-1044.

Neuman, S.P., 1973. Supplementary comments on theory of flow in unconfined aquifers considering delayed response of the watertable, *Water Resources Res.*, 9:4:1102-1103.

Neuman, S.P., 1974. A.S.P. Neuman effect of partial penetration on flow in unconfined aquifers considering delayed gravity response, *Water Resour. Res.*, 10:2:303-312.

Neuman, S.P., 1975. Analysis of pumping test data from anisotropic unconfined aquifers considering delayed gravity response, *Water Resources Res.*, 11:2:329-342.

Neuman, S.P., G.R. Walter, H.W. Bentley, J.J.Ward, and D.D. Gonzales, 1984. Determination of horizontal aquifer anisotropy with three wells, *Ground Water* 22:1:66-72.

Nwankwor, G.I., R.W. Gillham, G. van der Kamp, and F.F. Akindunni, 1992. Unsaturated and saturated flow in response to pumping of an unconfined aquifer: Field evidence of delayed drainage. *Ground Water*, 30:5:690-700.

Oberhettinger, F. and L. Badii, 1973. *Tables of Laplace Transforms*, Springer-Verlag, 428 pp.

Papadopulos, J.S., 1965. Nonsteady flow to a well in an infinite anisotropic aquifer, In Proc. of the Dubrovnik Symposium on Hydrology of Fractured Rocks, pp. 21-31, Inter. Assoc. Sci. Hydrology.

Prickett, T.A., 1965. Type curve solution to aquifer tests under water table conditions, *Ground Water.*, 3:3:5-14.

Rolfes, L., 1980. A numerical method for the calculation of the average drawdown in a fully penetrating observaton well in an unconfined aquifer, *Water Resour. Res.* 16:5:887-890.

Sneddon, I.N., 1972. *The Use of Integral Transforms*, McGraw-Hill.

Stehfest, H., 1970. Algorithm 368 numerical inversion of Laplace transforms, *Commun. ACM*, 13:1:47-48.

Stephens, D.B., W. Cox and J. Havlena, 1988. *Field Study of Ephemeral Stream Infiltration and Recharge*. New Mexico Water Resources Research Institute, Technical Completion Report No. 228, New Mexico State University, Las Cruces, New Mexico.

Stoner, J.D., 1981. 1 Horizontal anisotropy determined by pumping in Two Powder River basin coal aquifers, Montana, *Ground Water* 19:1:34-40.

Streltsova, T.D., 1987. *Well Testing in Heterogeneous Formations*, an Exxon Monograph, John Wiley, 413 pp.

Theis, C.V., 1935. The relation between the lowering of the piezometric surface and the rate and duration of discharge of a well using groundwater storage, *Trans. Amer. Geophys. Union,* 16:519-524.

Tiab, D., and A. Kumar, 1980. Application of the P_D' function to interference analyses, *J. Petrol. Tech.*, August:1465-1470.

Vukovic, M. and A. Soro, 1992. Determination of hydraulic conductivity of porous media from grain-size composition: *Water Resources Publications*, Littleton, Colorado.

Walton, W.C., 1960. Application and limitation of methods used to analyze pumping test data, *Water Well J.*

Walton, W.C., 1987. *Groundwater Pumping Tests*, Lewis Publishers, 201 pp.

Way, S.C. and C.R. McKee, 1982. In-situ determination of three-dimensional aquifer permeability, *Ground Water* 20:5:594-603.

Wenzel, L.K., 1942. Methods of determining permeability of water-bearing materials, with special reference to discharging-well methods, USGS Water Supply Paper 887.

Zody, S.P., 1989. Seismic refraction investigation of the shallow subsurface of the lower Rio Salado, northwest of San Acacia, New Mexico, unpublished M.S. Thesis, Geoscience Department, New Mexico Tech, Socorro, New Mexico.

APPENDIX A

Asymptotic Calculation of Laplace Inverse in Analytical Solutions of Groundwater Problems

WATER RESOURCES RESEARCH, VOL. 29, NO. 1, PAGES 207–209, JANUARY 1993

Asymptotic Calculation of Laplace Inverse in Analytical Solutions of Groundwater Problems

CHIA-SHYUN CHEN

Department of Geoscience, New Mexico Tech, Socorro

WILLIAM D. STONE

Department of Mathematics, New Mexico Tech, Socorro

The Laplace transform with respect to time, t, is normally used in finding analytical solutions for transient groundwater problems. The behavior of a function at large or small t is known to correspond to that of its Laplace transform counterpart at small or large p, respectively; p is the Laplace transform parameter of t. This condition is generally translated as t being inversely related to p and vice versa. By this relationship many asymptotic solutions for large or small t have been determined from the Laplace domain solutions valid only for small or large p. However, an example is given here which shows this kind of asymptotic calculation may fail to yield correct asymptotic solutions. Hence, the asymptotic calculation must be exercised with care. To deal with this possible failure, the Tauberian theorem is offered to evaluate the asymptotic behavior of functions from their Laplace transform counterparts.

INTRODUCTION

The Laplace transform technique has been frequently used to find analytical solutions for transient groundwater problems. In such instances, the Laplace transform is applied with respect to time, t, to the function of interest. Taking the drawdown function for a well, $h(r, t)$, for example, the Laplace transform of $h(r, t)$ with respect to t is $H(r, p)$ as defined by

$$H(r, p) = \int_0^\infty e^{-pt} h(r, t)\, dt \tag{1}$$

where p is the transform parameter for t, and r represents the spatial coordinate.

When the original mathematical models of $h(r, t)$ are transformed through (1) to the Laplace p domain, the governing equations of $H(r, p)$ become ordinary differential equations, for which the analytical solutions usually can be determined without difficulty. To obtain the original t domain solutions of $h(r, t)$, the Laplace inverse needs to be carried out on $H(r, p)$ with respect to p. If $H(r, p)$ is complicated, the Laplace inverse can be rather difficult. To avoid this, sometimes the Laplace inverse is only carried out on the asymptotic forms of $H(r, p)$, which are less complicated and valid only for small or large p. Given that the behavior of a function at large t (or small t) corresponds to that of its Laplace transform counterpart at small p (or large p), the Laplace inverse of the asymptotic $H(r, p)$ for small p (or large p) gives the solutions of $h(r, t)$ for large t (or small t).

Although this kind of asymptotic calculation has been successfully employed to deal with different problems [e.g., *Van Everdingen and Hurst*, 1949; *Hantush*, 1960; *Neuman and Witherspoon*, 1969; *Chen*, 1986], its usage requires careful consideration. Here, we give one example invalidating this kind of asymptotic calculation and offer an alternative method for determining the correct asymptotic answers.

Paper number 92WR02216.
0043-1397/93/92WR-02216$02.00

EXAMPLE

The example deals with drawdown distributions caused by a flowing well in an extensive, confined aquifer. The flowing well is subject to a constant drawdown, h_0. This problem was studied by *Jacob and Lohman* [1952], where the analytical solution for the time-dependent flow rate instead of the drawdown distribution is given. The complete model is

$$\frac{\partial^2 h}{\partial r^2} + \frac{1}{r}\frac{\partial h}{\partial r} = \frac{S}{T}\frac{\partial h}{\partial t} \tag{2}$$

$$h(r, 0) = 0 \tag{3}$$

$$h(r_w, t) = h_0 \tag{4}$$

$$h(\infty, t) = 0 \tag{5}$$

where r_w is the finite well radius; that is, the flowing well is simulated as a cylindrical sink with a radius of r_w on which a constant drawdown h_0 is maintained. This model differs from the well-known Theis model in the well bore boundary condition; the latter assumes a constant pumping rate maintained at the well which is simulated as a line sink.

Application of the Laplace transform defined by (1) to (2)–(5) and making necessary calculations on the transformed model gives the Laplace domain solution of drawdown as

$$H(r, p) = \frac{h_0}{p}\frac{K_0[r(\alpha p)^{1/2}]}{K_0[r_w(\alpha p)^{1/2}]} \tag{6}$$

where $\alpha = S/T$ and $K_0(x)$ is the modified Bessel function of the second kind of order zero. Application of Darcy's law to (6) and setting r equal to r_w gives the Laplace domain solution of flow rate at the well bore, $Q_w(p)$, as

$$Q_w(p) = 2\pi T r_w \frac{h_0}{p}(\alpha p)^{1/2} \frac{K_1[r_w(\alpha p)^{1/2}]}{K_0[r_w(\alpha p)^{1/2}]} \tag{7}$$

where $K_1(x)$ is the modified Bessel function of the second kind of order one. Now the question of interest is, What is $Q_w(t)$ as t is large? The answer is readily found; $Q_w(t)$ decreases as t increases and is zero at large t. However, we are going to determine $Q_w(t)$ for large t from (7) with the asymptotic calculation mentioned above.

Since large t corresponds to small p, the two Bessel functions in (7) can be substituted by their asymptotic expansions of small arguments; that is,

$$\lim_{p\to 0} K_1[r_w(\alpha p)^{1/2}] = \frac{1}{r_w(\alpha p)^{1/2}} \tag{8}$$

$$\lim_{p\to 0} K_0[r_w(\alpha p)^{1/2}] = \log \frac{2}{r_w(\alpha p)^{1/2}} = -\tfrac{1}{2}\log \frac{p}{a} \qquad a = \frac{4}{r_w^2\alpha} \tag{9}$$

As a result, the asymptotic form of $Q_w(p)$ for small p is

$$\lim_{p\to 0} Q_w(p) = -4\pi T h_0/[p \log (p/a)] \tag{10}$$

The Laplace inverse of (10) gives $Q_w(t)$ for large t. This can be accomplished by the tabulated Laplace inverse formula given by *Oberhettinger and Badii* [1973, equation 6.75, p. 276],

$$\lim_{t\to\infty} Q_w(t) = -4\pi\ Th_0 \int_0^\infty \frac{(at)^x}{\Gamma(x+1)}\,dx \tag{11}$$

where $\Gamma(x)$ is the gamma function. The Gamma function has the special property that $\Gamma(x+1) = x\Gamma(x) = x!$ and its integral definition is given below.

In (11), $Q_w(t)$ changes with t in the sense governed by the integral. Therefore, to evaluate how $Q_w(t)$ behaves at large t one needs to understand the limit of the integral as t approaches infinity. Denoting the integral by $I(t)$ and using the special property of $\Gamma(x)$, in a straightforward manner one can obtain an inhomogeneous ordinary differential equation for $I(t)$ as

$$\frac{dI}{dt} - I = \int_0^1 \frac{t^{x-1}}{\Gamma(x)}\,dx \tag{12}$$

Subject to the condition of $I(0) = 0$, the solution of (12) is

$$I(t) = e^t \int_0^1 \int_0^t e^{-y}\, y^{x-1} \frac{1}{\Gamma(x)}\,dy\,dx \tag{13}$$

As t approaches infinity, the double integral in (13) can be rewritten as

$$\int_0^1 \frac{1}{\Gamma(x)}\,dx \int_0^\infty e^{-y}y^{x-1}dy = \int_0^1 \frac{1}{\Gamma(x)}\,\Gamma(x)\,dx = 1 \tag{14}$$

where the infinite integral is the integral definition of $\Gamma(x)$.

By (14), the limit of $I(t)$, the integral in (11), as t approaches infinity can be found as

$$\lim_{t\to\infty} I(t) = \lim_{t\to\infty} e^t(1) = \infty$$

or

$$\lim_{t\to\infty} Q_w(t) = -\infty$$

This formally proves that the asymptotic solution of $Q_w(t)$ for large t approaches negative infinity, which is incorrect. This example demonstrates the asymptotic calculation normally used can be subject to error and should be used with care. That is, although t and p are inversely related, application of this general rule to the determination of the asymptotic Laplace inverse may yield inaccurate results. Unfortunately, there are no mathematical laws that can guide us to avoid this pitfall. Nevertheless, we noticed that the Tauberian theorem (e.g., see *Sneddon* [1972, pp. 184, 185] and *Wylie and Barrett* [1982, pp. 420, 421]) provides an effective alternative in evaluating the asymptotic behaviors of a function from its Laplace domain counterpart. In essence, the Tauberian theorem states that if a function $f(t)$ is bounded and its limits at $t = 0$ and ∞ exist, as denoted by $f(0^+)$ and $f(\infty)$ respectively, then

$$f(0^+) = \lim_{p\to\infty} pF(p) \tag{15}$$

$$f(\infty) = \lim_{p\to 0} pF(p) \tag{16}$$

where $F(p)$ is the Laplace transform of $f(t)$. Equations (15) and (16) indicate that the correct asymptotic Laplace inverse can be obtained by applying the inverse relationship between t and p to the product of p and $F(p)$. However, (15) and (16) do not involve the operation of the Laplace inverse and yield information on $f(0^+)$ and $f(\infty)$ not in terms of t domain asymptotic "functions" but in terms of their "magnitudes."

Application of (16) to (10) leads to

$$Q_w(\infty) = \lim_{p\to 0} \frac{-4\pi\ Th_0}{\log (p/a)} = 0 \tag{17}$$

which is the correct result. It should be noted that the aforementioned asymptotic solutions given by *Van Everdingen and Hurst* [1949], *Hantush* [1960], *Neuman and Witherspoon* [1969] and *Chen* [1986] yield corfrect results at small and large t values as predicted by the Tauberian theorem.

CONCLUSIONS

In the Laplace transform technique, t is inversely related to p. This relationship can be used to aid in finding asymptotic solutions for the Laplace inverse. However, it should be used with care because of possible failure as demonstrated above. It is suggested that the Tauberian theorem be used in evaluating the asymptotic behaviors of $f(t)$ from its Laplace transform counterpart $F(p)$, regardless of whether the asymptotic calculation usually conducted fails or succeeds.

Acknowledgments. Work reported here is part of the research projects supported by USGS (14-08-0001-G1744) and WRRI of New Mexico (1423640 and 4-23952). This support is highly appreciated.

REFERENCES

Chen, C. S., Solutions for radionuclide transport from an injection well into a single fracture in a porous formation, *Water Resour. Res.*, *22*(4), 508–518, 1986.

Hantush, M. S., Modification of the theory of leaky aquifers, *J. Geophys. Res.*, *65*(11), 3713–3725, 1960.

Jacob, C. E., and S. W. Lohman, Nonsteady flow to a well of constant drawdown in an extensive aquifer, *Eos. Trans. AGU*, *23*(4), 559–569, 1952.

Neuman, S. P., and P. A. Witherspoon, Theory of flow in a confined two-aquifer system, *Water Resour. Res.*, *5*(4), 803–816, 1969.

Oberhettinger, F., and L. Badii, *Tables of Laplace Transforms*, 428 pp., Springer-Verlag, New York, 1973.

Sneddon, I. H., *The Use of Integral Transforms*, 539 pp., McGraw-Hill, New York, 1972.

Van Everdingen, A. F., and W. Hurst, The application of the Laplace transformation to flow problems in reservoirs, *Trans. Am. Inst. Min. Metall. Eng.*, *186*, 305–324, 1949.

Wylie, C. R., and L. C. Barrett, *Advanced Engineering Mathematics*, 1103 pp., McGraw-Hill, New York, 1982.

C.-S. Chen, Department of Geoscience, New Mexico Tech., Socorro, NM 87801.

W. D. Stone, Department of Mathematics, New Mexico Tech, Socorro, NM 87801.

(Received April 15, 1992;
revised September 8, 1992;
accepted September 16, 1992.)